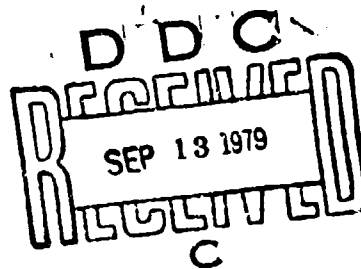


AFWL-TR-78-82



AFWL-TR-
78-82

Handwritten circled '2' and signature.

EXPERIMENTAL METHODS FOR THE CHARACTERIZATION OF MULTICONDUCTOR CABLE SYSTEMS

Howard M. Fowles et al.

Mission Research Corporation
Albuquerque, NM 87108

March 1979

Final Report

LEVEL III stamp with handwritten signature.

Approved for public release; distribution unlimited.

AD A073767



DDC FILE COPY

AIR FORCE WEAPONS LABORATORY
Air Force Systems Command
Kirtland Air Force Base, NM 87117

BEST

AVAILABLE

COPY

This final report was prepared by Mission Research Corporation, Albuquerque, New Mexico, under Contract F29601-77-C-9040, Job Order 12090531 with the Air Force Weapons Laboratory, Kirtland Air Force Base, New Mexico. Captain Howard G. Hudson (ELT) was the Laboratory Project Officer-in-Charge.

When US Government drawings, specifications, or other data are used for any purpose other than a definitely related Government procurement operation, the Government thereby incurs no responsibility nor any obligation whatsoever, and the fact that the Government may have formulated, furnished, or in any way supplied the said drawings, specifications, or other data, is not to be regarded by implication or otherwise, as in any manner licensing the holder or any other person or corporation, or conveying any rights or permission to manufacture, use, or sell any patented invention that may in any way be related thereto.

This report has been authored by a contractor of the United States Government. Accordingly, the United States Government retains a nonexclusive, royalty-free license to publish or reproduce the material contained herein, or allow others to do so, for the United States Government purposes.

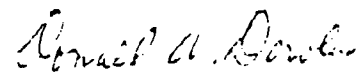
This report has been reviewed by the Information Office (OI) and is releasable to the National Technical Information Service (NTIS). At NTIS, it will be available to the general public, including foreign nations.

This technical report has been reviewed and is approved for publication.


HOWARD G. HUDSON
Captain, USAF
Project Officer

FOR THE COMMANDER


J. PHILIP CASTILLO
Chief, Technology Branch


DONALD A. DOWLEP
Colonel, USAF
Chief, Electromagnetics Division

UNCLASSIFIED

SECURITY CLASSIFICATION OF THIS PAGE (When Data Entered):

REPORT DOCUMENTATION PAGE		READ INSTRUCTIONS BEFORE COMPLETING FORM
1. REPORT NUMBER AFWL-TR-78-82	2. GOVT ACCESSION NO.	3. RECIPIENT'S CATALOG NUMBER
4. TITLE (and Subtitle) EXPERIMENTAL METHODS FOR THE CHARACTERIZATION OF MULTICONDUCTOR CABLE SYSTEMS	5. TYPE OF REPORT & PERIOD COVERED Final Report	
	6. PERFORMING ORG. REPORT NUMBER AMRC-R-120	
7. AUTHOR(s) Howard M. Fowles, Ashok K. Agrawal, Larry D. Scott, Larry Simpson	8. CONTRACT OR GRANT NUMBER(s) F29501-77-C-0040	
9. PERFORMING ORGANIZATION NAME AND ADDRESS Mission Research Corporation Albuquerque, NM 87108	10. PROGRAM ELEMENT, PROJECT, TASK AREA & WORK UNIT NUMBERS 64747F/12090531	
11. CONTROLLING OFFICE NAME AND ADDRESS Air Force Weapons Laboratory (ELT) Kirtland Air Force Base, NM 87117	12. REPORT DATE March 1979	
	13. NUMBER OF PAGES 120	
14. MONITORING AGENCY NAME & ADDRESS (if different from Controlling Office)	15. SECURITY CLASS. (of this report) UNCLASSIFIED	
	15a. DECLASSIFICATION/DOWNGRADING SCHEDULE	
16. DISTRIBUTION STATEMENT (of this Report) Approved for public release; distribution unlimited.		
17. DISTRIBUTION STATEMENT (of the abstract entered in Block 20, if different from Report)		
18. SUPPLEMENTARY NOTES		
19. KEY WORDS (Continue on reverse side if necessary and identify by block number) Transmission Lines Aircraft Cable Multiconductor Experimental		
20. ABSTRACT (Continue on reverse side if necessary and identify by block number) This report presents the results of an experimental investigation of pulse propagation on cross-sectional inhomogeneous multiconductor cable systems. Time domain and frequency domain measurement techniques are described and verified. The modal analysis of a 5-wire branched cable and the common mode analysis of a simple cable network are given in the time domain and verified experimentally. Some practical applications of the results of this study to measurements of multiconductor transmission line characteristics in situ are discussed.		

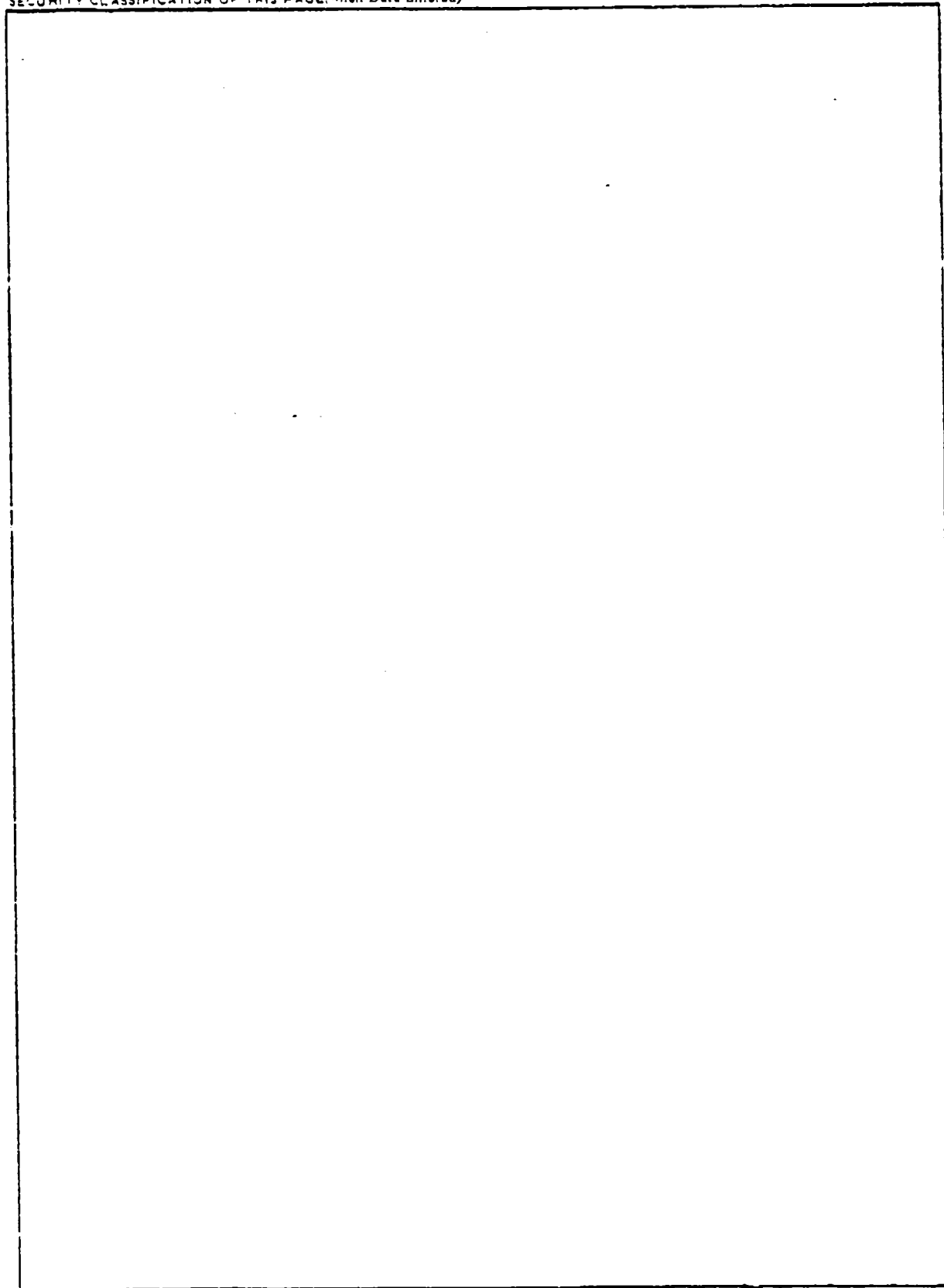
DD FORM 1473, JAN 73 EDITION OF 1 NOV 65 IS OBSOLETE

UNCLASSIFIED

SECURITY CLASSIFICATION OF THIS PAGE (When Data Entered)

UNCLASSIFIED

SECURITY CLASSIFICATION OF THIS PAGE (When Data Entered)

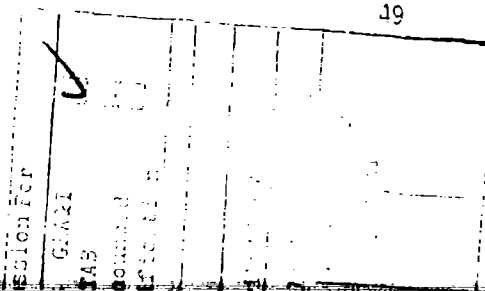


UNCLASSIFIED

SECURITY CLASSIFICATION OF THIS PAGE (When Data Entered)

CONTENTS

<u>Section</u>		<u>Page</u>
I	INTRODUCTION	7
II	MODAL ANALYSIS OF UNIFORM LINE SEGMENTS	9
III	EXPERIMENTAL CHARACTERIZATION OF MULTICONDUCTORS	15
	1. BACKGROUND	15
	2. TDR PRINCIPLES	16
	3. CHARACTERISTIC ADMITTANCE MEASUREMENTS	17
	a. Direct Method	17
	b. Indirect Method	17
	4. MODAL AMPLITUDE AND VELOCITY MEASUREMENTS	18
	5. INDUCTANCE AND CAPACITANCE MATRICES	20
	6. EXPERIMENTAL RESULTS FOR THREE-, FOUR-, AND FIVE-WIRE LINES OVER A GROUND PLANE	21
	a. Three-Wire Line	21
	b. Four-Wire and Five-Wire Lines	29
	c. Result Summary and Error Analysis	34
IV	PULSE PROPAGATION ON BRANCHED MULTICONDUCTORS FORMED BY UNIFORM LINE SEGMENTS	40
	1. BACKGROUND	40
	2. ANALYSIS USING THE REFLECTION AND TRANSMISSION MATRICES	41
	a. Methodology	41
	b. Examples	43
	3. ANALYSIS USING THE SCATTERING MATRIX OF THE JUNCTION	49



CONTENTS (Continued)

<u>Section</u>	<u>Page</u>
4. EXPERIMENTAL RESULTS	54
5. ANALYSIS OF CABLE NETWORKS	69
a. Background	69
b. Special Case of a Network Modeled with Single Conductor Line Segments	69
V APPLICATIONS TO MULTICONDUCTOR CHARACTERIZATION <i>IN SITU</i>	79
1. INTRODUCTION	79
2. CABLE INTERFACE REFLECTIONS	79
3. ANALYSIS OF MULTIPLE REFLECTIONS	88
4. PRACTICAL CONSIDERATIONS	90
REFERENCES	93
APPENDIX EXPERIMENTAL CHARACTERIZATION OF MULTICONDUCTOR TRANSMISSION LINES IN FREQUENCY DOMAIN	95

ILLUSTRATIONS

<u>Figure</u>		<u>Page</u>
1	Schematic of a Three-Wire Line Over a Ground Plane	12
2	Three-Wire Cable (Over a Ground Plane) Geometry	22
3	Waveforms measured with a time domain reflectometer to determine the impedance Z_{ij}^m and the modal velocities.	23
4	Voltage waveform at the load end; (a) wire 1 driven, (b) wire 2 driven, (c) wire 3 driven.	25
5	Voltage and current waveforms at the driven end; (a) wire #1 driven, (b) wire #2 driven, (c) wire #3 driven.	28
6	Cross sections of four-wire and five-wire cables (over a ground plane), dimensions in cm.	30
7	Four-wire and five-wire line input voltage pulse.	31
8	Voltage waveforms at load end of four-wire and five-wire lines.	32
9	A Multiconductor Transmission Line with a Branch	44
10	Five-Wire Cable (Over a Ground Plane) Cross Section	55
11	Input waveform used to drive the wire in the cable.	58
12	Voltage waveform at the load end of wire 1 of tube 2, with wire 4 of tube 1 driven.	58
13	Voltage waveform at the load end of wire 2 of tube 2, with wire 4 of tube 1 driven.	58
14	Voltage waveform at the load end of wire 3 of tube 2, with wire 4 of tube 1 driven.	59
15	Voltage waveform at the load end of wire 4 of tube 3, with wire 4 of tube 1 driven.	59
16	Voltage waveform at the load end of wire 5 of tube 3, with wire 4 of tube 1 driven.	59

ILLUSTRATIONS (Continued)

<u>Figure</u>		<u>Page</u>
17	Voltage waveform at the load end of wire 1 of tube 1, with wire 1 of tube 2 driven.	61
18	Voltage waveform at the load end of wire 2 of tube 1, with wire 1 of tube 2 driven.	61
19	Voltage waveform at the load end of wire 3 of tube 1, with wire 1 of tube 2 driven.	61
20	Voltage waveform at the load end of wire 4 of tube 1, with wire 1 of tube 2 driven.	62
21	Voltage waveform at the load end of wire 5 of tube 1, with wire 1 of tube 2 driven.	62
22	Voltage waveform at the load end of wire 4 of tube 3, with wire 1 of tube 2 driven.	62
23	Voltage waveform at the load end of wire 5 of tube 3, with wire 1 of tube 2 driven.	63
24	Voltage waveform at the load end of wire 1 of tube 1, with wire 4 of tube 3 driven.	63
25	Voltage waveform at the load end of wire 2 of tube 1, with wire 4 of tube 3 driven.	63
26	Voltage waveform at the load end of wire 3 of tube 1, with wire 4 of tube 3 driven.	64
27	Voltage waveform at the load end of wire 4 of tube 1, with wire 4 of tube 3 driven.	64
28	Voltage waveform at the load end of wire 5 of tube 1, with wire 4 of tube 3 driven.	64
29	Voltage waveform at the load end of wire 1 of tube 2, with wire 4 of tube 3 driven.	65
30	Voltage waveform at the load end of wire 2 of tube 2, with wire 4 of tube 3 driven.	65

ILLUSTRATIONS (Continued)

<u>Figure</u>		<u>Page</u>
31	Voltage waveform at the load end of wire 3 of tube 2, with wire 4 of tube 3 driven.	65
32	Current waveform at short circuit termination on wire 1 of tube 1 with tube 2 driven in the common mode.	66
33	Current waveform at short circuit termination on wire 2 of tube 1 with tube 2 driven in the common mode.	66
34	Current waveform at short circuit termination on wire 3 of tube 1 with tube 2 driven in the common mode.	66
35	Current waveform at short circuit termination on wire 4 of tube 1 with tube 2 driven in the common mode.	67
36	Current waveform at short circuit termination on wire 5 of tube 1 with tube 2 driven in the common mode.	67
37	Current waveform at short circuit termination on wire 5 of tube 3 with tube 2 driven in the common mode.	68
38	Current waveform at short circuit termination on wire 5 of tube 3 with tube 2 driven in the common mode.	62
39	Network Layout	71
40	Pulse Generator Output Signals	77
41	Measured and Predicted Network Response	78
42	Cable Interface Approximate Equivalent Circuit	80
43	Typical Interface Reflections for an Ideal Step Input	83
44	Typical Interface Reflections for a Nonideal Step Input	84
45	Interface reflections from actual aircraft cable connectors.	36
46	Typical interface reflections for a nonideal step input for various load impedances.	87

ILLUSTRATIONS (Continued)

<u>Figure</u>		<u>Page</u>
47	Multiple Reflection Diagram	89
48	Example of the reflection produced by foil tape around a multiconductor.	92

TABLES

<u>Table</u>		<u>Page</u>
1	Comparison of Three-Wire Line Parameters From Frequency Domain and Time Domain Measurements	35
2	Comparison of Four-Wire Line Parameters From Frequency Domain and Time Domain Measurements	36
3	Comparison of Five-Wire Line Parameters From Frequency Domain and Time Domain Measurements	37
4	Branched Multiconductor Characteristic Impedance and Scattering Matrices	57

SECTION I

INTRODUCTION

Electronic subsystems on aircraft, missiles and ground electronic systems are generally connected by closely coupled multiconductor cables. These multiconductor cables are generally made of conductors with different insulating materials resulting in a cross-sectionally inhomogeneous media. Such cables often have branches where some of the conductors of the cable branch and/or some other conductors may join the cable. Determination of the transient response of such cables illuminated by an electromagnetic pulse (EMP) from nuclear detonations is becoming of increasing importance (ref. 1).

The use of multiconductor transmission line theory in EMP interaction problems is well documented (refs. 1, 2). The analysis usually proceeds from transmission line models which are characterized by specifying the per unit-length inductance and capacitance matrices of the line. However, it is also possible to characterize a line in terms of the characteristic admittance or impedance and the modal amplitudes and velocities that can exist on the line. Either set of parameters is sufficient to determine the coupling and propagation characteristics of a lossless multiconductor in an inhomogeneous medium.

Analyses of uniform multiconductor transmission lines have been reported by several investigators both in the frequency and the time domain (refs. 2 through 12). The propagation modes for multiconductor transmission lines with inhomogeneous dielectrics are discussed in reference 4. The analysis of multiconductor transmission line networks in the frequency domain is given in reference 5.

This report presents the results of a multiconductor cable characterization study which was undertaken to investigate multimode pulse propagation on cable systems and to develop measurement techniques applicable

to cable testing *in situ*. Multimode propagation is discussed in section II of this report. Section III describes experimental methods for the time domain characterization of multiconductors. Frequency domain methods were also investigated and are described in the appendix. Two methods for the analysis of a branched cable configuration are presented in section IV. While many individual parts of this problem appear elsewhere (refs. 4 and 5), section IV presents a complete time domain analysis of a multiconductor transmission line with branches and includes experimental verification of the results. The common mode response of a cable network containing two branch points is included as a special case. Section V discusses some practical applications of this study for the characterization *in situ* of multiconductor cable systems.

SECTION II

MODAL ANALYSIS OF UNIFORM LINE SEGMENTS

Consider a lossless line formed by N conductors, plus a reference conductor (ground). The line is assumed to be uniform along its length (z coordinate), but with arbitrary cross section. In general, the dielectric surrounding the line is inhomogeneous (e.g., cable made of insulated conductors having different geometries and dielectric materials).

In the presence of materials of different dielectric constants, the propagation cannot strictly be TEM. However, for many applications propagation may be considered "quasi-TEM" (refs. 4 and 13), and the analysis can proceed from the generalized telegrapher's equations. These equations for the lossless case are (refs. 3 and 14),

$$\frac{\partial}{\partial z} [V_n(z,t)] = -[L'_{nm}] \frac{\partial}{\partial t} [I_m(z,t)] \quad (1)$$

$$\frac{\partial}{\partial z} [I_n(z,t)] = -[C'_{nm}] \frac{\partial}{\partial t} [V_m(z,t)] \quad (2)$$

with

$$\begin{aligned} n &= 1, 2, \dots, N \\ m &= 1, 2, \dots, N \end{aligned}$$

Where V_m and I_m represent the voltage with respect to the reference conductor and current on the m th conductor, respectively, as a function of distance z along the line at time, t . $[L'_{nm}]$ and $[C'_{nm}]$ are respectively per unit-length coefficients of inductance and capacitance matrices of $N \times N$ size. The diagonal elements are self- and the off-diagonal elements are mutual quantities. Both $[L'_{nm}]$ and $[C'_{nm}]$ are real, symmetric and dominant. The elements of the capacitance matrix $[C'_{nm}]$ and inductance matrix $[L'_{nm}]$ are further characterized by the following properties (ref. 15):

$$L'_{nm} \geq 0 \text{ for all } n \text{ and } m$$

$$C'_{nn} \geq 0 \text{ for all } n$$

$$C'_{nm} \leq 0 \text{ for all } n \neq m$$

$$\sum_{m=1}^N C'_{nm} \geq 0 \text{ for all } n$$

$$\sum_{n=1}^N C'_{nm} \geq 0 \text{ for all } m$$

(3)

The per unit-length inductance matrix $[L'_{nm}]$ and capacitance matrix $[C'_{nm}]$ can be measured experimentally using the methods described in section III. The determination of $[L'_{nm}]$ and $[C'_{nm}]$ analytically is generally a difficult problem; however, numerical approximations can be employed to determine $[L'_{nm}]$ and $[C'_{nm}]$ (refs. 16 and 17).

The voltage and current vectors which satisfy equations (1) and (2) can be written as (ref. 4)

$$[V_n(z,t)] = [V_n] \cdot f(z-vt) \quad (4)$$

$$[I_n(z,t)] = [I_n] \cdot f(z-vt) \quad (5)$$

where $[V_n]$ and $[I_n]$ are constant vectors. From equations (1), (2), (4) and (5) the eigenvalue equation for $[V_n]$ can be written as

$$[L'_{nm}][C'_{nm}][V_n]_i = 1/v_i^2 [V_n]_i \quad (6)$$

where $1/v_i^2$ is a eigenvalue of the matrix $[L'_{nm}][C'_{nm}]$, and $[V_n]_i$ is the associated voltage eigenvector. In the case of inhomogeneous dielectrics, there will in general be N distinct eigenvalues. Associated with the eigenvalues $1/v_i^2$, $i=1, \dots, N$, there are also current eigenvectors $[I_n]_i$. The $[I_n]_i$ are the eigenvectors of the adjoint matrix $[C'_{nm}][L'_{nm}]$ and have the same eigenvalues $1/v_i^2$ (ref. 4). The eigenvalue equation for this case can be written as

$$[C'_{nm}][L'_{nm}][I_n]_i = 1/v_i^2 [I_n]_i \quad (7)$$

It can be shown that in order for the modes to represent unattenuated traveling waves, the velocities must be real; i.e., the eigenvalues $1/v_i^2$ must be real and positive (ref. 4). The v_i 's represent the velocities of N propagating modes.

The eigenvectors of voltage or current are determined to within an arbitrary constant by solving the set of linear homogeneous equations (6) or (7) for $[V_n]_i$ or $[I_n]_i$. Each solution for $i=1, 2, \dots, N$ represents a mode of propagation on the line. Since the modes of propagation are orthogonal to each other, the eigenvectors form a set of linearly independent vectors and an arbitrary vector $[E_n]$ can be represented as a sum of voltage eigenvectors in the form (ref. 4)

$$[E_n] = [V_{nm}][A_m] \quad (8)$$

where $[A_m]$ is a vector.

Let a wave traveling in the forward direction be characterized at some point in space and time by the voltage vector $[V_{fn}(z, t)]$ which can be expressed in terms of the voltage eigenvectors as

$$[V_{fn}(z, t)] = [V_{nm}][A_m(t)] \quad (9)$$

where the vector $[A_m(t)] = A_m f(t - z/v_m)$.

The matrix $[V_{nm}]$ is the modal matrix of the line which is defined as a square matrix whose columns are the eigenvectors determined from equation (6) or (7). The vector $[A_m f(t - z/v_m)]$ represents forward traveling waves of unspecified amplitude. The amplitude coefficients A_m are determined from boundary conditions.

Consider a line of length ℓ connected to arbitrary terminal networks at each end (figure 1), and excited at the input end $z = 0$. The modal amplitudes are given in terms of the total voltage at the input $[V_{fn}]_0$ by evaluating equation (9) at $z = 0$ and solving for the amplitude coefficients A_m .

The forward traveling voltage wave on the n^{th} wire at any point $z = \ell$ on the line is then

$$V_{fn}(\ell, t) = \sum_{m=1}^N V_{nm} A_m(t - \tau_m) \quad (10)$$

where τ_m is the transit time for each mode

$$\tau_m = \ell/v_m, m=1, 2, \dots, N \quad (11)$$

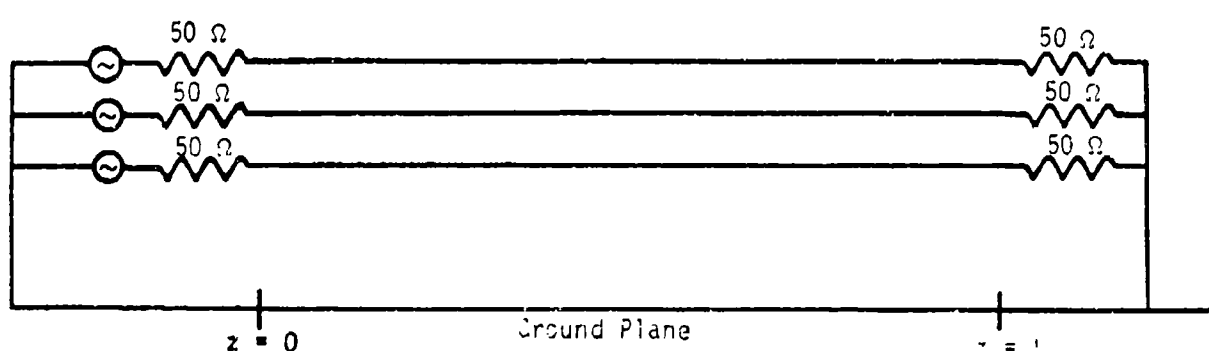


Figure 1. Schematic of a Three-Wire Line Over a Ground Plane

This is illustrated by considering an example of a four conductor line. For this case, equation (10) can be written as

$$\begin{bmatrix} V_{f_1}(z,t) \\ V_{f_2}(z,t) \\ V_{f_3}(z,t) \end{bmatrix} = \begin{bmatrix} V_{11} & V_{12} & V_{13} \\ V_{21} & V_{22} & V_{23} \\ V_{31} & V_{32} & V_{33} \end{bmatrix} \begin{bmatrix} A_1(t-\tau_1) \\ A_2(t-\tau_2) \\ A_3(t-\tau_3) \end{bmatrix} \quad (12)$$

$$V_{f_1}(z,t) = V_{11} \cdot A_1(t-\tau_1) + V_{12} \cdot A_2(t-\tau_2) + V_{13} \cdot A_3(t-\tau_3) \quad (13)$$

with expressions similar to equation (13) for the voltage on wires 2 and 3.

Note that in equation (13) the voltage wave incident at the point $z = z$ on the conductors has three components. These voltages represent the modal amplitudes of the different modes. The voltage wave, traveling in the forward direction at $z = 0$ can be obtained from the following relation

$$[V_{f_n}(0,t)] = [Z_{c_{nm}}][Z_{c_{nm}} + Z_{s_{nm}}]^{-1}[V_{s_n}(0,t)] \quad (14)$$

where $[Z_{c_{nm}}]$ is the characteristic impedance matrix of the line, $[Z_{s_{nm}}]$ the termination impedance matrix at the driven end and $[V_{s_n}(0,t)]$ the source voltage vector at $z = 0$. Thus, from equations (13) and (14) the modal amplitudes at any point on the line can be obtained. The waves on a lossless line travel unattenuated. At any discontinuity or load, the voltage or current can be obtained using the reflection and transmission coefficients. For a uniform section of line (figure 1) the voltage vector at the load is given by the following relation

$$[V_{L_n}(t)]_m = 2[Z_{L_{nm}}][Z_{L_{nm}} + Z_{c_{nm}}]^{-1}[V_{f_n}(z,t)]_m \quad (15)$$

where $[V_{L_n}(t)]_m$ is the load voltage vector for the m^{th} mode, $[Z_{L_{nm}}]$ and $[Z_{C_{nm}}]$ are the load and characteristic impedance matrices, respectively. $[V_{f_n}(x,t)]_m$ is the incident voltage vector at the load for the m^{th} mode.

SECTION III

EXPERIMENTAL CHARACTERIZATION OF MULTICONDUCTORS

1. BACKGROUND

The propagation of transient signals on lossless multiconductor cables is completely specified by the inductance and capacitance matrices of the cable system. These parameters can be obtained from frequency domain measurements and used to calculate the characteristic impedance matrix and the modal amplitudes and velocities that can exist on the line. The technique is described in the appendix.

It is also possible, using time domain techniques, to measure the characteristic impedance and modal amplitudes and velocities directly, from which the inductance and capacitance matrices can be computed (ref. 18). The time domain technique has a distinct advantage for *in situ* impedance measurements since it has the ability to "look through" stray impedances at the input. The measurements are completed before reflections from the load arrive and are, therefore, independent of the load. When both ends of the cable are accessible, the modal velocities and amplitudes can also be measured, either by terminating the load end in a known impedance and measuring the current or voltage at the load, or by simply disconnecting or shorting the load end of the cable to produce an open or short circuit with a reflection coefficient of ± 1 . In the latter case all of the measurements can be made from the driven end of the cable with simple instrumentation.

An investigation of multiconductor transmission line characterization techniques has been carried out utilizing bundles of closely spaced insulated wires located near a ground plane. The wires were insulated with different dielectric materials to form a cross sectionally inhomogeneous bundle which supports nondegenerate modes of propagation with discrete modal velocities.

Time domain reflectometry (TDR) methods have been reported for the characterization of cross sectionally homogeneous bundles in which the eigenmodes are totally degenerate and, therefore, propagate with the same velocity (ref. 19). The measurement techniques described here for the nondegenerate case are an extension of the methods developed in reference 19 for homogeneous bundles.

2. TDR PRINCIPLES

Standard TDR techniques for the measurement of an unknown impedance utilize a fast (0.1 ns rise time) voltage step as input to a "standard" line of known characteristic impedance Z_c , which is terminated in an unknown impedance Z_L . The pulse reflected by the discontinuity between Z_c and Z_L is recorded (usually with a sampling scope) and compared with the input pulse. For resistive loads, the incident and reflected voltages are of the same pulse shape and the reflection coefficient ρ is given by the ratio of the reflected (A_r) to incident (A_i) pulse amplitude. The pulse amplitudes are related to the impedances by the equation

$$\rho = A_r/A_i = \frac{Z_L - Z_c}{Z_L + Z_c} \quad (16)$$

from which the load impedance can be computed as

$$Z_L = Z_c \left(\frac{1 + \rho}{1 - \rho} \right) \quad (17)$$

Equations (16) and (17) also apply to complex impedances; however, in this case the reflection coefficient is a complex function of frequency given by the ratio of the frequency spectra of the reflected and incident pulses.

3. CHARACTERISTIC ADMITTANCE MEASUREMENTS

The characteristic admittance matrix of an N-wire cable can be determined directly or indirectly using the procedures described in reference 19. Both procedures apply to homogeneous or inhomogeneous bundles and treat the cable as an N-port network with an input admittance matrix equal to the characteristic admittance matrix of line. These parameters are equal for times less than the round trip travel time on the line.

a. Direct Method

Direct measurement of the characteristic admittance is performed by driving each wire of the bundle in turn with all other wires grounded at the input. Voltage and current probes are used to measure the voltage pulse on the driven wire and the current pulses on all wires. Since the pulse shapes are the same, the elements of the admittance matrix can be determined from the amplitude ratios given by

$$y_{ij} = I_i/V_j \quad \begin{array}{l} i = 1, 2, \dots, N \\ j = 1, 2, \dots, N \end{array} \quad (18)$$

b. Indirect Method

A conventional TDR is used for indirect measurements of the characteristic admittance. Formulas for the diagonal and off-diagonal elements of the characteristic admittance matrix in terms of measured impedance values are given in reference 19 as:

$$y_{ii} = 1/Z_{ii}^m \quad (\text{diagonal}) \quad (19)$$

$$y_{ij} = y_{ji} = 1/2(1/Z_{ij}^m - 1/Z_{ii}^m - 1/Z_{jj}^m) \quad (\text{off-diagonal}) \quad (20)$$

where Z_{ii}^m is the measured impedance of wire i with all other wires grounded at the input and Z_{ij}^m is the measured impedance of wires i and j connected in parallel at the input with all other wires grounded at the input.

4. MODAL AMPLITUDE AND VELOCITY MEASUREMENTS

On an infinitely long multiconductor, the forward traveling voltage or current pulse on each wire can be expressed as a sum of eigenmodes of the form given by equation (10) where the product $A_m V_{nm}$ has been replaced by V'_{nm} .

$$V_{fn}(z,t) = \sum_{m=1}^N V'_{nm} f(t - z/v_m) \quad n = 1, 2, \dots, N \quad (21)$$

$$I_{fn}(z,t) = \sum_{m=1}^N I'_{nm} f(t - z/v_m) \quad n = 1, 2, \dots, N \quad (22)$$

The index n denotes the wire number, m is the mode number, V'_{nm} is the modal voltage amplitude coefficient, I'_{nm} is the modal current amplitude coefficient, and v_m is the modal velocity. These equations apply to a lossless nondispersive line; e.g., the modal velocities are constant and the pulse shape is independent of distance. They also apply to a line of finite length which is terminated at the load end by either an open or a short circuit, when all reflections after the first are ignored. Since a reflection coefficient of ± 1 at the end of the line reflects all modes without distortion, no mode conversion occurs on reflection. The reflected pulse of voltage or current incident back at the driving point is given by equations (21) or (22) evaluated at $z = 2L$, where L is the line length.

For an arbitrary input pulse at $z = 0$, the reflected pulse is seen as a superposition of time delayed pulses which arrive at times

$$t_m = 2L/v_m \quad (23)$$

with amplitudes given by the coefficients V'_{nm} and I'_{nm} of equations (21) and (22). The modal velocities are found from equation (23) by measuring the arrival times t_m (round trip travel times) of each mode.

The coefficients V'_{nm} and I'_{nm} are voltage and current eigenvectors of the line which can be determined by recording the voltage or current pulse train described by equations (21) and (22) at a known termination network. No mode conversion would occur at the termination if the network were matched to the characteristic impedance of the line; however, this would require a complicated matching network for cables containing several wires. A more reasonable approach is to use an arbitrary known unmatched termination and to correct the data for distortion caused by mode conversion at the termination. This is easily carried out since it is known that the observed pulse is just the sum of the incident and reflected pulses.

For a two conductor line of characteristic impedance Z_c the voltage pulse V_L measured across a load of impedance Z_L is given by

$$V_L = V_i + \rho V_i = (1 + \rho)V_i \quad (24)$$

where V_i is the incident pulse amplitude and the voltage reflection coefficient ρ is given by equation (16). The same relationship applies to an N-wire multiconductor; however, for this case the impedances used in equation (16) to compute the reflection coefficient are $N \times N$ matrices and the voltages V_L and V_i are N-dimensional vectors for each mode of propagation. Solving equation (24) for V_i and expressing the result in matrix form gives

$$[V_i]_m = (I + [\rho])^{-1} [V_L]_m \quad (25)$$

where I is the unit matrix and $[\rho]$ is an $N \times N$ matrix given by

$$[\rho] = ([Z_L] - [Z_c])([Z_L] + [Z_c])^{-1} \quad (26)$$

where the subscripts L and c denote the termination impedance and line

characteristic impedance, respectively. The eigenvectors $[V_{1n}^m]$ are determined from equations (25) and (26) using measured terminal voltages for each mode on each wire of the cable. Similar equations apply to the eigenvectors of current. In this case the order of multiplication of the factors which define the voltage reflection coefficient given by equation (26) are transposed and the polarity is reversed.

5. INDUCTANCE AND CAPACITANCE MATRICES

Relationships between the inductance and capacitance matrices and the characteristic admittance, modal amplitudes and velocities can be obtained directly from the matrix form of the transmission line differential equations given by equations (1) and (2). Rewriting equations (21) and (22) in matrix form and substitution into equations (1) and (2) leads to

$$[V_{nm}'] = [L_{mn}'] [I_{nm}'] [v_{mm}] \quad (27)$$

$$[I_{nm}'] = [C_{mn}'] [V_{nm}'] [v_{mm}] \quad (28)$$

The modal velocity matrix $[v_{mm}]$ is diagonal in form with the modal velocities v_m as elements.

Equations (27) and (28) can be solved for the inductance and capacitance matrices of the line to give

$$[L_{nm}'] = [V_{nm}'] [v_{mm}]^{-1} [I_{nm}']^{-1} \quad (29)$$

$$[C_{nm}'] = [I_{nm}'] [v_{mm}]^{-1} [V_{nm}']^{-1} \quad (30)$$

These equations can be further simplified by making use of the relationships

$$[V'_{nm}] = [Z_{c_{nm}}][I'_{mn}] \quad (31)$$

and

$$[I'_{nm}] = [Y_{c_{nm}}][V'_{mn}] \quad (32)$$

Substitution of these expressions into equations (29) and (30) give the L and C matrices of the line in terms of the measured characteristic impedance Z_c or admittance matrix Y_c and the measured modal velocities and modal current or voltage amplitudes. The results are

$$[L'_{nm}] = [Z_{c_{nm}}][I'_{mn}][v_{nm}]^{-1}[I'_{nm}]^{-1} \quad (33)$$

$$[C'_{nm}] = [Y_{c_{nm}}][V'_{mn}][v_{nm}]^{-1}[V'_{nm}]^{-1} \quad (34)$$

It is not necessary to measure both the modal voltage and modal current since if either L or C is known, the other can be computed from the equations

$$[C'_{nm}] = [Y_{c_{nm}}][L'_{mn}][Y_{c_{nm}}]; \quad [L'_{nm}] = [Z_{c_{nm}}][C'_{mn}][Z_{c_{nm}}] \quad (35)$$

6. EXPERIMENTAL RESULTS FOR THREE-, FOUR-, AND FIVE-WIRE LINES OVER A GROUND PLANE

a. Three-Wire Line

For purposes of demonstrating the validity of the methods described, a three-wire cable (over a ground plane) 20 meters in length was constructed using wires insulated with solid polyethylene (wire #1), neoprene (wire #2), and rubber (wire #3). The wires were wrapped with a dielectric tape to insure a constant cable cross section over the length of the cable. The cable was supported with Styrofoam blocks above an aluminum ground plane in the configuration shown in figure 2.

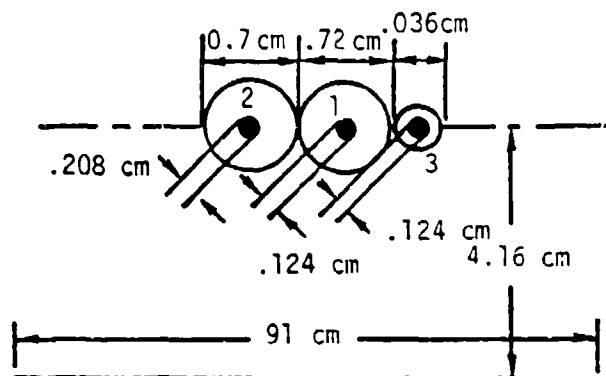
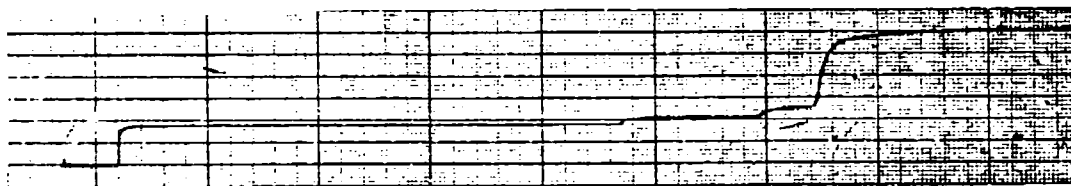


Figure 2. Three-Wire Cable (Over a Ground Plane) Geometry

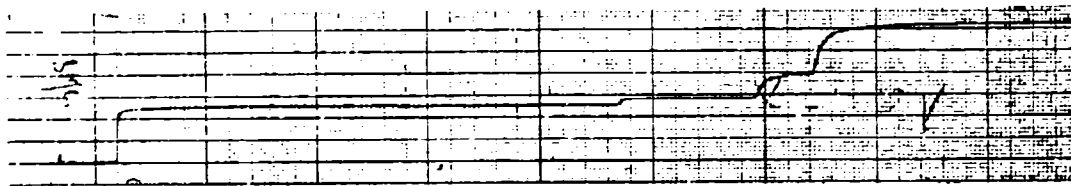
(1) Indirect Measurements

TDR recordings obtained by driving each wire in turn with the others grounded at the input end and with the load end open, are presented in figure 3. Similar data (not shown) was recorded with wires 1 and 2, 2 and 3, and 1 and 3 connected in parallel at the input. The results were used in equations (19) and (20) to obtain the diagonal and off-diagonal terms of the characteristic admittance matrix. The reflected pulses shown in figure 3a, 3b and 3c each exhibit three time-delayed step functions corresponding to the three discrete propagation modes on the line. The measured round trip travel times of each mode and the known line length were used in equation (23) to determine the propagation velocities.

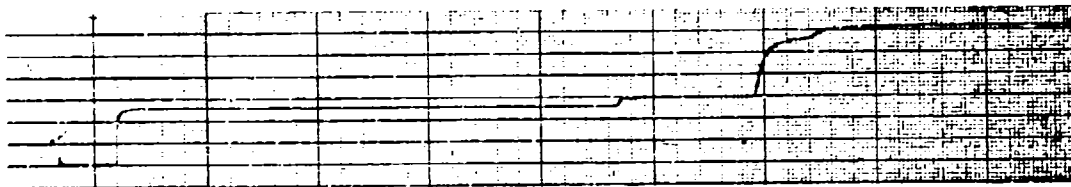
Measurement of the voltage eigenvectors was accomplished by driving one of the wires with a short duration pulse from a 50 ohm source and terminating the ends of each wire in 50 ohm resistive loads. Pulse distortion caused by the stray inductance of the probe ground lead and the carbon resistors was minimized by erecting grounded plates at right angles to the ground plane at the input and load ends of the line (see figure A-1 of the appendix). This provided a very low impedance to the ground plane and allowed the probe ground connection and resistor leads to be kept to a minimum. The output voltage pulses on each wire were recorded using a



(a) Z_{11}^m



(b) Z_{22}^m



(c) Z_{23}^m

Figure 3. Waveforms measured with a time domain reflectometer to determine the impedance Z_{ij}^m and the modal velocities. The vertical scale is 200 mV/div; horizontal scale is 6 ns/div.

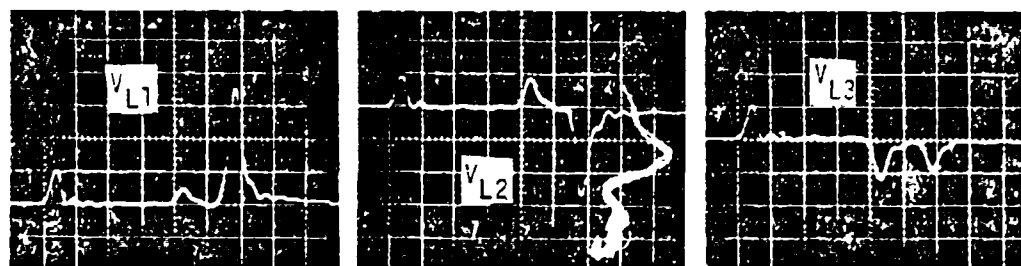
high impedance voltage probe and a 200 MHz oscilloscope. The modal amplitudes were computed from the measured load voltages using equation (25). Only one set of data was required to determine the modal matrix of line; however, three sets were obtained by driving each wire in turn in order to determine the consistency of the measurements. The recorded pulse data are shown in figure 4.

The modal matrix normalized to the first element in each column, the modal velocities and the characteristic impedance matrix determined from measurements on the three-wire line are as follows:

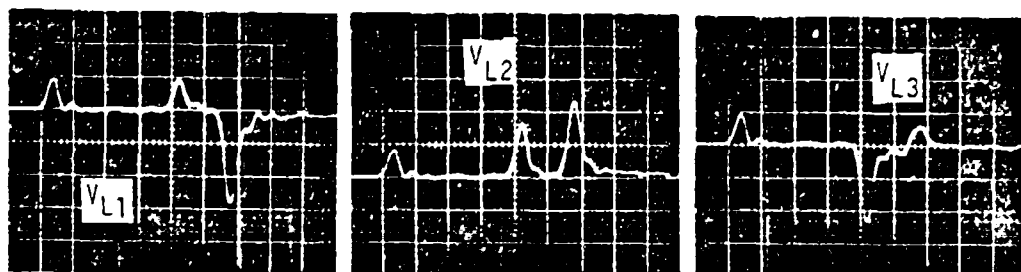
$$[Z_c]_3(\text{ohms}) = \begin{bmatrix} 231 & 139 & 157 \\ 139 & 230 & 112 \\ 157 & 112 & 258 \end{bmatrix}$$

$$[v_{nm}]_3(\text{m/sec}) = \begin{bmatrix} 2.77 & 0 & 0 \\ 0 & 2.19 & 0 \\ 0 & 0 & 2.03 \end{bmatrix} \times 10^8$$

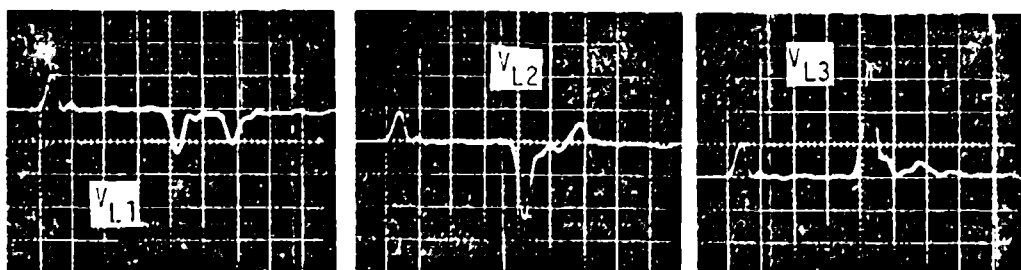
$$[V_{nm}]_3 = \begin{array}{c} \text{Wire \#1 Driven} \\ \begin{bmatrix} 1 & 1 & 1 \\ 0.92 & 4.31 & -1.14 \\ 1.01 & -5.46 & -0.16 \end{bmatrix} \end{array} \begin{array}{c} \text{Wire \#2 Driven} \\ \begin{bmatrix} 1 & 1 & 1 \\ 0.90 & 3.89 & -1.25 \\ 0.98 & -4.64 & -0.03 \end{bmatrix} \end{array} \begin{array}{c} \text{Wire \#3 Driven} \\ \begin{bmatrix} 1 & 1 & 1 \\ 0.91 & 5.32 & -1.00 \\ 1.00 & -7.40 & -0.70 \end{bmatrix} \end{array}$$



(a)



(b)



(c)

Figure 4. Voltage waveform at the load end: (a) wire 1 driven, (b) wire 2 driven, (c) wire 3 driven. Vertical scale is 0.2 V/div; horizontal scale is 5 ns/div.

The corresponding per unit-length inductance and capacitance matrices are:

(a) Wire #1 Driven

$$[L_{nm}] = \begin{bmatrix} 0.895 & 0.468 & 0.544 \\ 0.455 & 0.924 & 0.359 \\ 0.537 & 0.359 & 1.01 \end{bmatrix} \mu\text{H/m} \quad [C_{nm}] = \begin{bmatrix} 44.33 & -18.88 & -20.19 \\ -19.40 & 32.55 & -3.54 \\ -20.21 & -3.77 & 30.47 \end{bmatrix} \text{pF/m}$$

(b) Wire #2 Driven

$$[L_{nm}] = \begin{bmatrix} 0.893 & 0.467 & 0.539 \\ 0.456 & 0.927 & 0.359 \\ 0.542 & 0.360 & 1.00 \end{bmatrix} \mu\text{H/m} \quad [C_{nm}] = \begin{bmatrix} 44.21 & -18.89 & -20.28 \\ -19.46 & 32.67 & -3.50 \\ -19.94 & -3.85 & 30.41 \end{bmatrix} \text{pF/m}$$

(c) Wire #3 Driven

$$[L_{nm}] = \begin{bmatrix} 0.888 & 0.469 & 0.547 \\ 0.454 & 0.924 & 0.363 \\ 0.524 & 0.366 & 1.01 \end{bmatrix} \mu\text{H/m} \quad [C_{nm}] = \begin{bmatrix} 44.35 & -18.97 & -20.18 \\ -19.14 & 32.35 & -3.58 \\ -20.99 & -3.27 & 30.8 \end{bmatrix} \text{pF/m}$$

The elements of the inductance and capacitance matrices are seen to be in good agreement for each of the three driving conditions even though some elements of the modal matrices were inaccurately measured due to the low modal amplitudes of some modes. This consistency indicates that the transformations given by equations (33) and (34) are tolerant to errors in the modal matrix. Large errors in some elements of the modal matrix

have been observed to have only a small effect on the accuracy of [L] and [C]. The propagation of errors of this type is discussed further at the end of this section.

(2) Direct Measurements

Direct measurement of the characteristic admittance, modal currents, and modal velocities was also carried out on the three-wire line. This technique has an advantage over the indirect method in that fewer measurements are required and all data are recorded at the driven end of the cable with the load end open or short circuited.

The measurements were performed by driving each wire in turn with a voltage step and recording the voltage on the driven wire and the currents on all three wires. All wires but the driven wire were grounded at the input and the load end was open circuited. For this example it was possible to record the input and reflected pulses on the same oscilloscope trace. The recorded waveforms are shown in figure 5.

The pulse amplitudes, prior to arrival of the reflections were used in equation (18) to compute the characteristic admittance matrix. The modal current matrix was determined by measuring the modal amplitudes in the reflected pulse and correcting for the effects of the termination impedance. For this case the termination impedance was a 3×3 matrix with a single 25 ohm load on the diagonal element of the driven wire and zeros elsewhere. The set of modal velocities can be obtained from any one of the recordings by measuring the time delay between the input and reflected pulses. These line constants were then used in equation (33) to determine the inductance matrix, and in equation (35) to determine the capacitance matrix. The results are as follows:

$$[Z_c]_3(\text{ohms}) = \begin{bmatrix} 247 & 157 & 166 \\ 157 & 249 & 126 \\ 166 & 126 & 268 \end{bmatrix}$$

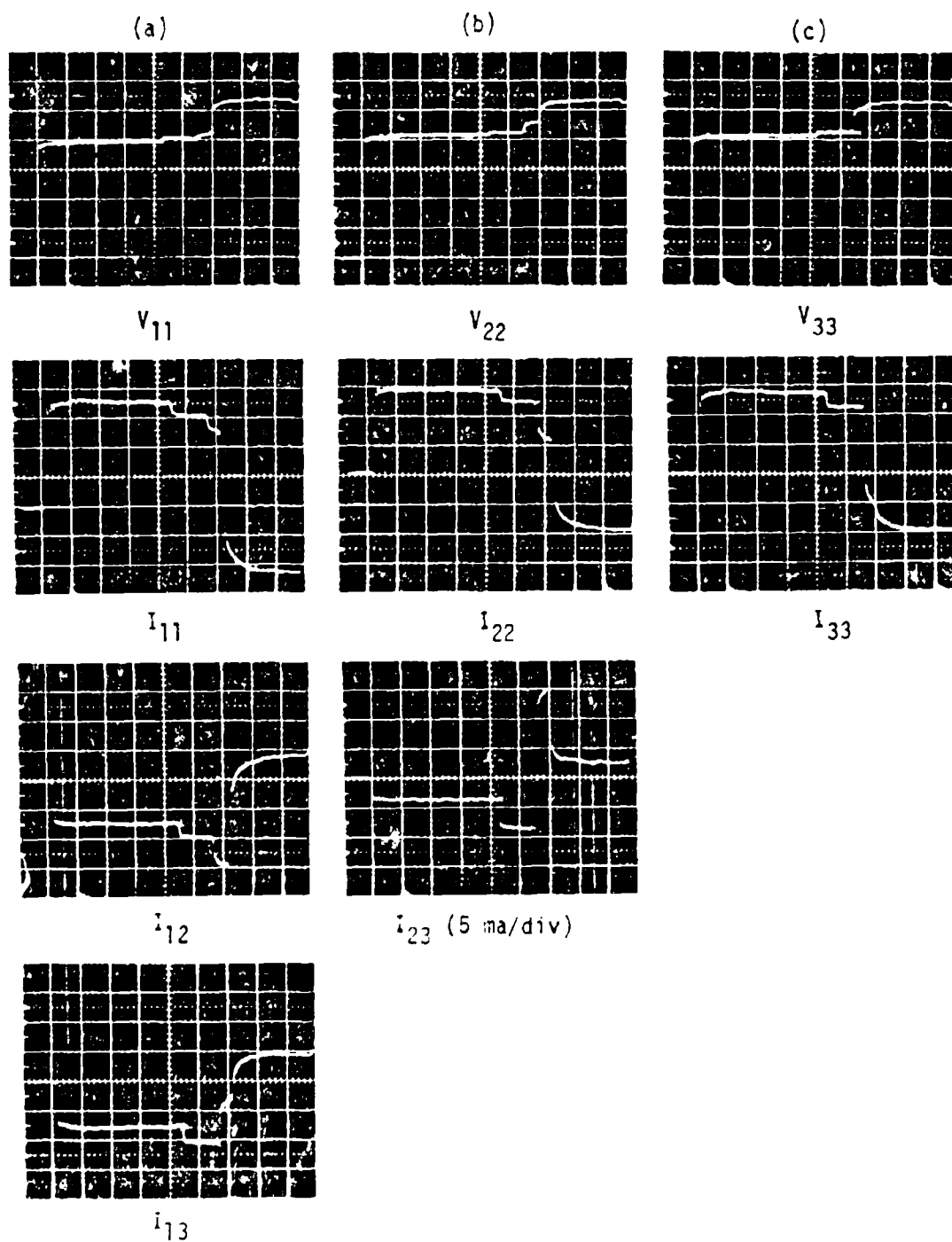


Figure 5. Voltage and current waveforms at the driven end; (a) wire #1 driven, (b) wire #2 driven, (c) wire #3 driven.
 Vertical Sens: 1 v/div or 10 ma/div unless otherwise noted.
 Horizontal Sens: 32.6 nanoseconds/div.

$$[v_{nm}]_3 (\text{m/sec}) = \begin{bmatrix} 2.85 & 0 & 0 \\ 0 & 2.24 & 0 \\ 0 & 0 & 2.04 \end{bmatrix} \times 10^8$$

$$[I_{nm}]_3 = \begin{bmatrix} 1 & 1 & 1 \\ 1.35 & 1.72 & -0.88 \\ 1.15 & -2.79 & -0.28 \end{bmatrix}$$

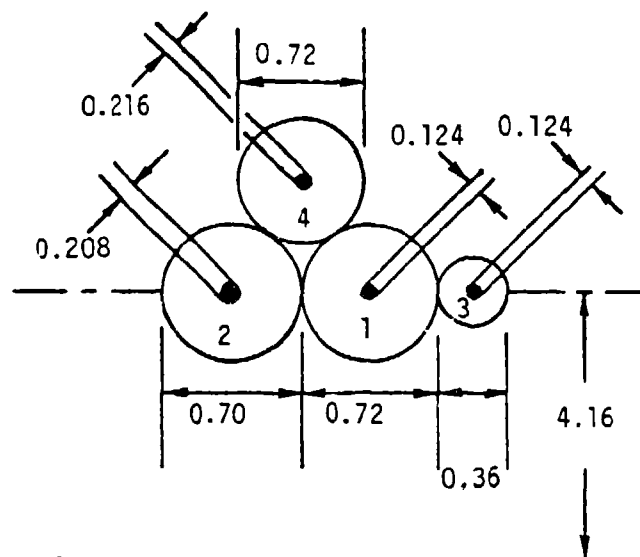
$$[L'_{nm}] = \begin{bmatrix} 0.93 & 0.53 & 0.57 \\ 0.49 & 0.98 & 0.40 \\ 0.55 & 0.40 & 1.04 \end{bmatrix} \times 10^{-6} \text{ H/m}$$

$$[C'_{nm}] = \begin{bmatrix} 43.0 & -19.4 & -18.7 \\ -20.6 & 32.4 & -3.87 \\ -19.2 & -4.0 & 29.6 \end{bmatrix} \times 10^{-12} \text{ F/m}$$

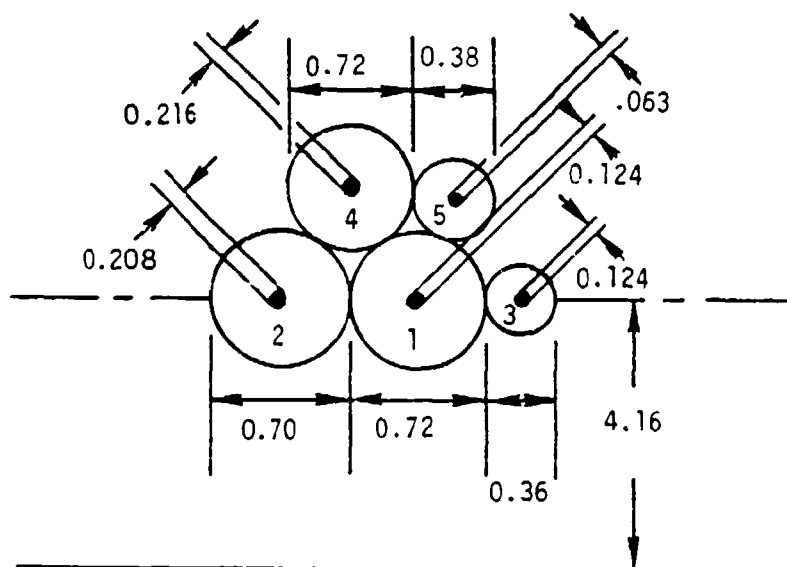
b. Four-Wire and Five-Wire Lines

To further investigate the applicability and limitations of the indirect time domain method, measurements were carried out on two other transmission line configurations. The first consisted of a 10 meter section of a four-wire cable constructed by adding a fourth wire insulated with cellular polyethylene to the three-wire cable geometry. The second was 20 meters in length and contained a fifth wire of semisolid polyethylene which was added to the four-wire geometry. The cable cross-sections are shown in figures 6a and 6b.

The methodology used to make the measurements and to perform the calculations was the same as that used for the three-wire cable. For the four-wire cable, measurements were made with each of the four wires driven in turn. To avoid duplication, measurements on the five-wire line were made by driving only one wire of the cable. For illustration, a



(a) Four-wire cable



(b) Five-wire cable

Figure 6. Cross sections of four-wire and five-wire cables (over a ground plane), dimensions in centimeters.

complete set of the voltage waveforms recorded at the load end of the cables with the input pulse applied to wire #1 is presented in figure 8 for these two configurations.

The input in each case was the short duration voltage pulse shown in figure 7. Pulse amplitudes of 21.8 and 4.1 volts were applied to wire 1 of the four-wire and five-wire lines, respectively.

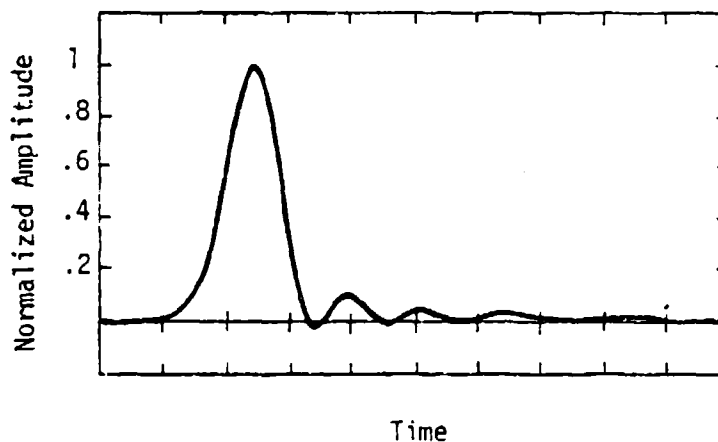


Figure 7. Four-wire and Five-wire line input voltage pulse
(Horizontal Sens: 2 ns/Div)

The pulse responses of figure 8 show the time resolved modal components arriving at the load to be consistent with nondegenerate propagation on multiconductor lines. Some interference is present due to line irregularities and the nonideal input pulse from the pulse generator; however, the resolution is adequate to allow identification of the N modal components present on each wire in nearly every case.

The line parameters determined experimentally for the four-wire and five-wire lines are as follows:

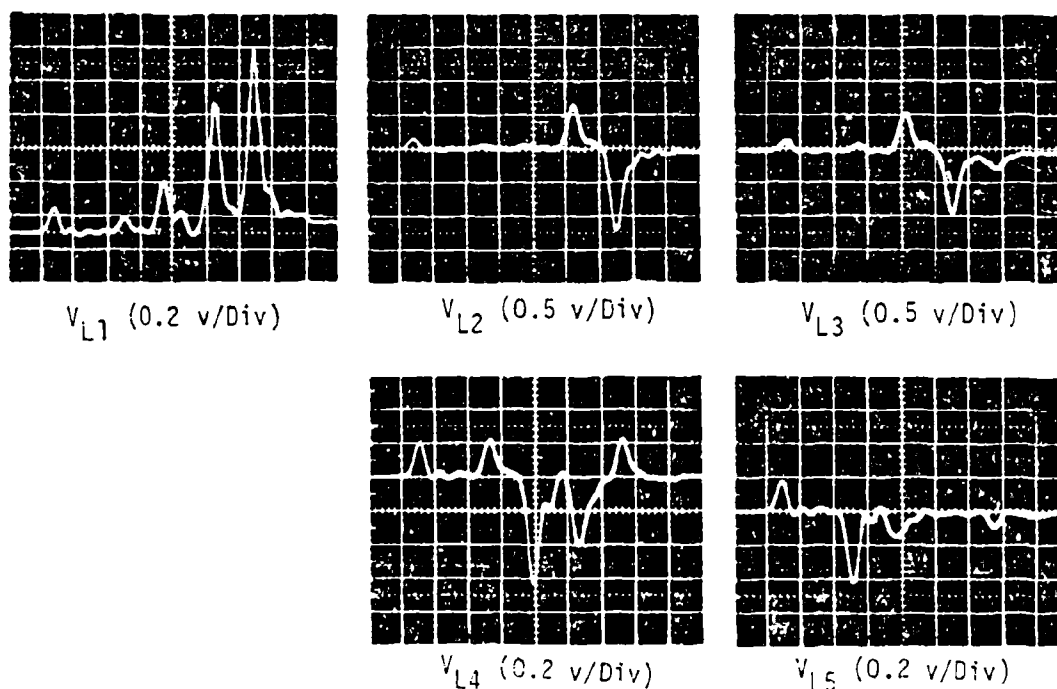
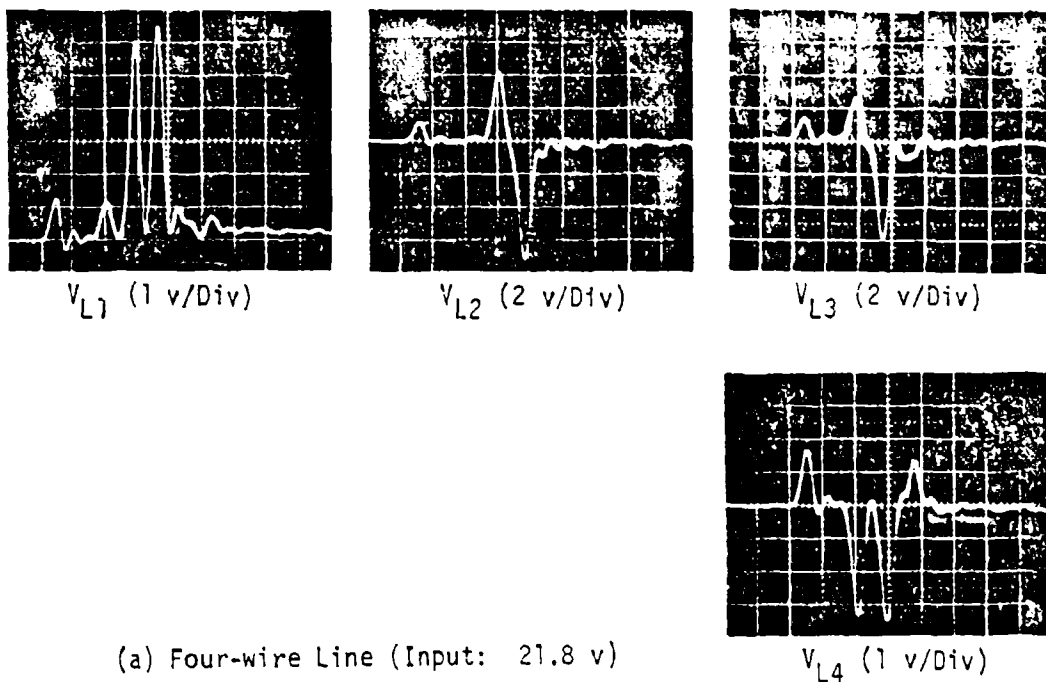


Figure 8. Voltage waveforms at load end of four- and five-wire lines (Horizontal Sens: 5 ns/Div).

Four-Wire Line

$$[Z_c]_4(\text{ohms}) = \begin{bmatrix} 252 & 176 & 189 & 173 \\ 176 & 259 & 155 & 175 \\ 189 & 155 & 275 & 160 \\ 173 & 175 & 160 & 258 \end{bmatrix}$$

$$[v_{nm}]_4(\text{m/sec}) = \begin{bmatrix} 2.86 & 0 & 0 & 0 \\ 0 & 2.36 & 0 & 0 \\ 0 & 0 & 2.15 & 0 \\ 0 & 0 & 0 & 1.99 \end{bmatrix} \times 10^8$$

$$[V_{nm}]_4 = \begin{bmatrix} 1 & 1 & 1 & 1 \\ 0.93 & 0.28 & 1.03 & -2.35 \\ 1.03 & 1.85 & -1.10 & -1.44 \\ 1.02 & -1.14 & -0.36 & 0.58 \end{bmatrix}$$

Five-Wire Line:

$$[z_c]_5(\text{ohms}) = \begin{bmatrix} 252 & 160 & 176 & 164 & 175 \\ 160 & 250 & 135 & 165 & 150 \\ 176 & 135 & 273 & 148 & 176 \\ 164 & 165 & 148 & 251 & 182 \\ 175 & 150 & 176 & 182 & 320 \end{bmatrix}$$

$$[v_{nm}]_5(\text{m/sec}) = \begin{bmatrix} 2.78 & 0 & 0 & 0 & 0 \\ & 2.44 & 0 & 0 & 0 \\ & & 2.26 & 0 & 0 \\ & & & 2.08 & 0 \\ & & & & 1.94 \end{bmatrix} \times 10^8$$

$$[V_{nm}]_5 = \begin{bmatrix} 1 & 1 & 1 & 1 & 1 \\ 0.93 & 1.02 & 0.18 & 1.22 & -1.98 \\ 0.97 & 1.25 & 1.77 & -1.31 & -0.38 \\ 1.02 & 2.09 & -1.12 & -0.27 & -0.12 \\ 1.10 & -6.36 & -0.17 & -0.09 & -0.34 \end{bmatrix}$$

c. Result Summary and Error Analysis

The multiconductor transmission line characteristics of the three-, four-, and five-wire lines were also determined from swept frequency measurements using the technique described in the appendix. These results are compared in tables 1, 2, and 3 with those obtained from time domain measurements. The frequency domain results were derived from averages of several independent measurements of the short circuit impedance and open circuit admittance matrices in the 0.1 to 2 MHz frequency range. The parameters obtained from the indirect time domain method are average values for the different driving conditions used.

Comparison of the frequency domain and indirect time domain results for the three-wire line shows agreement to within 5 percent for the inductance matrix elements, 10 percent for the capacitance matrix elements, and 7 percent for the characteristic impedance elements. The set of parameters obtained from a single application of the direct method is also in good agreement with those from the indirect method, with a maximum difference of approximately 10 percent in the elements of L , C , or Z_C .

Similar comparisons between the frequency and time domain methods can be made for the four- and five-wire parameters listed in tables 2 and 3. However, in these cases the agreement is not as good, with differences of up to 30 percent observed in some elements. To isolate the source of this difference, an error propagation analysis was performed. The goal of this analysis was to determine how errors in the measurement of the voltage eigenvectors and the TDR reflection coefficients modify the calculated values of $[L]$, $[C]$, and $[Z_C]$.

To determine the effects of an inaccurate measurement of the voltage eigenvector matrix upon the calculated inductance and capacitance matrices, various elements in the measured matrix were perturbed and then the $[L]$ and $[C]$ matrices were calculated. A number of cases were considered. In two cases a small valued element was replaced with zero in order to determine

Table 1. COMPARISON OF THREE-WIRE LINE PARAMETERS FROM FREQUENCY DOMAIN AND TIME DOMAIN MEASUREMENTS

Parameter	Frequency Domain	Time Domain (Indirect)	Time Domain (Direct)
$[L_{nm}](\mu H/m)$	$\begin{bmatrix} 0.884 & 0.484 & 0.535 \\ 0.484 & 0.940 & 0.379 \\ 0.535 & 0.379 & 0.992 \end{bmatrix}$	$\begin{bmatrix} 0.892 & 0.461 & 0.538 \\ 0.461 & 0.925 & 0.365 \\ 0.538 & 0.365 & 1.006 \end{bmatrix}$	$\begin{bmatrix} 0.93 & 0.51 & 0.56 \\ 0.51 & 0.98 & 0.40 \\ 0.56 & 0.40 & 1.04 \end{bmatrix}$
$[C_{nm}](pF/m)$	$\begin{bmatrix} 46.48 & -20.91 & -20.55 \\ -20.91 & 33.83 & -4.15 \\ -20.55 & -4.15 & 31.0 \end{bmatrix}$	$\begin{bmatrix} 44.30 & -19.12 & -20.30 \\ -19.12 & 32.52 & -3.58 \\ -20.30 & -3.58 & 30.56 \end{bmatrix}$	$\begin{bmatrix} 43.0 & -20.0 & -19.0 \\ -20.0 & 32.4 & -3.9 \\ -19.0 & -3.9 & 29.6 \end{bmatrix}$
$[Z_{c_{nm}}](\Omega)$	$\begin{bmatrix} 232.4 & 148.4 & 159.8 \\ 148.4 & 237.9 & 121.3 \\ 159.8 & 121.3 & 258.3 \end{bmatrix}$	$\begin{bmatrix} 231.4 & 139.2 & 157.2 \\ 139.2 & 230.6 & 112.5 \\ 157.2 & 112.5 & 257.6 \end{bmatrix}$	$\begin{bmatrix} 247 & 157 & 166 \\ 157 & 249 & 126 \\ 166 & 126 & 268 \end{bmatrix}$
$v_1(m/s)$	2.829×10^8	2.772×10^8	2.85×10^8
$v_2(m/s)$	2.178×10^8	2.187×10^8	2.24×10^8
$v_3(m/s)$	2.009×10^8	2.028×10^8	2.04×10^8

Table 2. COMPARISON OF FOUR-WIRE LINE PARAMETERS FROM
FREQUENCY DOMAIN AND TIME DOMAIN MEASUREMENTS

Parameter	Frequency Domain				Time Domain			
$[L_{nm}](\mu\text{H/m})$	$\begin{bmatrix} 0.840 & 0.490 & 0.561 & 0.493 \\ 0.490 & 0.938 & 0.396 & 0.489 \\ 0.561 & 0.396 & 0.974 & 0.432 \\ 0.493 & 0.439 & 0.432 & 0.855 \end{bmatrix}$	$\begin{bmatrix} 0.949 & 0.598 & 0.642 & 0.582 \\ 0.598 & 1.033 & 0.514 & 0.591 \\ 0.642 & 0.514 & 1.031 & 0.529 \\ 0.582 & 0.591 & 0.529 & 0.937 \end{bmatrix}$						
$[C_{nm}](\text{pF/m})$	$\begin{bmatrix} 57.26 & -18.75 & -22.75 & -11.59 \\ -18.75 & 43.79 & -2.33 & -15.82 \\ -22.75 & -2.33 & 34.99 & -4.77 \\ -11.59 & -15.82 & -4.77 & 37.87 \end{bmatrix}$	$\begin{bmatrix} 54.89 & -18.03 & -22.27 & -11.30 \\ -18.03 & 43.49 & -3.00 & -16.46 \\ -22.27 & -3.00 & 35.65 & -5.81 \\ -11.30 & -16.46 & -5.81 & 37.84 \end{bmatrix}$						
$[Z_{c_{nm}}](\Omega)$	$\begin{bmatrix} 218.7 & 144.9 & 161.1 & 142.4 \\ 144.9 & 229.7 & 122.7 & 143.8 \\ 161.1 & 122.7 & 252.2 & 128.4 \\ 142.4 & 143.8 & 128.4 & 227.8 \end{bmatrix}$	$\begin{bmatrix} 251.8 & 176.1 & 188.9 & 172.9 \\ 176.1 & 259.3 & 154.8 & 175.4 \\ 188.9 & 154.8 & 274.8 & 159.9 \\ 172.9 & 175.4 & 159.9 & 257.8 \end{bmatrix}$						
$v_1(\text{m/s})$	2.807×10^8	2.865×10^8						
$v_2(\text{m/s})$	2.338×10^8	2.357×10^8						
$v_3(\text{m/s})$	2.147×10^8	2.151×10^8						
$v_4(\text{m/s})$	1.954×10^8	1.986×10^8						

Table 3. COMPARISON OF FIVE-WIRE LINE PARAMETERS FROM
FREQUENCY DOMAIN AND TIME DOMAIN MEASUREMENTS

	Frequency Domain					Time Domain				
$[L_{nm}](\mu H/m)$	0.902	0.478	0.540	0.485	0.513	0.984	0.552	0.614	0.562	0.609
	0.478	0.951	0.384	0.486	0.424	0.552	1.024	0.457	0.579	0.522
	0.540	0.384	1.007	0.425	0.534	0.614	0.457	1.084	0.506	0.624
	0.485	0.486	0.425	0.851	0.557	0.562	0.579	0.506	0.942	0.641
	0.513	0.424	0.534	0.557	1.116	0.609	0.522	0.624	0.641	1.200
$[C_{nm}](pF/m)$	52.56	-16.13	-17.76	-8.90	-5.63	50.08	-14.64	-17.20	-9.13	-6.53
	-16.13	42.15	-2.32	-15.36	-1.43	-14.64	41.34	-1.78	-15.77	-1.70
	-17.76	-2.32	35.78	-3.15	-6.84	-17.20	-1.78	34.72	-3.67	-6.82
	-8.90	-15.36	-3.15	41.77	-9.71	-9.13	-15.77	-3.67	41.88	-9.75
	-5.63	-1.43	-6.84	-9.71	25.36	-6.53	-1.70	-6.82	-9.75	26.05
$[Z_{c_{nm}}](\Omega)$	223.1	139.0	150.9	138.3	145.4	251.7	159.7	175.5	164.1	175.3
	139.0	229.2	115.6	141.0	125.5	159.7	249.7	134.6	164.6	150.3
	150.9	115.6	248.0	123.8	149.1	175.5	134.6	272.7	148.5	175.5
	138.3	141.0	123.8	225.1	155.6	164.1	164.6	148.5	251.3	181.7
	145.4	125.5	149.1	155.6	295.4	175.3	150.3	175.5	181.7	320.5
$v(m/s)$	2.762 $\times 10^8$					2.784 $\times 10^8$				
	2.465 $\times 10^8$					2.445 $\times 10^8$				
	2.260 $\times 10^8$					2.256 $\times 10^8$				
	2.071 $\times 10^8$					2.082 $\times 10^8$				
	1.917 $\times 10^8$					1.944 $\times 10^8$				

the sensitivity of the calculated matrices to low amplitudes and inaccurately measured modal amplitudes. In other calculations single elements were perturbed by amounts ranging from 8 to 17 percent, and as a final check five elements were perturbed before the calculations were made.

The conclusions drawn from this study are that calculation of the $[L]$ and $[C]$ matrices is stable with respect to errors in the measured values of the voltage eigenvectors. Typically a perturbation of 10 percent in a single element of a voltage eigenvector resulted in a difference of less than 1 percent in the calculated values of the elements of the $[L]$ and $[C]$ matrices.

The accuracy with which the indirect time domain method can be applied to measure $[Z_0]$ is limited by the accuracy of the reflection coefficients which are measured from the TDR records. These are limited by noise and line irregularities to about ± 5 percent. To observe the effects of a 5 percent change in the measured value of the reflection coefficient upon the calculated value of the characteristic impedance matrix, one of the measured values of the reflection coefficient was increased by 5 percent. The corresponding change in the impedance matrix was found to be approximately the same with increases of from 3 to 8 percent observed in individual elements.

The elements of the impedance matrices of the four- and five-wire lines which were determined using the indirect time domain method were found to be consistently larger by as much as 20 percent when compared with frequency domain measurements. To observe the effect of these larger values on the calculated $[L]$ and $[C]$ matrices, the calculations were repeated using the $[Z_c]$ determined from frequency domain techniques. For the four-wire line this resulted in a maximum difference of 3.3 percent in an element of the $[L]$ matrix and 7.6 percent in an element of the $[C]$ matrix when compared to frequency domain results. For the five-wire line these maximum differences were found to be -3.1% and -9.4% for the $[L]$ and $[C]$ matrices, respectively.

Based on the preceding analysis, it is concluded that the difference in the characteristic impedance matrix determined from time domain and frequency domain measurements is largely responsible for the discrepancy between the values of the $[L]$ and $[C]$ matrices. It appears that the limiting factor in these applications is the accuracy with which the characteristic impedance matrix can be measured.

SECTION IV

PULSE PROPAGATION ON BRANCHED MULTICONDUCTORS FORMED BY UNIFORM LINE SEGMENTS

1. BACKGROUND

Multiconductor cable runs are often characterized by abrupt changes in impedance at various points along the cable, as might be caused by the branching of some wires away from the main bundle or changes in the cable cross section or ground plane distances. Cables of this type can sometimes be modeled as uniform line segments with constant transmission line properties over the length of each segment. The analysis can be carried out in a manner similar to that for a two-conductor transmission line except that the characteristic impedance of each N -wire segment is an $N \times N$ matrix and the voltages and currents are N -dimensional vectors.

Multiconductors may support nondegenerate or partially degenerate propagation modes. For these cases the voltages and currents are represented as sums of eigenmodes of the line as given by equations (21) and (22). Separate N -dimensional voltage and current vectors then exist for each mode of propagation. Multimode analysis is further complicated by mode conversion at a discontinuity. For example, when a discontinuity exists between a segment which supports p modes and a second segment which supports q modes, each mode of the first segment will excite q modes in the second. A total of $p \times q$ modes will then propagate on the second segment, each with a distinct modal velocity. The resultant signal at the load end of a segmented multiconductor is then a superposition of all modal components present.

The analysis of branched multiconductors or multiconductors which can be represented by uniform line segments can be performed either by (1) computing the reflection and transmission matrices at each discontinuity or by (2) computing the scattering matrix at the junction of uniform line

segments. The first method is a step-by-step procedure which is analogous to methods used to analyze a two-conductor line and is simple to apply. The second is a more general formulation which is well suited to computer calculations. Both methods lead to identical results.

2. ANALYSIS USING THE REFLECTION AND TRANSMISSION MATRICES

a. Methodology

For a multiconductor line which is composed of uniform segments the transmitted and reflected signal components at a discontinuity are determined in the same manner as for a two-conductor line. At each discontinuity the voltage and current vectors are represented as sums of the incident and reflected signals by the equations

$$[V_n]^t = [V_n]^i + [V_n]^r \quad (36)$$

$$[I_n]^t = [I_n]^i + [I_n]^r \quad (37)$$

The currents and voltages are related by the characteristic impedance of the adjacent segments by

$$[V_n]^i = [Z_c][I_n]^i \quad [V_n]^r = -[Z_c][I_n]^r \quad [V_n]^t = [Z_L][I_n]^t \quad (38)$$

The super scripts i, r, and t in the above equations refer to the incident, reflected, and transmitted signal components. $[Z_c]$ and $[Z_L]$ are the characteristic impedance matrices at the discontinuity on the source and load sides, respectively. The transmission matrix which relates the incident and transmitted signal components is obtained by eliminating the reflected signals in equations (36) and (37) and solving for the transmitted voltage or current. This gives the equation

$$[V_n]^t = [\tau_V][V_n]^i \quad (39)$$

where

$$[\tau_v] = 2[Z_L]([Z_L] + [Z_c])^{-1} \quad (40)$$

and

$$[I_n]^t = [\tau_I][I_n]^i \quad (41)$$

where

$$[\tau_I] = 2([Z_L] + [Z_c])^{-1} [Z_c] \quad (42)$$

The corresponding reflection matrices are obtained by substituting these results back into equations (36) and (37) and solving for the reflected components. This gives

$$[V_n]^r = [\rho_v][V_n]^i \quad (43)$$

where

$$[\rho_v] = ([Z_L] - [Z_c])([Z_L] + [Z_c])^{-1} \quad (44)$$

and

$$[I_n]^r = [\rho_I][I_n]^i \quad (45)$$

where

$$[\rho_I] = ([Z_L] + [Z_c])^{-1} ([Z_L] - [Z_c]) \quad (46)$$

These relationships are seen to be nearly the same as for a two-conductor line. The only difference is that the order of multiplication of the factors which define the current transmission and reflection matrices is transposed.

The analysis of a branched multiconductor proceeds by computing the reflection and transmission matrices at each discontinuity. The transmitted voltage or current vectors at a discontinuity become the incident vectors at the next discontinuity and so on down the line. When multi-mode propagation exists, each incident pulse is a superposition of time delayed modes and each must be treated independently.

The method described was used to analyze the branched multiconductor above a ground plane shown in figure 9. Several cases were studied by (1) driving a single wire of each segment with a pulse generator and measuring the voltages at each load and (2) driving each segment with the wires connected in parallel at the input (common mode) and measuring the individual wire currents in short circuit terminations. Examples of the analytical procedure followed for each of the above cases are included.

b. Examples

Case 1. Prediction of pin voltages at 50-ohm terminations on the three- and five-wire segments. Wire #4 of the two-wire segment was driven with a voltage step from 50-ohm pulse generator. Wire #5 was terminated in 50 ohms at the source end.

The characteristic impedance matrices required in equations (40) and (44) to compute the transmission and reflection matrices at the junction are

$$Z_c = \begin{bmatrix} [Z_{ij}]_3 & 0 \\ 0 & [Z_{ij}]_2 \end{bmatrix} \quad (47)$$

and

$$Z_L = [Z_{ij}]_5 \quad (48)$$

where $[Z_{ij}]_{2,3,5}$ are the characteristic impedance matrices of the two-, three-, and five-wire segments of the branched multiconductor. The off-diagonal terms of the partitioned matrix of equation (47) are zero because the two-wire and three-wire line segments are branched at right angles and no cross coupling exists between segments.

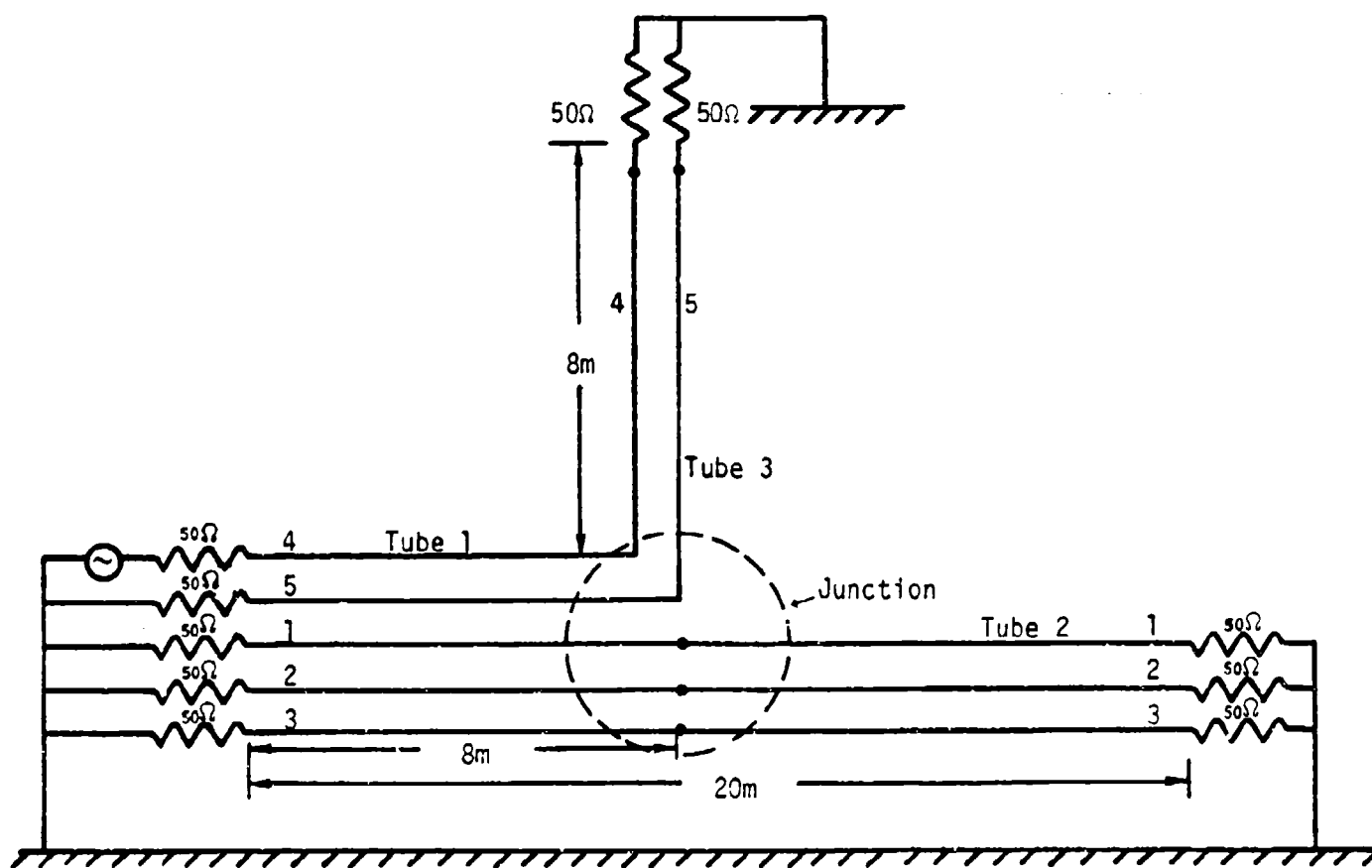


Figure 9. A Multiconductor Transmission Line With a Branch

The voltage waveforms incident on the junction are determined by first computing the input voltage on each wire at the source. For the two-wire segment with wire #4 driven, the input voltages are given by

$$\begin{bmatrix} V_4 \\ V_5 \end{bmatrix}_s = 2[Z_{ij}]_2([Z_{ij}]_s + [Z_{ij}]_2)^{-1} \times \begin{bmatrix} 1 \\ 0 \end{bmatrix} \times V_g \quad (49)$$

where V_g is the generator voltage and $[Z_{ij}]_s$ is the source impedance

$$[Z_{ij}]_s = \begin{bmatrix} 50 & 0 \\ 0 & 50 \end{bmatrix} \quad (50)$$

The two modes of propagation in the forward direction are determined by expanding the line voltages at the source in terms of the eigenvectors of the line. This amounts to determining the constants A and B at $z = 0$ in the simultaneous equations

$$\begin{bmatrix} V_4 \\ V_5 \end{bmatrix}_s = [V_{nm}]_2 \begin{bmatrix} A U(t - z/v_A) \\ B U(t - z/v_B) \end{bmatrix} \quad z = 0 \quad (51)$$

The coefficients $[V_{nm}]_2$ are elements of the modal matrix of the two-wire segment, defined by placing each eigenvector of the line in a column of the modal matrix. The velocities v_A and v_B are the corresponding modal velocities of the line.

The voltages incident on the junction are given by equation (51) evaluated at $z = z_j$. The incident vectors for modes A and B are then

$$\begin{bmatrix} V_1 \\ V_2 \\ V_3 \\ V_4 \\ V_5 \end{bmatrix}_A^i = \begin{bmatrix} 0 \\ 0 \\ 0 \\ A V_{11} \\ A V_{21} \end{bmatrix} \times U(t-T_A); \quad \begin{bmatrix} V_1 \\ V_2 \\ V_3 \\ V_4 \\ V_5 \end{bmatrix}_B^i = \begin{bmatrix} 0 \\ 0 \\ 0 \\ B V_{12} \\ B V_{22} \end{bmatrix} \times U(t-T_B) \quad (52)$$

where $T_A = \ell_3/v_A$, $T_B = \ell_3/v_B$ are the arrival times of modes A and B at the junction.

Each incident mode $[V_n]_{A,B}^i$ given by equation (52) is treated independently in equations (39) and (43) to compute the transmitted and reflected pulses.* The transmitted voltages on wires 1 through 5 for each mode are then expanded in terms of the modal matrix $[V_{nm}]_5$ of the five-wire segment and the reflected voltages on wires 1 through 3 are expanded in terms of the modal matrix $[V_{nm}]_3$ of the three-wire segment following the same procedure as used to define the modes of propagation on the two-wire segment. The signal incident at the load end of the three-wire segment is the superposition of six terms given by the sum

$$[V_n]_A + [V_n]_B \quad n = 1, 2, 3 \quad (53)$$

where

$$V_{1A} = C_{1A}V_{11}U(t-T_{1A}) + C_{2A}V_{12}U(t-T_{2A}) + C_{3A}V_{13}U(t-T_{3A}) \quad (54)$$

$$V_{2A} = C_{1A}V_{21}U(t-T_{1A}) + \dots\dots\dots$$

$$V_{3A} = C_{1A}C_{31}U(t-T_{1A}) + \dots\dots\dots$$

*The transmitted and reflected pulses are identical on wires 1, 2, and 3 for this case because there is no incident pulse on these wires.

$$V_{1B} = C_{1B}V_{11}U(t-T_{1B}) + C_{2B}V_{12}U(t-T_{2B}) + C_{3B}V_{13}U(t-T_{3B}) \quad (55)$$

$$V_{2B} = C_{1B}V_{21}U(t-T_{1B}) + \dots\dots\dots$$

$$V_{3B} = C_{1B}V_{31}U(t-T_{1B}) + \dots\dots\dots$$

The arrival times of the six modes at the load are

$$T_{1A} = T_A + \ell_2/v_1 \quad T_{1B} = T_B + \ell_2/v_1 \quad (56)$$

$$T_{2A} = T_A + \ell_2/v_2 \quad T_{2B} = T_B + \ell_2/v_2$$

$$T_{3A} = T_A + \ell_2/v_3 \quad T_{3B} = T_B + \ell_2/v_3$$

where v_1 , v_2 , and v_3 are the modal velocities on the three-wire segment.

The load voltages (transmitted voltages) on each wire are computed from equation (15) with $Z_c = [Z_{ij}]_3$ and where Z_L is a 3×3 diagonal matrix with 50 ohm loads for elements. The calculation is performed for each of the six modal components given by equations (53) and (55).

The same procedure is applied to the five-wire segment with the transmitted junction voltages expanded in terms of the modal matrix $[V_{nm}]_5$ of the five-wire line. Since each of the incident modes A and B generate five new modes, the voltage incident at the load end of the five-wire segment is the superposition of 10 modal components given by the sum

$$[V_n]_A + [V_n]_B \quad n = 1, 2, 3, 4, 5 \quad (57)$$

where

$$\begin{aligned} V_{1A} &= D_{1A} V_{11} U(t-\tau_{1A}) + D_{2A} V_{12} U(t-\tau_{2A}) + \dots + D_{5A} V_{15} U(t-\tau_{5A}) \\ &\vdots \\ V_{5A} &= D_{1A} V_{51} U(t-\tau_{1A}) + \dots \end{aligned} \quad (58)$$

$$\begin{aligned} V_{1B} &= D_{1B} V_{11} U(t-\tau_{1B}) + \dots \\ &\vdots \\ V_{5B} &= D_{5B} V_{51} U(t-\tau_{5B}) + \dots \end{aligned} \quad (59)$$

the arrival times at the load end of the five-wire segment are

$$\begin{aligned} \tau_{1A} &= T_A + \ell_1/v_1 & \tau_{1B} &= T_B + \ell_1/v_1 \\ &\vdots & &\vdots \\ \tau_{5A} &= T_A + \ell_1/v_5 & \tau_{5B} &= T_B + \ell_1/v_5 \end{aligned} \quad (60)$$

The load voltages are calculated for each modal component in the same manner as for the three-wire segment.

Case 2. Prediction of individual wire currents at short circuit terminations on the two- and five-wire segments when the wires of tube 3 are driven in parallel (common mode) with a voltage step from a 50-ohm pulse generator.

For this case the potential of each wire of the three-wire segment is the same and the total input current is known. The individual wire currents at the source are

$$\begin{bmatrix} I_1 \\ I_2 \\ I_3 \end{bmatrix} = [Y_{ij}]_3 \begin{bmatrix} 1 \\ 1 \\ 1 \end{bmatrix} \times V_g \quad (61)$$

where the $[Y_{ij}]_3$ matrix is the characteristic admittance of the three-wire segment $[Y_{ij}]_3 = [Z_{ij}]_3^{-1}$. Since the total current is just the sum of the individual wire currents, the ratio of the current on each wire to the total current is the sum of the admittance elements in each row divided by the sum of the elements of the matrix. The latter is also equal to the bulk characteristic admittance of the line.

The analysis from this point is the same as that given in case 1 for the voltages, except eigenvectors of current are used in the modal expansions rather than eigenvectors of voltage. The current and voltage eigenvectors are related by the equation

$$[I_{nm}] = [Y_{nm}][V_{mn}] \quad (62)$$

where $[Y_{nm}]$ is the characteristic admittance of the line segment. The transmission and reflection matrices for current are given by equations (42) and (46). No mode conversion occurs at the short circuit terminations of the two- and five-wire segments. The reflection coefficient is +1 for all modes in this case and the individual wire currents for each incident mode are doubled in amplitude.

3. ANALYSIS USING THE SCATTERING MATRIX OF THE JUNCTION

For distributed circuits, the reflected and incident waves at a junction can be related by a scattering matrix (ref. 20). The procedures for evaluating the scattering matrix for transmission line junctions are discussed in detail in reference 5. In this section these procedures will be described briefly and the scattering matrix for a branched multiconductor line will be evaluated.

For the junction shown in figure 9, the incident and reflected voltages for a lossless case are related by the following relation

$$\begin{bmatrix} [V_n^{(re)}]_1 \\ [V_n^{(re)}]_2 \\ [V_n^{(re)}]_3 \end{bmatrix} = [S_{nm}] \begin{bmatrix} [V_n^{(i)}]_1 \\ [V_n^{(i)}]_2 \\ [V_n^{(i)}]_3 \end{bmatrix} \quad (63)$$

where $[V_n^{(re)}]_i$, $i = 1, 2, 3$ are the reflected voltage vectors for the various tubes meeting at the junction and $[V_n^{(i)}]_i$, $i = 1, 2, 3$ are the incident voltage vectors for the various tubes meeting at the junction. The size of the vectors $[V_n^{(re)}]_i$ and $[V_n^{(i)}]_i$ is equal to the number of the conductors in the tube. The components of these vectors represent the voltages on the individual conductors. $[S_{nm}]$, in equation (63), is the scattering matrix of the junction which is considered lossless. For the junction shown in figure 9, the scattering matrix is of 10×10 size.

At the junction where there are several tubes interconnected to one another, the Kirchhoff's current and voltage laws have to be enforced in order to evaluate the scattering matrix of the junction.

Kirchhoff's current law states that the sum of the current flowing into a node is zero. For the case where n_1 -th wire of tube 1 is connected to the n_2 -th wire of tube 2 and to the n_k -th wire of tube k, etc., then

$$(I_{n1})_1 + (I_{n2})_2 + \dots + (I_{nk})_k = 0 \quad (64)$$

where the subscripts on the parentheses denote the tube number and the subscripts and I denote the wire number in the tube. Equation (64) can be put into matrix form, i.e.,

$$\begin{array}{c} \text{Tube 1} \quad \text{Tube 2} \quad \dots \quad \text{Tube k} \\ [0 \ 0 \ \dots \ 1 \ \dots 0 \ 0 \ 0 \ \dots \ 1 \ \dots 0 \ \dots \ 0 \ 0 \ \dots \ 1 \ \dots] \end{array} \begin{bmatrix} [I_n]_1 \\ [I_n]_2 \\ \vdots \\ [I_n]_k \end{bmatrix} = [0] \quad (65)$$

In equation (65) all elements in the left matrix are zero unless they correspond to the conductors which are connected at the node. For N_c connections within the junction, there are N_c equations similar to equation (65), and we can define the junction connection matrix $[C_{I_{nm}}]$ so that

$$[C_{I_{nm}}] \begin{bmatrix} [I_n]_1 \\ [I_n]_2 \\ \vdots \\ [I_n]_k \end{bmatrix} = [0_n] \quad (66)$$

where $[C_{I_{nm}}]$ is a $N_c \times M_j$ matrix, and M_j is the total number of conductors connected to junction.

Kirchhoff's voltage law, for the case of simple connections, requires all voltages associated with each conductor to be the same at the same node. Thus, for the above example, we have

$$\begin{aligned} (V_{n1})_1 - (V_{n2})_2 &= 0 \\ (V_{n2})_2 - \dots &= 0 \\ &\dots\dots\dots \\ \dots\dots - (V_{nk})_k &= 0 \end{aligned} \quad (67)$$

For a consistent set of connections, there are $M_j - N_c$ equations. The above equation can be easily written in matrix form. Let us denote the corresponding matrix as $[C_{V_{nm}}]$ such that

$$[C_{V_{nm}}] \begin{bmatrix} [V_n]_1 \\ [V_n]_2 \\ \vdots \\ [V_n]_k \end{bmatrix} = [0_n] \quad (68)$$

where $[C_{V_{nm}}]$ is a $(M_j - N_c) \times M_j$ matrix.

At the junction the total current and voltage is the sum of the two components, i.e., the incident and reflected components (ref. 20),

$$[V_n] = [V_n^{(i)}] + [V_n^{(re)}] \quad (69)$$

$$[I_n] = [I_n^{(i)}] - [I_n^{(re)}] \quad (70)$$

Using equations (66), (68), (69) and (70) the relation between the reflected and incident voltage components at the junction can be written as

$$\begin{bmatrix} [V_n^{(re)}]_1 \\ [V_n^{(re)}]_2 \\ \vdots \\ [V_n^{(re)}]_k \end{bmatrix} = \begin{bmatrix} [-C_{V_{nm}}] \\ [C_{I_{nm}}][Y_{c_{nm}}] \end{bmatrix}^{-1} \begin{bmatrix} [C_{V_{nm}}] \\ [C_{I_{nm}}][Y_{c_{nm}}] \end{bmatrix} \begin{bmatrix} [V_n^{(i)}]_1 \\ [V_n^{(i)}]_2 \\ \vdots \\ [V_n^{(i)}]_k \end{bmatrix} \quad (71)$$

From equation (71) the voltage scattering matrix is

$$[S_{nm}] = \begin{bmatrix} [-C_{V_{nm}}] \\ [C_{I_{nm}}][Y_{c_{nm}}] \end{bmatrix}^{-1} \begin{bmatrix} [C_{V_{nm}}] \\ [C_{I_{nm}}][Y_{c_{nm}}] \end{bmatrix} \quad (72)$$

where $[Y_{c_{nm}}]$ is the characteristic admittance matrix of the junction. $[Y_{c_{nm}}]$ can be obtained from the characteristic impedance matrix $[Z_{c_{nm}}]$. The matrix $[Z_{c_{nm}}]$ contains all the matrices of all branches involved at the junction and for the junction shown in figure 9 it can be expressed as

$$[Z_{c_{nm}}] = \begin{bmatrix} [Z_{c_{nm}}]_1 & [0_{nm}] & [0_{nm}] \\ [0_{nm}] & [Z_{c_{nm}}]_2 & [0_{nm}] \\ [0_{nm}] & [0_{nm}] & [Z_{c_{nm}}]_3 \end{bmatrix} \quad (73)$$

The characteristic impedance matrix $[Z_{c_{nm}}]$ can be obtained by methods described in section III.

The voltage modal amplitudes incident at the junction are computed using the method described in section II. From equation (63) the voltage amplitudes reflected in different branches at the junction are obtained. The method of analysis described in section II is used to compute the voltage waves arriving at the loads in different branches using the reflected wave in the branch at the junction as excitations.

As mentioned earlier, multiple modes are excited on a multi-conductor transmission line in inhomogeneous media. Each mode reflected from the junction or the load excites again multiple modes in the branch. Thus, using the analysis described in this paper all the modes excited at different times can be calculated and by following the step-by-step

procedure, the response of the line in the time domain can be obtained. It should be noted that when multiple reflections from the junction and the loads are considered, the number of modes traveling on the line becomes large. In some cases, some of the weaker modes having small amplitudes can be neglected for multiple reflections.

4. EXPERIMENTAL RESULTS

To substantiate the theory, a five-wire cable (over a ground plane) with a two-wire branch was constructed and tested. Wires insulated with solid polyethylene, neoprene, rubber, foam polyethylene and semisolid polyethylene were used for the cable construction. The configuration is shown in figure 9. The cable was supported with Styrofoam blocks above an aluminum ground plane. The cross-sectional configuration of the five-wire line is shown in figure 10. The wires 4 and 5 branch out at a 90 degree angle at 8 meters distance and the wires 1, 2 and 3 continue with the same cross-sectional configuration. The radii of the conductors, r , and the distance between the centers of the wires, d_{ij} are as follows:

$r_1 = 0.108$ cm	$d_{12} = 0.70$ cm	$d_{24} = 0.68$ cm
$r_2 = 0.062$ cm	$d_{13} = 0.54$ cm	$d_{25} = 1.02$ cm
$r_3 = 0.062$ cm	$d_{14} = 0.69$ cm	$d_{34} = 0.93$ cm
$r_4 = 0.111$ cm	$d_{15} = 0.60$ cm	$d_{35} = 0.49$ cm
$r_5 = 0.0125$ cm	$d_{23} = 1.16$ cm	$d_{45} = 0.59$ cm

The transmission line characteristics of each segment were determined from previous measurements. The three- and five-wire characteristic impedance matrices, modal velocities, and modal matrices are given in tables 1 and 3 of section III. The two wire segment was found to have the following characteristics:

$$[Z_{ij}]_2 = \begin{bmatrix} 228 & 157 \\ 157 & 303 \end{bmatrix} \text{ ohms}$$

$$[V_{nm}]_2 = \begin{bmatrix} 1 & 1 \\ 1 & -1 \end{bmatrix}$$

$$v_1 = 2.895 \times 10^8 \text{ m/s}$$

$$v_2 = 2.538 \times 10^8 \text{ m/s}$$

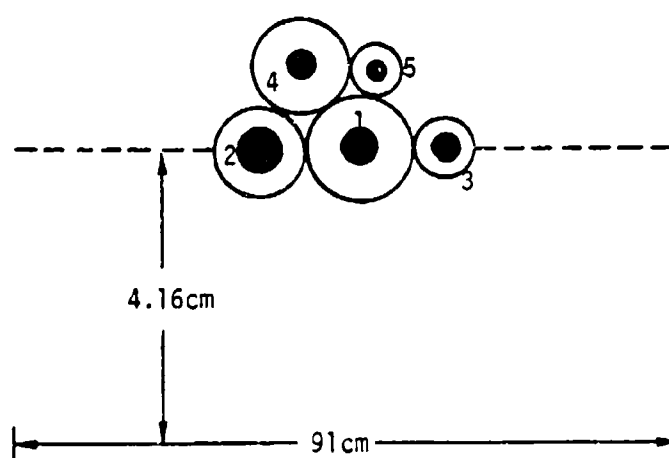


Figure 10. Five-Wire Cable (Over a Ground Plane) Cross Section

Analysis in terms of the scattering matrix requires the connection matrices given by

$$[C_{I_{nm}}] = \begin{bmatrix} 1 & 0 & 0 & 0 & 0 & 1 & 0 & 0 & 0 & 0 \\ 0 & 1 & 0 & 0 & 0 & 0 & 1 & 0 & 0 & 0 \\ 0 & 0 & 1 & 0 & 0 & 0 & 0 & 1 & 0 & 0 \\ 0 & 0 & 0 & 1 & 0 & 0 & 0 & 0 & 1 & 0 \\ 0 & 0 & 0 & 0 & 1 & 0 & 0 & 0 & 0 & 1 \end{bmatrix}$$

$$[C_{V_{nm}}] = \begin{bmatrix} 1 & 0 & 0 & 0 & 0 & -1 & 0 & 0 & 0 & 0 \\ 0 & 1 & 0 & 0 & 0 & 0 & -1 & 0 & 0 & 0 \\ 0 & 0 & 1 & 0 & 0 & 0 & 0 & -1 & 0 & 0 \\ 0 & 0 & 0 & 1 & 0 & 0 & 0 & 0 & -1 & 0 \\ 0 & 0 & 0 & 0 & 1 & 0 & 0 & 0 & 0 & -1 \end{bmatrix}$$

The characteristic impedance and the scattering matrix are shown in table 4.

The voltage measurements were obtained by recording the voltages with a Tektronix 475 oscilloscope using a high impedance voltage probe. The upper frequency limit of the recording system was approximately 200 MHz, which produced some low-pass filtering of the experimental data. Measurements of the current pulses were obtained by replacing the voltage probe with a Tektronix P 6022 200 MHz clip-on current probe. The signal source in all cases was a Tektronix 109 pulse generator with a 175 nanosecond charging line. The pulse generator rise time was approximately 0.7 nanoseconds.

Figure 11 shows the input pulse waveform which is used to drive the wires. Figures 12 through 16 show the comparison of voltage waveforms recorded at the load ends of tubes 2 and 3, when wire 4 of tube 1 is driven, with the waveforms computed using the analysis described in this

Table 4. BRANCHED MULTICONDUCTOR CHARACTERISTIC IMPEDANCE AND SCATTERING MATRICES

$$[Z_{c_{nm}}] = \begin{bmatrix} 223.073 & 138.964 & 150.885 & 138.278 & 145.372 & 0 & 0 & 0 & 0 \\ 138.964 & 229.164 & 115.579 & 140.97 & 125.528 & 0 & 0 & 0 & 0 \\ 150.885 & 115.579 & 247.95 & 123.761 & 149.056 & 0 & 0 & 0 & 0 \\ 138.278 & 140.97 & 123.761 & 225.051 & 155.647 & 0 & 0 & 0 & 0 \\ 145.372 & 125.528 & 149.056 & 155.647 & 295.409 & 0 & 0 & 0 & 0 \\ 0 & 0 & 0 & 0 & 0 & 232.419 & 148.328 & 159.83 & 0 \\ 0 & 0 & 0 & 0 & 0 & 148.382 & 237.879 & 121.279 & 0 \\ 0 & 0 & 0 & 0 & 0 & 159.83 & 121.279 & 258.32 & 0 \\ 0 & 0 & 0 & 0 & 0 & 0 & 0 & 0 & 227.59 \\ 0 & 0 & 0 & 0 & 0 & 0 & 0 & 0 & 156.939 \\ 0 & 0 & 0 & 0 & 0 & 0 & 0 & 0 & 302.948 \end{bmatrix}$$

$$[S_{nm}] = \begin{bmatrix} 0.06775 & 0.07147 & 0.05039 & -0.25665 & -0.15288 & 0.93224 & -0.07147 & -0.05039 & 0.25665 & 0.15288 \\ 0.07334 & 0.07258 & 0.03348 & -0.30059 & -0.09414 & -0.07334 & 0.92741 & -0.03348 & 0.300592 & 0.09414 \\ 0.06688 & 0.05086 & 0.05896 & -0.19562 & -0.18852 & -0.06688 & -0.05086 & 0.94103 & 0.19527 & 0.18852 \\ -0.16315 & -0.20131 & -0.09141 & 0.10854 & 0.05009 & 0.16315 & 0.20131 & 0.09141 & 0.89145 & -0.05009 \\ -0.17621 & -0.11906 & -0.17501 & 0.08759 & 0.07822 & 0.17621 & 0.11906 & 0.17501 & -0.08759 & 0.92177 \\ 1.06776 & 0.07147 & 0.05039 & -0.25665 & -0.15288 & -0.06775 & -0.07147 & -0.05039 & 0.25665 & 0.15288 \\ 0.07334 & 1.07259 & 0.03348 & -0.30059 & -0.09414 & -0.07334 & -0.07258 & -0.03348 & 0.30059 & 0.09414 \\ 0.06688 & 0.05086 & 1.05896 & -0.19562 & -0.18852 & -0.06688 & -0.05086 & -0.05896 & 0.19562 & 0.18852 \\ -0.16315 & -0.20131 & -0.09141 & 1.10855 & 0.05009 & 0.16315 & 0.20131 & 0.09141 & -0.10854 & -0.05009 \\ -0.17621 & -0.11906 & -0.17501 & 0.08759 & 1.07822 & 0.176218 & 0.11906 & 0.17501 & -0.08759 & -0.07822 \end{bmatrix}$$

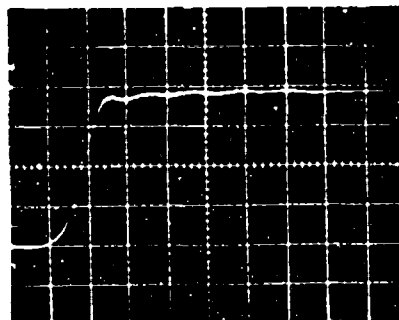


Figure 11. Input waveform used to drive the wire in the cable.
Vertical scale is 1.0 V/div; horizontal scale is 2 ns/div.

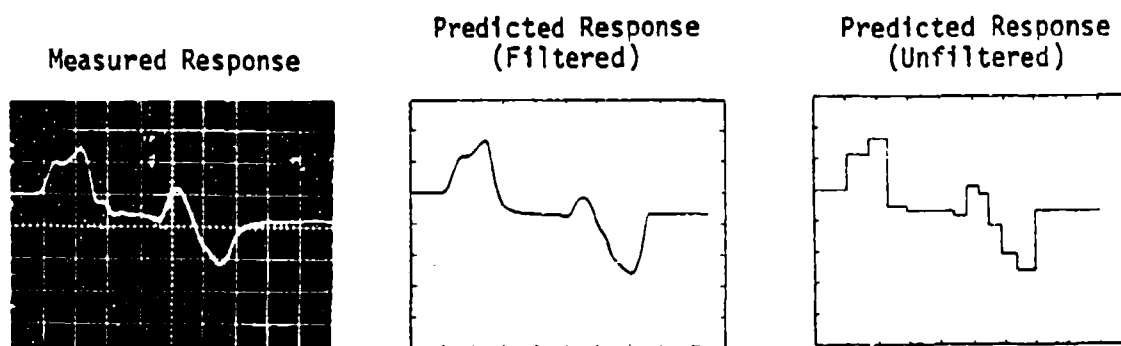


Figure 12. Voltage waveform at the load end of wire 1 of tube 2, with wire 4 of tube 1 driven. Vertical scale is 0.2 V/div; horizontal scale is 5 ns/div.

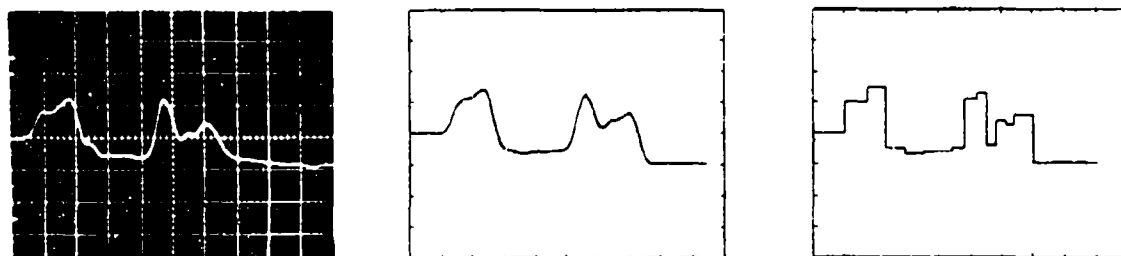


Figure 13. Voltage waveform at the load end of wire 2 of tube 2, with wire 4 of tube 1 driven. Vertical scale is 0.2 V/div; horizontal scale is 5 ns/div.

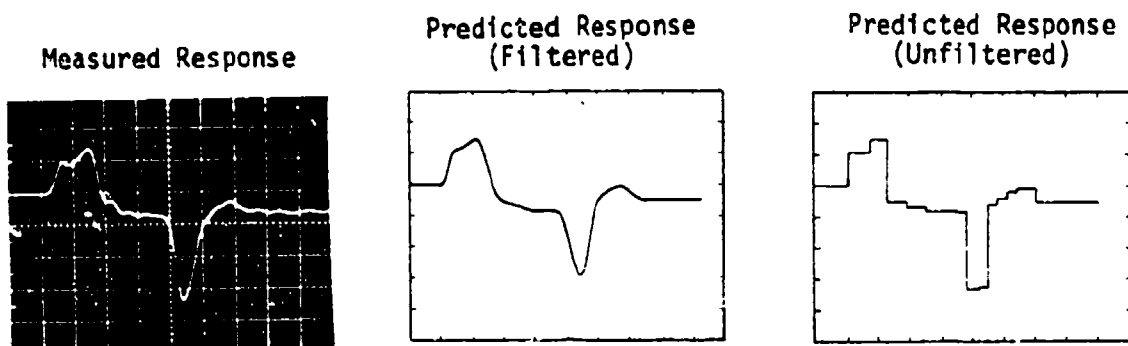


Figure 14. Voltage waveform at the load end of wire 3 of tube 2, with wire 4 of tube 1 driven. Vertical scale is 0.2 V/div; horizontal scale is 5 ns/div.



Figure 15. Voltage waveform at the load end of wire 4 of tube 3, with wire 4 of tube 1 driven. Vertical scale is 0.5 V/div; horizontal scale is 5 ns/div.

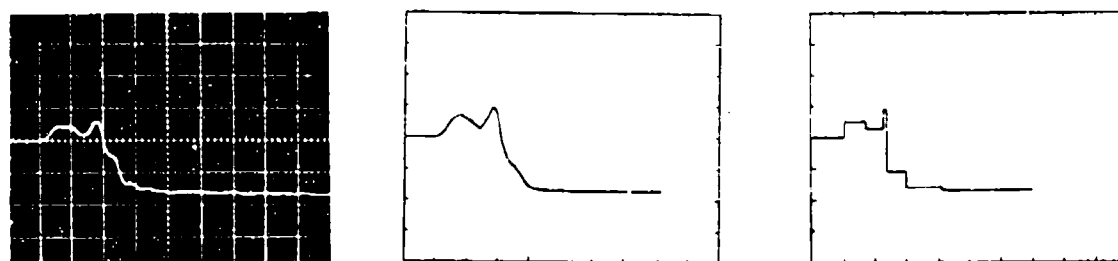


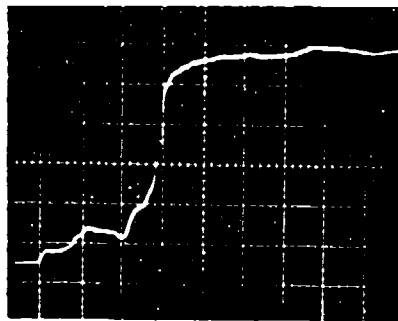
Figure 16. Voltage waveform at the load end of wire 5 of tube 3, with wire 4 of tube 1 driven. Vertical scale is 0.5 V/div; horizontal scale is 5 ns/div.

section. These waveforms have been filtered to simulate the 200 MHz bandwidth of the oscilloscope for comparison of the measured and predicted responses. The unfiltered waveforms clearly show the times of arrival of different modes. Figures 17 through 23 show the comparison of voltage waveforms recorded at the load ends of tubes 1 and 3, when wire 1 of tube 2 is driven, with the waveforms computed. Figures 24 through 31 show the comparison of voltage waveforms recorded at the load ends of tubes 1 and 2, when wire 4 of tube 3 is driven, with the waveforms computed.

The computed waveforms in figures 12 through 31 have been obtained by assuming an ideal step function voltage pulse as the input. The comparison in figures 12 through 31 shows that the predicted waveforms agree very closely with the measured waveforms. Note that, in figures 12 through 16, predicted waveforms, after being filtered for the 200 MHz bandwidth of the oscilloscope, are of a shape which is similar to the measured waveforms. The predicted amplitudes of different modes, and their times of arrival, compare closely with those of the measured data. The predicted waveforms for the actual input pulse can be obtained by applying the method of convolution. These figures show that the waveforms obtained by using the analysis described in this section agree very closely with the measured waveforms.

The waveforms of current recorded with the three-wire section driven in the common mode are presented in figures 32 through 36 for the five-wire segment and figures 37 and 38 for the two-wire segment. The first reflections, which arrive after approximately 60 nanoseconds are included in the predicted waveforms of figures 32 through 36. The reflections are from the junction and from the end of the two-wire segment and arrive at the measurement point at approximately the same time. Similar results (not shown) were obtained by driving the two- and five-wire ends in the common mode.

Measured Response



Predicted Response

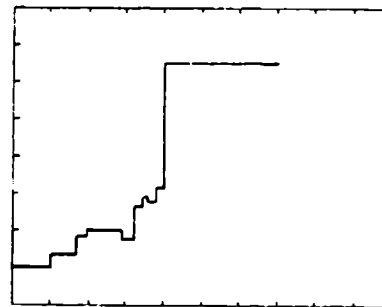


Figure 17. Voltage waveform at the load end of wire 1 of tube 1, with wire 1 of tube 2 driven. Vertical scale is 0.5 V/div; horizontal scale is 10 ns/div.

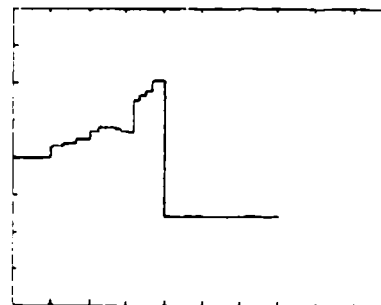
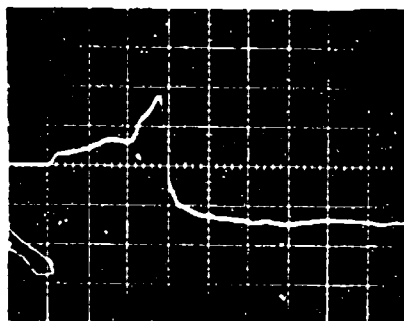


Figure 18. Voltage waveform at the load end of wire 2 of tube 1, with wire 1 of tube 2 driven. Vertical scale is 0.5 V/div; horizontal scale is 10 ns/div.

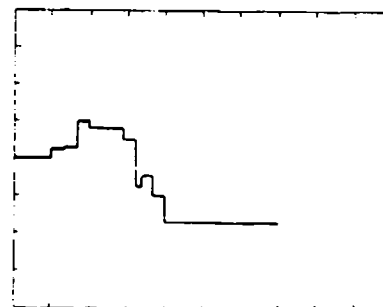
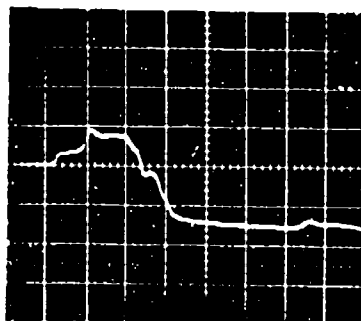
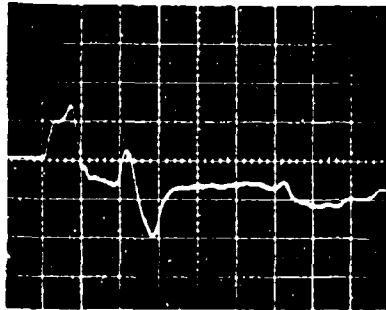


Figure 19. Voltage waveform at the load end of wire 3 of tube 1, with wire 1 of tube 2 driven. Vertical scale is 0.5 V/div; horizontal scale is 10 ns/div.

Measured Response



Predicted Response

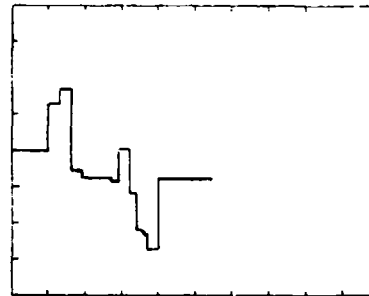


Figure 20. Voltage waveform at the load end of wire 4 of tube 1 with wire 1 of tube 2 driven. Vertical scale is 0.2 V/div; horizontal scale is 10 ns/div.

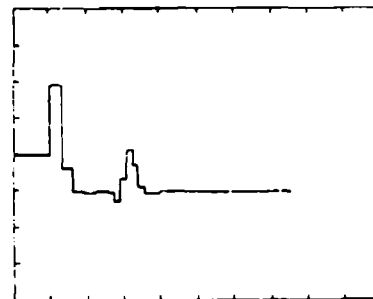
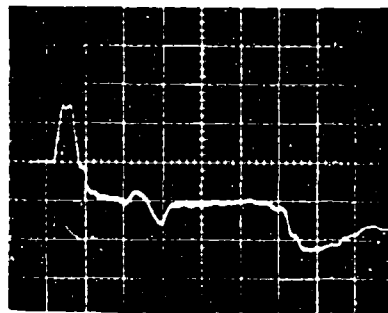


Figure 21. Voltage waveform at the load end of wire 5 of tube 1 with wire 1 of tube 2 driven. Vertical scale is 0.1 V/div; horizontal scale is 10 ns/div.

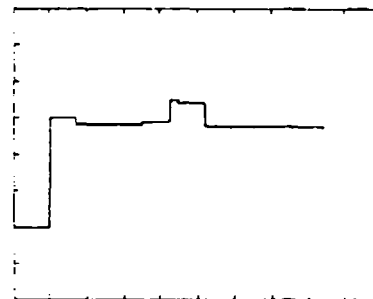
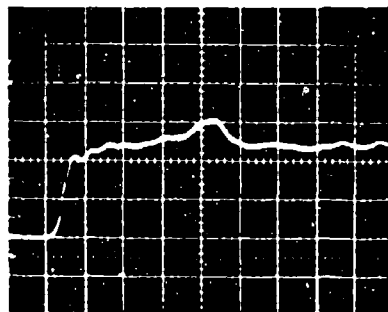
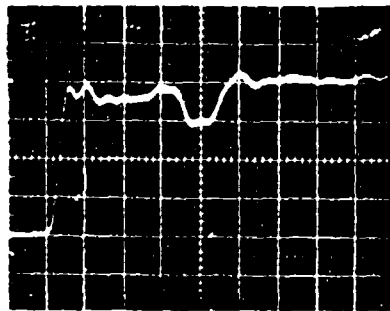


Figure 22. Voltage waveform at the load end of wire 4 of tube 3 with wire 1 of tube 2 driven. Vertical scale is 0.1 V/div; horizontal scale is 5 ns/div.

Measured Response



Predicted Response



Figure 23. Voltage waveform at the load end of wire 5 of tube 3 with wire 1 of tube 2 driven. Vertical scale is 0.05 V/div; horizontal scale is 5 ns/div.

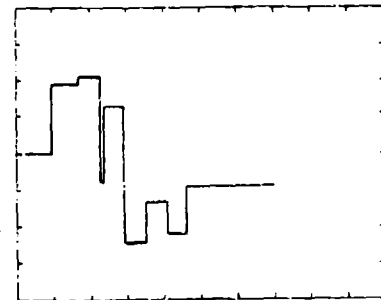
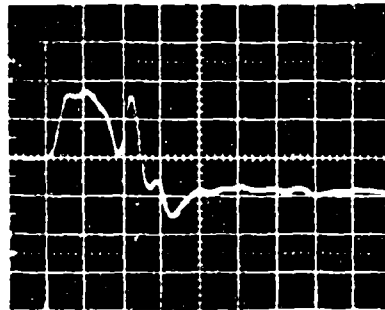


Figure 24. Voltage waveform at the load end of wire 1 of tube 1 with wire 4 of tube 3 driven. Vertical scale is 0.1 V/div; horizontal scale is 5 ns/div.

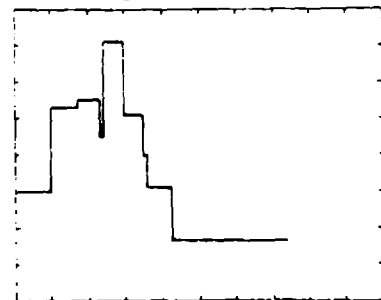
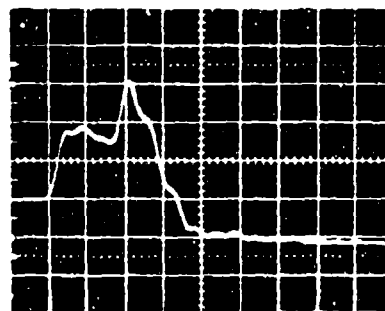
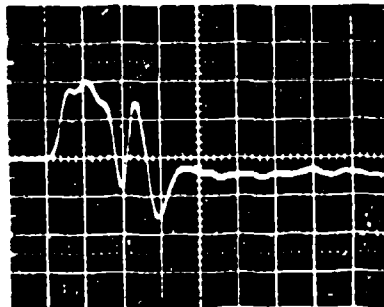


Figure 25. Voltage waveform at the load end of wire 2 of tube 1 with wire 4 of tube 3 driven. Vertical scale is 0.1 V/div; horizontal scale is 5 ns/div.

Measured Response



Predicted Response

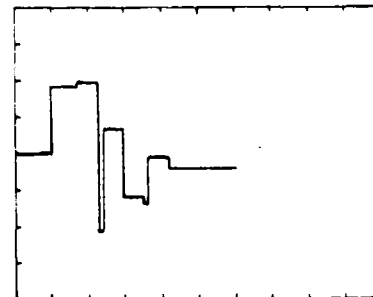


Figure 26. Voltage waveform at the load end of wire 3 of tube 1 with wire 4 of tube 3 driven. Vertical scale is 0.1 V/div; horizontal scale is 5 ns/div.

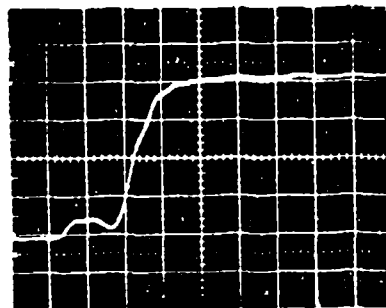


Figure 27. Voltage waveform at the load end of wire 4 of tube 1 with wire 4 of tube 3 driven. Vertical scale is 0.5 V/div; horizontal scale is 5 ns/div.

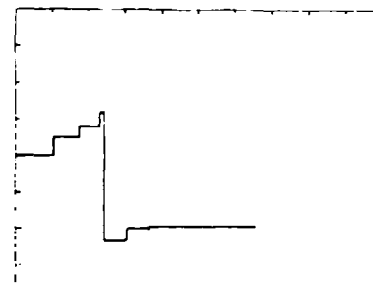
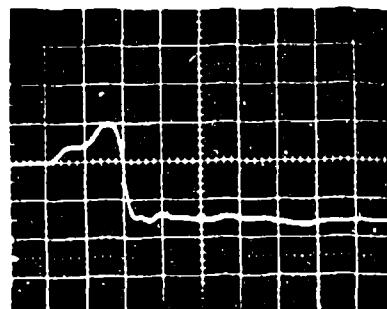
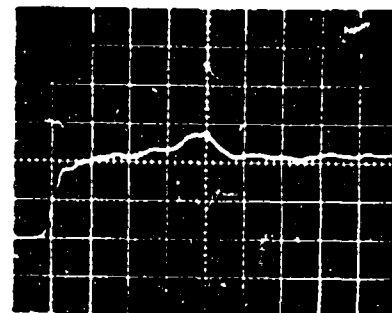


Figure 28. Voltage waveform at the load end of wire 5 of tube 1 with wire 4 of tube 3 driven. Vertical scale is 0.5 V/div; horizontal scale is 5 ns/div.

Measured Response



Predicted Response

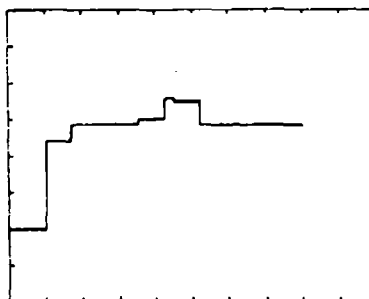


Figure 29. Voltage waveform at the load end of wire 1 of tube 2 with wire 4 of tube 3 driven. Vertical scale is 0.1 V/div; horizontal scale is 5 ns/div.

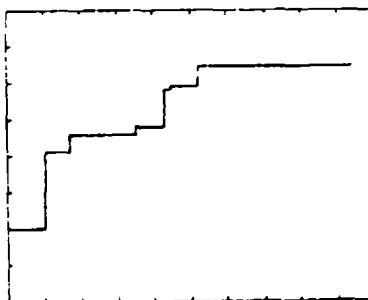
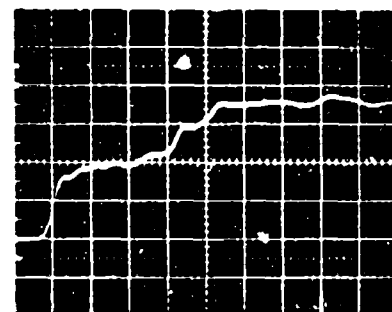


Figure 30. Voltage waveform at the load end of wire 2 of tube 2 with wire 4 of tube 3 driven. Vertical scale is 0.1 V/div; horizontal scale is 5 ns/div.

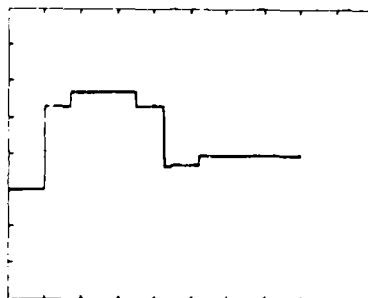
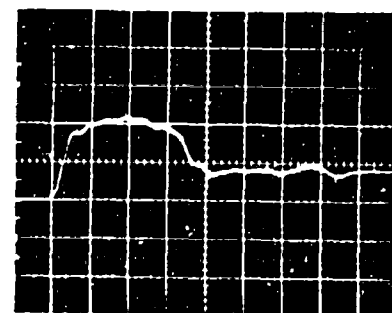
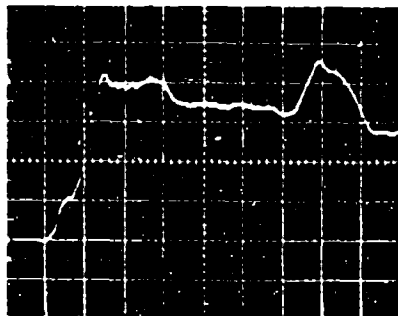


Figure 31. Voltage waveform at the load end of wire 3 of tube 2 with wire 4 of tube 3 driven. Vertical scale is 0.1 V/div; horizontal scale is 5 ns/div.

Measured Response



Predicted Response

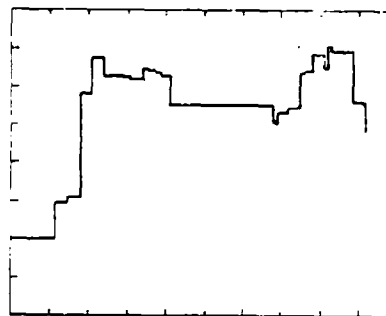


Figure 32. Current waveform at short circuit termination on wire 1 of tube 1 with tube 2 driven in the common mode. Vertical scale is 20 ma/div; horizontal scale is 10 ns/div.

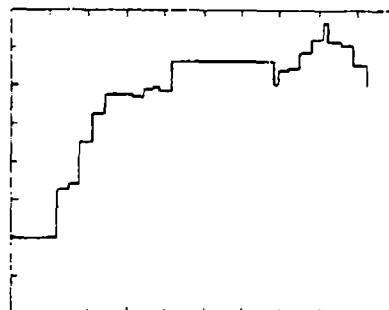
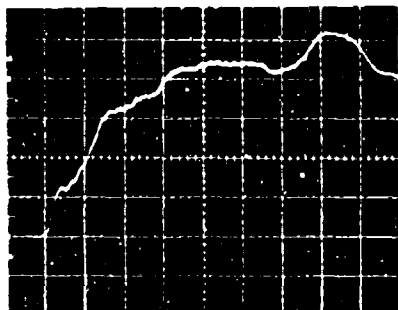


Figure 33. Current waveform at short circuit termination on wire 2 of tube 1 with tube 2 driven in the common mode. Vertical scale is 20 ma/div; horizontal scale is 10 ns/div.

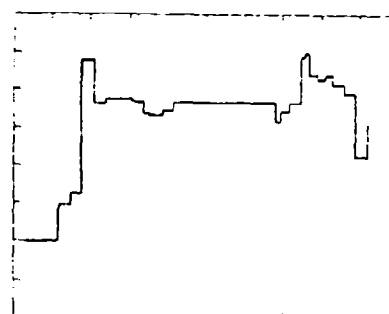
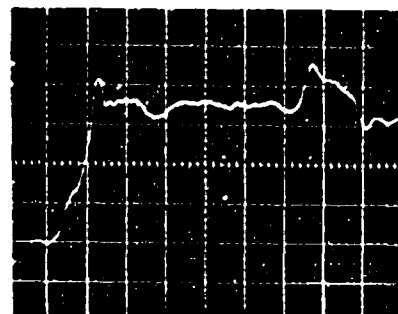
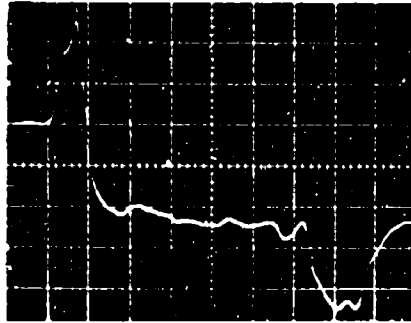


Figure 34. Current waveform at short circuit termination on wire 3 of tube 1 with tube 2 driven in the common mode. Vertical scale is 20 ma/div; horizontal scale is 10 ns/div.

Measured Response



Predicted Response

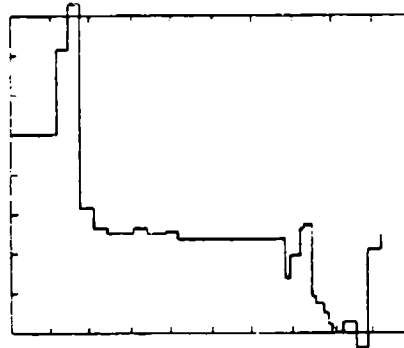


Figure 35. Current waveform at short circuit termination on wire 4 of tube 1 with tube 2 driven in the common mode. Vertical scale is 20 ma/div; horizontal scale is 10 ns/div.

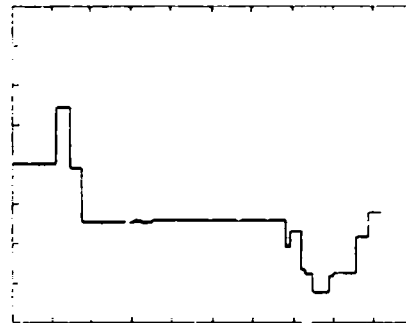
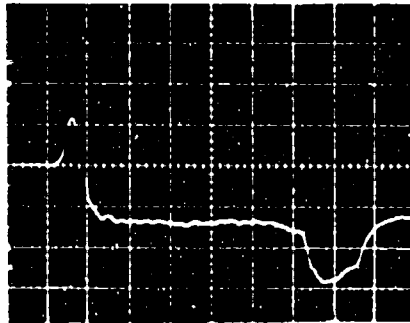
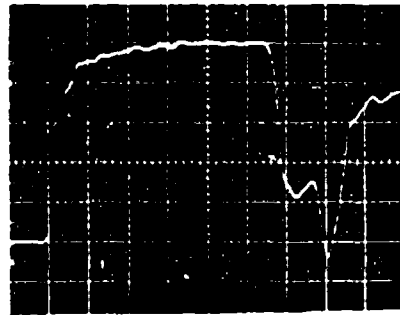


Figure 36. Current waveform at short circuit termination on wire 5 of tube 1 with tube 2 driven in the common mode. Vertical scale is 20 ma/div; horizontal scale is 10 ns/div.

Measured Response



Predicted Response

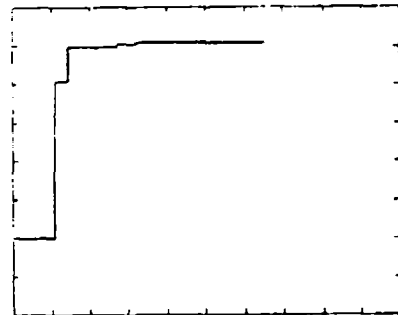


Figure 37. Current waveform at short circuit termination on wire 4 of tube 3 with tube 2 driven in the common mode. Vertical scale is 10 ma/div; horizontal scale is 10 ns/div.

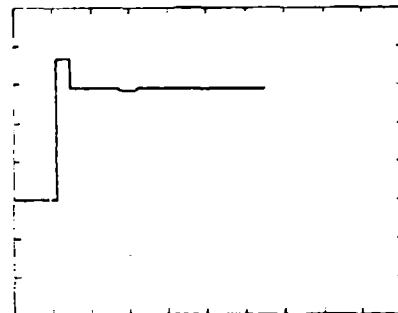
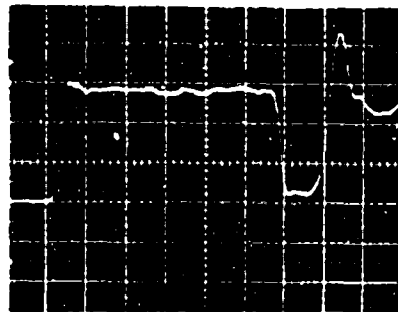


Figure 38. Current waveform at short circuit termination on wire 5 of tube 3 with tube 2 driven in the common mode. Vertical scale is 10 ma/div; horizontal scale is 10 ns/div.

Low-level signals were used in the current pulse measurements and consequently the signal-to-noise ratio was lower than for the voltage pulse measurements. Some noise pickup was observed due to the undesirable electric field response of the current probe; however this did not seriously effect the data and agreement with predictions was found to be satisfactory in all cases.

5. ANALYSIS OF CABLE NETWORKS

a. Background

The analytical concepts presented for the simple branched cable also apply to more complicated networks containing several branches. The direct time domain analysis discussed in section IV.2 leads to a solution for the voltage or current time function at a given point in the network which is a superposition of all possible modes arriving at that point. This approach involves simple analytical concepts and is readily applied to the early time pulse response of a cable network. However, as time progresses the pulse amplitude at any given time depends on an increasing number of superimposed modes caused by multiple reflections from the branch and end points, with each reflection and transmission accompanied by mode conversion. Direct time domain analysis in this case becomes complicated and requires elaborate computational schemes to keep track of the amplitudes and arrival times of the several modal components present.

b. Special Case of a Network Modeled with Single Conductor Line Segments

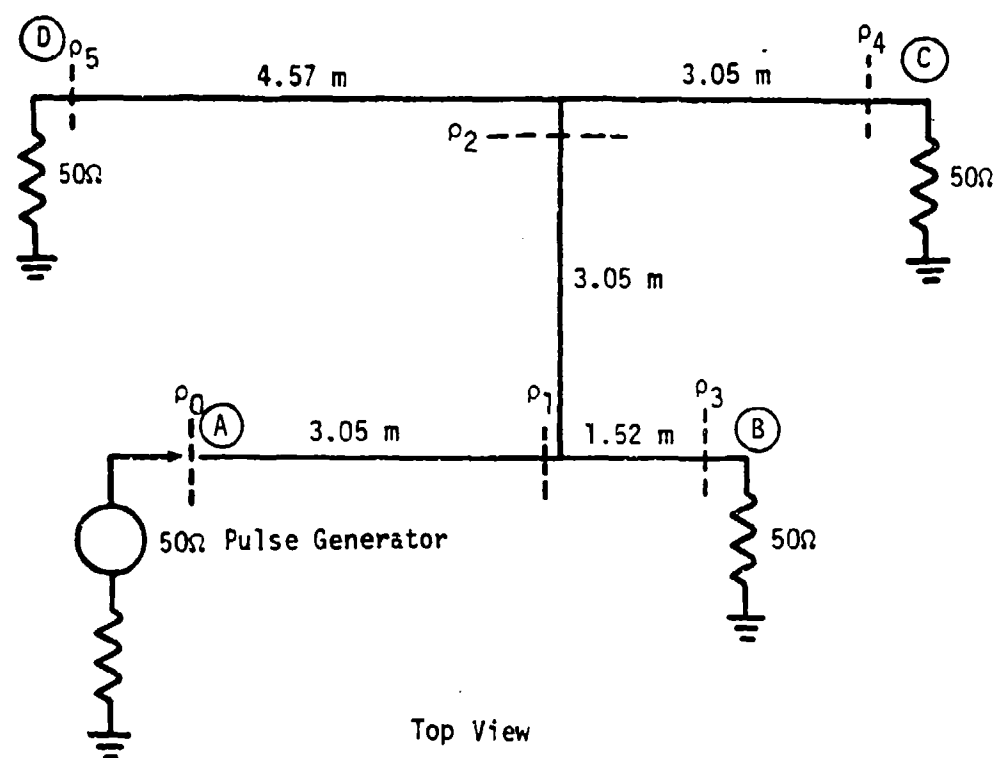
Interest in the response of a multiconductor to EMP excitation is often limited to common mode propagation on the bundle. Multiconductor segments can then be modeled as equivalent single conductors with characteristic impedances which are determined by the equivalent single conductor radius of the bundle (ref. 21). This greatly simplifies the analysis which is a special case of the more general multiconductor analysis presented in sections IV.2 and IV.3.

To validate the analytical concepts that have been discussed and to provide experimental data for the verification of prediction codes under development by other contractors, the pulse response of a simple transmission line network which supports only a single propagation mode (common mode) was determined experimentally. The results were compared with the calculated response obtained from a direct time domain analysis of the network.

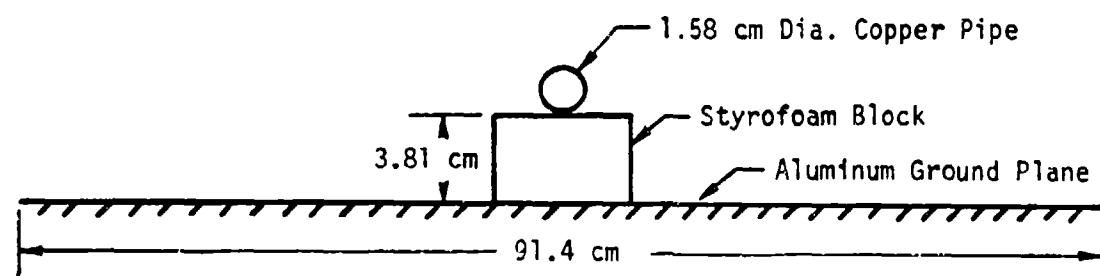
The network, shown in figure 39, was constructed of 1.58 cm diameter copper pipe in the form of an "H" with legs 4.57 and 7.62 meters in length separated by a 3.05 meter cross member. The configuration was supported by Styrofoam blocks 3.8 cm above an aluminum ground plane.

Measurements of the voltage at the input and the load voltages across 50 ohm loads at the end of each leg were obtained using impulse and step function input pulses to drive the network. Relatively long time base (100 ns) oscilloscope traces were recorded to show the multiple reflections from the two junctions and four end points. The impulse response data was primarily for verification of the time of arrival of the various reflected pulses at each measurement point. The step function data was obtained primarily for pulse amplitude measurements.

Time domain analysis of the network was carried out with the aid of a multiple reflection diagram (ref. 22). Multiple reflections and the construction of multiple reflection diagrams are discussed in more detail in section VI.3. The six reflection coefficients ρ_0 through ρ_5 that are required for the calculations were computed from equation (16). The line characteristic impedance is the same for each segment and was determined to be 150 ohms from TDR measurements. The load impedance at each junction is 75 ohms, given by the parallel impedance of the two segments which leave the junction. The reflection coefficients for pulse propagation in the forward direction (away from the pulse generator) are then



Top View



Cross Section - Any Segment

Figure 39. Network Layout

$$\rho_0 = \frac{150 - 50}{150 + 50} = 0.5$$

$$\rho_1 = \rho_2 = \frac{75 - 150}{75 + 150} = -0.333$$

$$\rho_3 = \rho_4 = \rho_5 = \frac{50 - 150}{50 + 150} = -0.5$$

The amplitude and arrival time of the first four signal components at each measurement point are listed as follows:

Measurement Point A

Component	TOA (ns)	Amplitude	Voltage
0	0	$(1+\rho_0)Vg$	6.00
1	20.4	$(1-\rho_0)\rho_1(1+\rho_0)Vg$	-1.00
2	30.5	$(1-\rho_0)(1+\rho_1)\rho_3(1+\rho_1)(1+\rho_0)Vg$	-0.67
3a	40.7	$(1-\rho_0)(1+\rho_1)\rho_2(1+\rho_1)(1+\rho_0)Vg$	-0.44
3b	40.7	$(1-\rho_0)\rho_1(-\rho_0)\rho_1(1+\rho_0)Vg$	-0.17
3c	40.7	$(1-\rho_0)(1+\rho_1)\rho_3\rho_1\rho_3(1+\rho_1)(1+\rho_0)Vg$	-0.11
			<hr/> -0.72

Measurement Point B

Component	TOA (ns)	Amplitude	Voltage
0	0	$(1+\rho_3)(1+\rho_1)(1+\rho_0)Vg$	2.00
1	10.2	$(1+\rho_3)\rho_1\rho_3(1+\rho_1)(1+\rho_0)Vg$	0.33
2a	20.4	$(1+\rho_3)(1+\rho_1)\rho_2(1+\rho_1)(1+\rho_0)Vg$	-0.44
2b	20.4	$(1+\rho_3)(1+\rho_1)(-\rho_0)\rho_1(1+\rho_0)Vg$	0.33
2c	20.4	$(1+\rho_3)\rho_1\rho_3\rho_1\rho_3(1+\rho_1)(1+\rho_0)Vg$	0.06
			<hr/> -0.06
3a	30.5	$(1+\rho_3)\rho_1\rho_3(1+\rho_1)\rho_2(1+\rho_1)(1+\rho_0)Vg$	-0.07
3b	30.5	$(1+\rho_3)(1+\rho_1)\rho_2(1+\rho_1)\rho_3(1+\rho_1)(1+\rho_0)Vg$	0.15
3c	30.5	$(1+\rho_3)\rho_1\rho_3(1+\rho_1)(-\rho_0)\rho_1(1+\rho_0)Vg$	0.06
3d	30.5	$(1+\rho_3)(1+\rho_1)(-\rho_0)(1+\rho_1)\rho_3(1+\rho_1)(1+\rho_0)Vg$	0.22
3e	30.5	$(1+\rho_3)(\rho_1\rho_3)^3(1+\rho_1)(1+\rho_0)Vg$	0.01
			<hr/> 0.37

Measurement Point C

Component	TOA (ns)	Amplitude	Voltage
0	0	$(1+\rho_4)(1+\rho_2)(1+\rho_1)(1+\rho_0)Vg$	1.34
1	10.2	$(1+\rho_4)(1+\rho_2)(1+\rho_1)\rho_3(1+\rho_1)(1+\rho_0)Vg$	-0.44
2a	20.4	$(1+\rho_4)\rho_2\rho_4(1+\rho_2)(1+\rho_1)(1+\rho_0)Vg$	0.22
2b	20.4	$(1+\rho_4)(1+\rho_2)\rho_1\rho_2(1+\rho_1)(1+\rho_0)Vg$	0.15
2c	20.4	$(1+\rho_4)(1+\rho_2)(1+\rho_1)(-\rho_0)\rho_1(1+\rho_0)Vg$	0.22
2d	20.4	$(1+\rho_4)(1+\rho_3)(1+\rho_1)\rho_3\rho_1\rho_3(1+\rho_1)(1+\rho_0)Vg$	-0.08
			<hr/> 0.51
3a	30.7	$(1+\rho_4)(1+\rho_2)\rho_5(1+\rho_2)(1+\rho_1)(1+\rho_0)Vg$	-0.44
3b	30.7	$(1+\rho_4)\rho_2\rho_4(1+\rho_2)(1+\rho_1)\rho_3(1+\rho_1)(1+\rho_0)Vg$	-0.08
3c	30.7	$(1+\rho_4)(1+\rho_2)\rho_1\rho_2(1+\rho_1)\rho_3(1+\rho_1)(1+\rho_0)Vg$	-0.05
3d	30.7	$(1+\rho_4)(1+\rho_2)(1+\rho_1)\rho_3(1+\rho_1)\rho_2(1+\rho_1)(1+\rho_0)Vg$	0.10
3e	30.7	$(1+\rho_4)(1+\rho_2)(1+\rho_1)\rho_3(1+\rho_1)(-\rho_0)\rho_1(1+\rho_0)Vg$	-0.08
3f	30.7	$(1+\rho_4)(1+\rho_2)(1+\rho_1)(-\rho_0)(1+\rho_1)\rho_3(1+\rho_1)(1+\rho_0)Vg$	0.15
3g	30.7	$(1+\rho_4)(1+\rho_2)(1+\rho_1)\rho_3\rho_1\rho_3\rho_1\rho_3(1+\rho_1)(1+\rho_0)Vg$	-0.01
			<hr/> -0.41

Measurement Point D

Component	TOA (ns)	Amplitude	Voltage
0	0	$(1+\rho_5)(1+\rho_2)(1+\rho_1)(1+\rho_0)Vg$	1.34
1	10.2	$(1+\rho_5)(1+\rho_2)(1+\rho_1)\rho_3(1+\rho_1)(1+\rho_0)Vg$	-0.45
2a	20.4	$(1+\rho_5)(1+\rho_2)\rho_4(1+\rho_2)(1+\rho_1)(1+\rho_0)Vg$	-0.44
2b	20.4	$(1+\rho_5)(1+\rho_2)\rho_1\rho_2(1+\rho_1)(1+\rho_0)Vg$	0.15
2c	20.4	$(1+\rho_5)(1+\rho_2)(1+\rho_1)\rho_3\rho_1\rho_3(1+\rho_1)(1+\rho_0)Vg$	-0.08
2d	20.4	$(1+\rho_5)(1+\rho_2)(1+\rho_1)(-\rho_0)\rho_1(1+\rho_0)Vg$	0.22
			<hr/> -0.15
3a	30.7	$(1+\rho_5)\rho_2\rho_5(1+\rho_2)(1+\rho_1)(1+\rho_0)Vg$	0.22
3b	30.7	$(1+\rho_5)(1+\rho_2)\rho_4(1+\rho_2)(1+\rho_1)\rho_3(1+\rho_1)(1+\rho_0)Vg$	0.15
3c	30.7	$(1+\rho_5)(1+\rho_2)\rho_1\rho_2(1+\rho_1)\rho_3(1+\rho_1)(1+\rho_0)Vg$	-0.05
3d	30.7	$(1+\rho_5)(1+\rho_2)(1+\rho_1)\rho_3(1+\rho_1)\rho_2(1+\rho_1)(1+\rho_0)Vg$	0.10
3e	30.7	$(1+\rho_5)(1+\rho_2)(1+\rho_1)\rho_3(1+\rho_1)(-\rho_0)\rho_1(1+\rho_0)Vg$	-0.08
3f	30.7	$(1+\rho_5)(1+\rho_2)(1+\rho_1)(-\rho_0)(1+\rho_1)\rho_3(1+\rho_1)(1+\rho_0)Vg$	0.15
3g	30.7	$(1+\rho_5)(1+\rho_2)(1+\rho_1)\rho_3\rho_1\rho_3\rho_1\rho_3(1+\rho_1)(1+\rho_0)Vg$	-0.01
			<hr/> 0.48

The input impulse and step function pulses used to drive the network are shown in figure 40. Figure 41 shows the network response recorded at each of the four measurement points A through D identified in figure 39. The predicted step function response for the first 40 nanoseconds is included for comparison and is found to be in satisfactory agreement with the measurements.

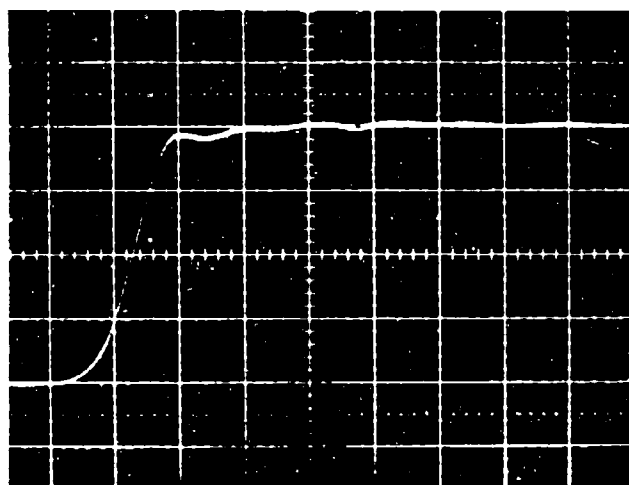
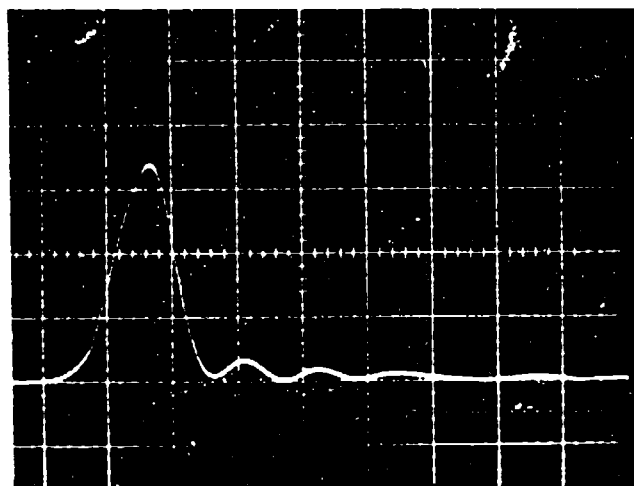


Figure 40. Pulse generator output signals;
 vert. sens: 1 v/div, horiz. sens:
 2 ns/div, 50 Ω termination.

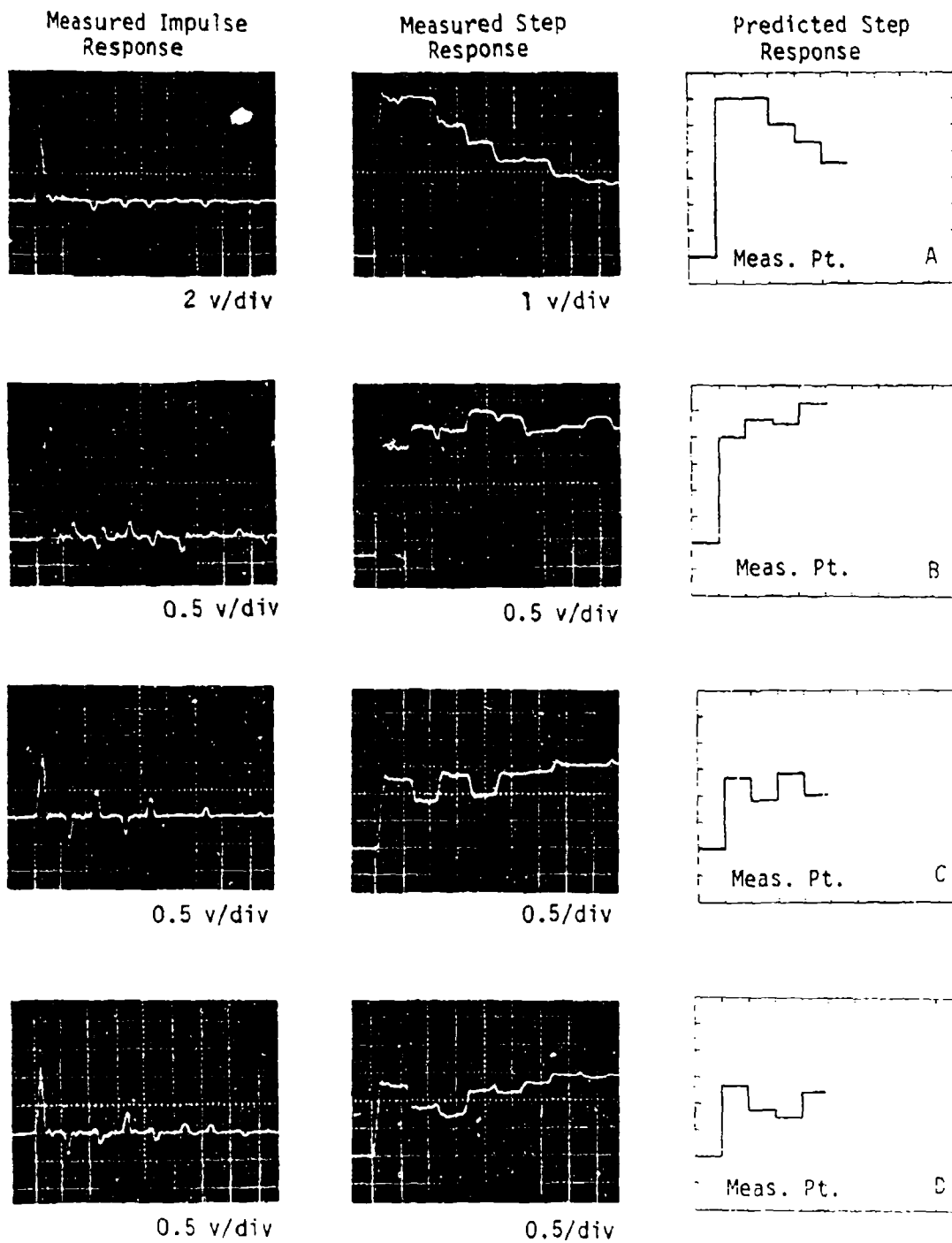


Figure 41. Measured and predicted network response;
Horiz. Sens: 10 ns/div.

SECTION V

APPLICATIONS TO MULTICONDUCTOR CHARACTERIZATION *IN SITU*

1. INTRODUCTION

Frequency domain methods for measurement of the L and C matrices of multiconductors have been reported previously (ref. 23). A complete description of the methodology is included in the appendix. The technique is useful for laboratory measurements on cable mockups; however, it is generally not suitable for measurements *in situ* because of its susceptibility to errors caused by stray capacitance and inductance. Complex loads due to multipin cable connectors, cable clamps, ground leads, etc., which are encountered in most cable installations behave in the frequency domain as distributed loads which affect the line parameter data over a wide frequency range.

The alternate methods for multiconductor line characterization developed in section III use time domain techniques. These techniques provide a direct measurement of the characteristic admittance matrix and are applicable to any cable or cable segment that has one end accessible. Time domain methods are well suited to measurements *in situ* because the pulse response of a complex load located at the input or elsewhere along the line is isolated in time and can be removed from the cable response data.

2. CABLE INTERFACE REFLECTIONS

Time domain reflectometry measurements *in situ* usually involve a non-ideal interface which must be made between the multipin connector attached to the cable under test and the reference line of the time domain reflectometer. In a typical connection, stray inductance is introduced by the connector pins and by the ground strap which joins the shield of the coaxial reference cable and the ground reference of the multiconductor.

Stray capacitance is also present due mainly to the metallic shell of the cable connector. The complex impedance of a typical interface can be modeled approximately as a lumped constant series inductance and shunt capacitance. An equivalent circuit of this model is shown in figure 42. The lumped parameters L and C represent the stray inductance and capacitance of the interface connection. The complex impedance Z_i which loads the TDR reference cable is obtained from the equivalent circuit of figure 42 and is given by

$$Z_i = j\omega L + \frac{Z_L}{1 + j\omega C Z_L} \quad (74)$$

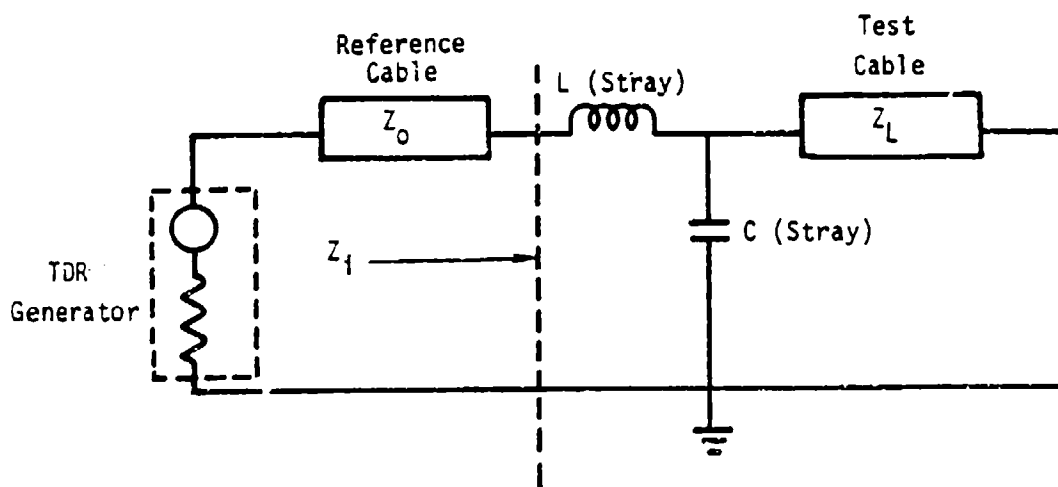


Figure 42. Cable Interface Approximate Equivalent Circuit

The complex reflection coefficient is given by equation (16) with Z_i from equation (74) substituted for Z_L . The pulse reflected by the complex load is computed by evaluating the inverse Fourier transform of the reflected signal $V_r(\omega)$ which is given in the frequency domain by

$$V_r(\omega) = \rho(\omega)V_i(\omega) \quad (75)$$

where $V_i(\omega)$ is the frequency spectrum of the input pulse. The solution of (75) for an ideal unit step input is readily obtained since in this case $V_i(\omega) = 1/(j\omega)$.

The results for critically damped, underdamped, and overdamped conditions are given in terms of the decay constants $k_1 = 1/(Z_0 C)$, $k_2 = Z_0/L$ and $k_3 = Z_L/L$ by the following equations:

Critically damped case $(k_1 + k_2)^2 = 4k_1(k_2 + k_3)$

$$v_r(t) = R + [(1-R) + A_1 t]e^{-\alpha_1 t} \quad (76)$$

where

$$\alpha_1 = (k_1 + k_2)/2, A_1 = (k_1 - 3k_2 - 2\alpha_1 R)/2$$

Underdamped case $(k_1 + k_2)^2 < 4k_1(k_2 + k_3)$

$$v_r(t) = R + (1-R)e^{-\alpha_2 t} \cos \beta_2 t + (A_2/\beta_2)e^{-\alpha_2 t} \sin \beta_2 t \quad (77)$$

where

$$\alpha_2 = (k_1 + k_2)/2, A_2 = k_1 - k_2 - \alpha_2(1 + R)$$

$$\beta_2 = [4k_1(k_2 + k_3) - (k_1 + k_2)^2]^{1/2}/2$$

Overdamped case $(k_1 + k_2)^2 > 4k_1(k_2 + k_3)$

$$v_r(t) = R + A_3 e^{-\alpha_3 t} - A_4 e^{-\beta_3 t} \quad (78)$$

where

$$\alpha_3 = (k_1 + k_2)/2 + [(k_1 + k_2)^2 - 4k_1(k_2 + k_3)]^{1/2}/2$$

$$\beta_3 = (k_1 + k_2)/2 - [(k_1 + k_2)^2 - 4k_1(k_2 + k_3)]^{1/2}/2$$

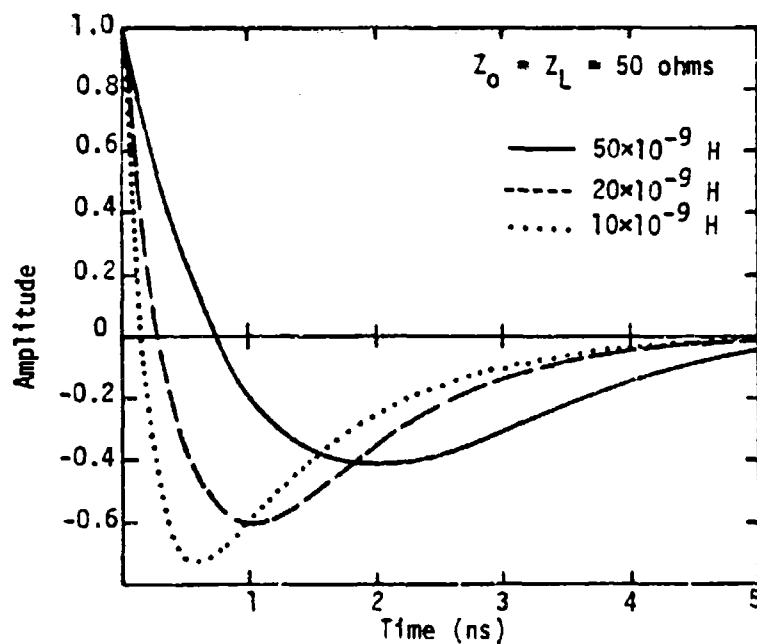
$$A_3 = (\alpha_3 - k_1 + k_2 + R\beta_3)/(\alpha_3 - \beta_3)$$

$$A_4 = (\beta_3 - k_1 + k_2 + R\alpha_3)/(\alpha_3 - \beta_3)$$

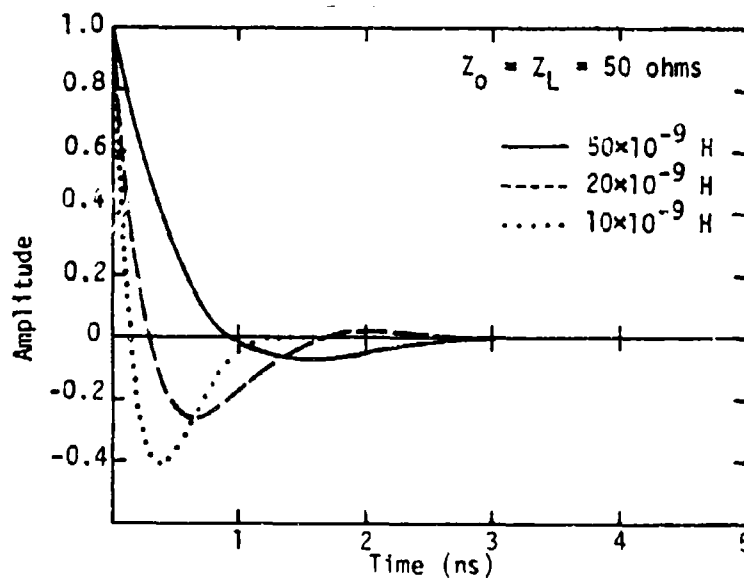
The constant R in the above equations is just the reflection coefficient $R = (Z_L - Z_0)/(Z_L + Z_0)$ that would exist for an ideal interface. The non-ideal interface is seen to produce an exponentially damped transient which decays to the constant R with a characteristic time governed by the magnitude of the stray L and C of the interface.

Examples of interface reflections calculated from equations (76) through (78) for a range of stray capacitance and inductance values that are typical of actual multipin cable connectors are shown in figure 43. The calculations are for capacitances of 10 and 50 picofarads and inductances of 10, 20 and 50 nanohenries, with an ideal unit step input pulse driving a 50 ohm reference cable terminated in a 50 ohm load. The reflection in each case is characterized by an initial positive step which decays exponentially or is exponentially damped and approaches the constant value R.

The effect of a nonideal step input with a finite risetime is to reduce the amplitude and round off the initial positive spike of the reflected pulse. Examples for an input pulse with a 0.2 nanosecond linear rise are shown in figure 44 for the same range of stray impedance as used to obtain the results of figure 43.

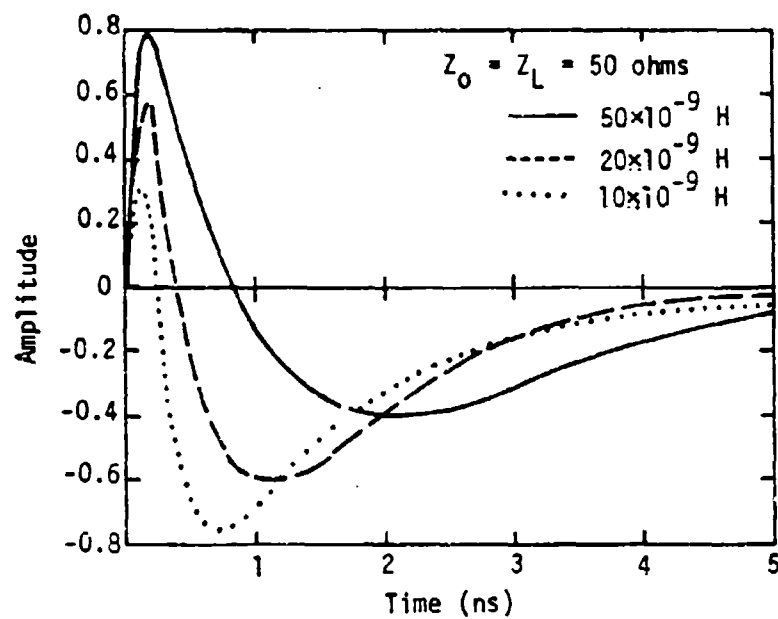


(a) 50×10^{-12} F Stray Capacitance

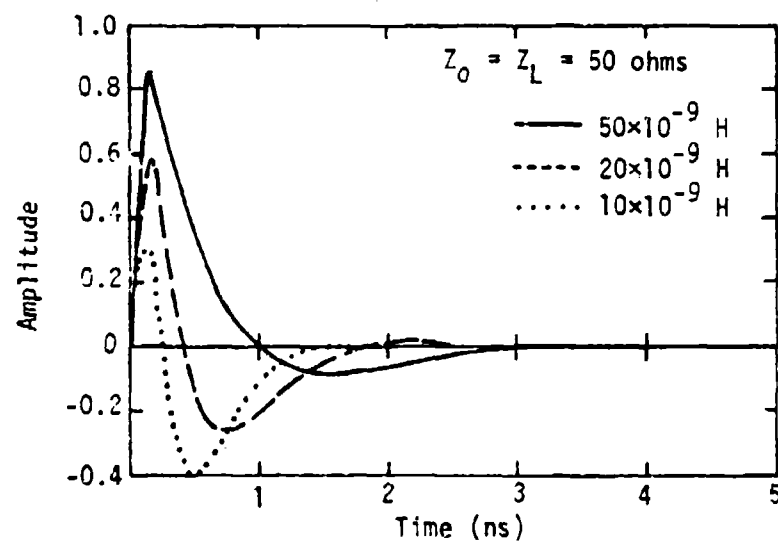


(b) 10×10^{-12} F Stray Capacitance

Figure 43. Typical Interface Reflections for an Ideal Step Input



(a) 10×10^{-12} F Stray Capacitance



(b) 10×10^{-12} F Stray Capacitance

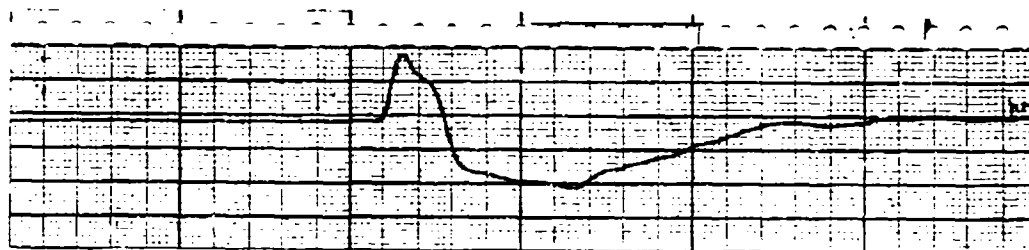
Figure 44. Typical Interface Reflections for a Nonideal Step Input

Measurements on some actual aircraft cable connectors with all of the pins connected in parallel are presented in figure 45. The transient response in each case is seen to closely approximate that predicted by the lumped constant L-C network of figure 42. The upper trace is for a Hughes Aircraft 158-pin rectangular connector which exhibits an unusually large capacitance.

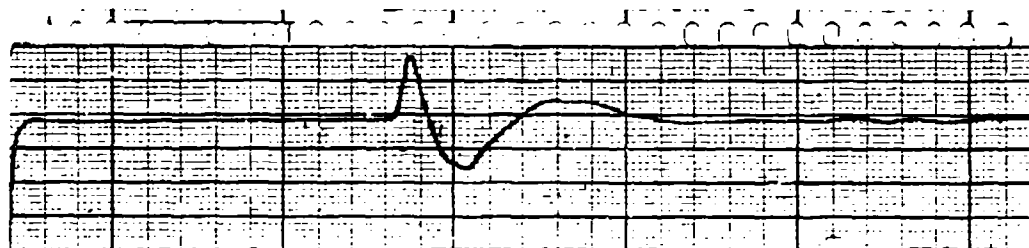
Examples of interface reflections in which the load impedance Z_L is not equal to the characteristic impedance of the reference cable are shown in figure 46. These examples correspond to an interface with a stray inductance of 20 nanohenries and a stray capacitance of 20 picofarads connected between a 50 ohm reference cable and loads in the 10 ohm to 200 ohm range. The input was assumed to be a nonideal step with a linear rise of 0.2 nanoseconds.

The results of this study show that the stray inductance and capacitance caused by typical multipin connectors introduces an exponentially damped transient at the beginning of the reflected pulse. The accuracy of cable impedance measurements obtained through nonideal interfaces of this type will not be seriously degraded as long as the perturbations from the interface decay before reflections from points farther down the line arrive back at the input. In the examples shown, the worst case exhibits a decay time of approximately 5 nanoseconds, which at the speed of light corresponds to the round trip travel time over a 2.5-foot length of cable. It is seen that the accuracy of TDR measurements on cables which are less than 2.5 feet in length, or have a discontinuity within 2.5 feet of the input connection would be degraded by the interface.

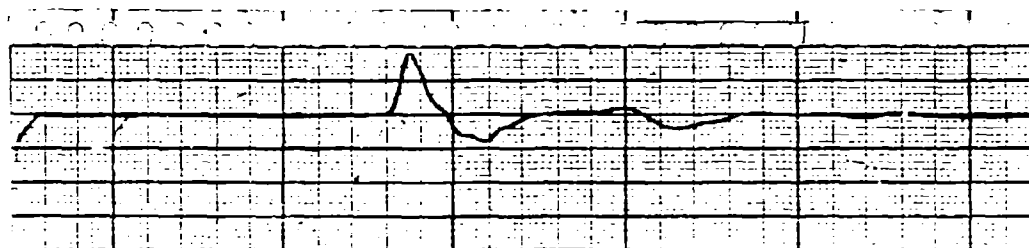
The interference caused by the stray inductance of an interface can be minimized through the use of short ground straps or conducting tape to connect the shield of the reference cable to the ground reference of the cable under test. The stray capacitance can also be minimized in some cases. On panel mounted connectors this can be accomplished by removing the connector mounting screws and allowing the connector shell to float during the measurements.



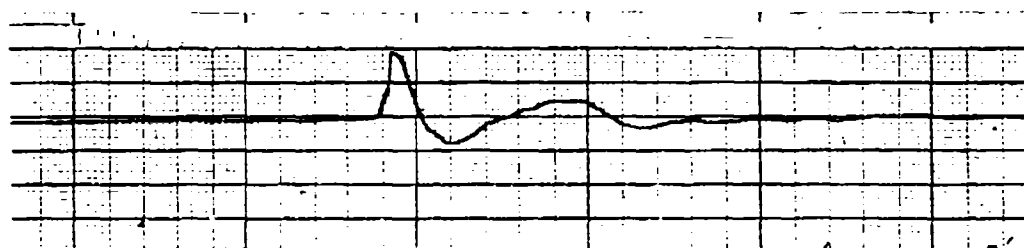
(a) CVC 6092/6093-8N (158 pin)



(b) CVC 6092/6093-6N (52 pin)



(c) CVC 6062E-12P/6066 AE-125 (12 pin)



(d) CVC 6062E 37x75 /6063 37x7P1 (7 pin coax)

Figure 45. Interface reflections from actual aircraft cable connectors.
Vertical Sens: 200 mV/div, Horizontal Sens: 0.8ns/div.
Tektronix 1502 TDR system.

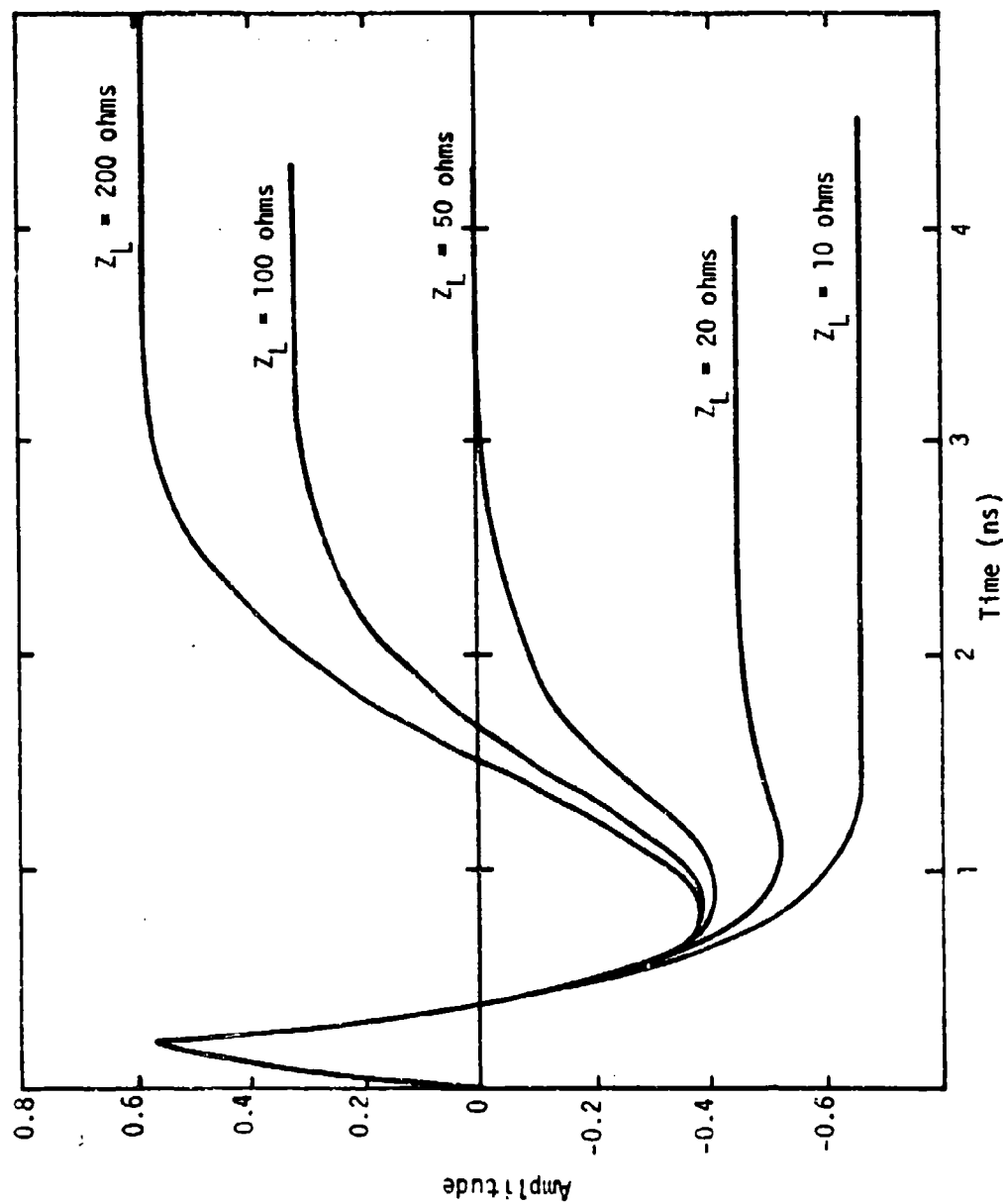


Figure 46. Typical interface reflections for a nonideal step input for various load impedances. $L = 20 \times 10^{-9}$ H, $C = 20 \times 10^{-12}$ F, $Z_0 = 50$ ohms

3. ANALYSIS OF MULTIPLE REFLECTIONS

Multiple reflections on a line terminated in a complex load and connected at the input through a nonideal interface are seen as a superposition of time delayed transients. The pulse shape is modified at each reflection and by transmission through the input interface to the TDR recorder. When the round trip travel time is short compared to the decay time of the reflected transients, the individual reflections overlap and produce complicated traces.

As an aid to the analysis of multiple reflections, the successive reflections can be diagrammed as shown in figure 47 (ref. 22). When the impedances are known, each reflection can be calculated separately and added with the proper time delay to predict the long time base TDR trace.

In principle, an unknown load impedance can be determined by unfolding the TDR record to obtain the load reflection coefficient ρ_2 . The procedure is readily applied when the first reflection from the load is separated in time from the other multiple reflections present. In this case it is only necessary to correct for the distortion caused by the input interface.

The first reflection from the load, shown in figure 47 as arriving at time t_2 , has the form

$$v_2(t) = [\delta(t) - \rho_1(t) * \rho_1(t)] * \rho_2(t) * v_i(t) \quad (79)$$

which transforms to the frequency domain as

$$V_2(\omega) = [1 - \rho_1^2(\omega)] \rho_2(\omega) V_i(\omega) \quad (80)$$

The input interface reflection coefficient ρ_1 is determined from the first reflection, which arrives at time t_1 , and has the form

$$v_1(t) = \rho_1(t) * v_i(t) \quad (81)$$

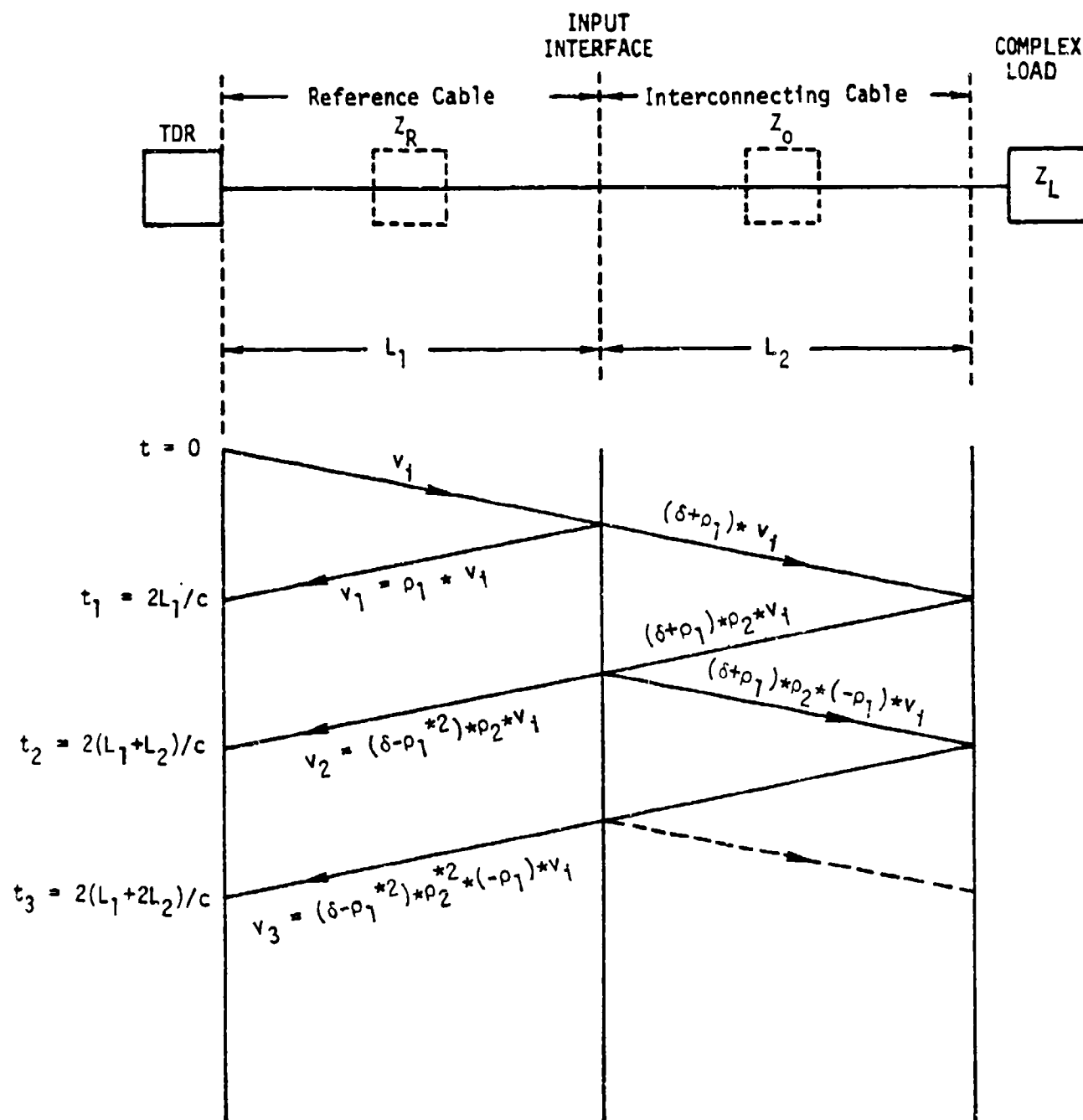


Figure 47. Multiple Reflection Diagram

Transforming to the frequency domain and solving for $\rho_1(\omega)$ gives

$$\rho_1(\omega) = \frac{V_1(\omega)}{V_i(\omega)} \quad (82)$$

Equation (80) is then solved for $\rho_2(\omega)$. The result is

$$\rho_2(\omega) = \frac{V_2(\omega)}{V_i(\omega)} \left\{ 1 - \left[\frac{V_1(\omega)}{V_i(\omega)} \right]^2 \right\}^{-1} \quad (83)$$

The load impedance is given by equation (17) with $\rho_2(\omega)$ from equation (83) substituted for ρ .

4. PRACTICAL CONSIDERATIONS

In many practical installations the cable runs may not be longitudinally or cross sectionally uniform and full characterization of the cable parameters may not be possible. These cases can sometimes be modeled as uniform line segments as discussed in section IV. Estimates of the transmission line properties of some inaccessible segments may then be necessary while partial characterization of those which are accessible can still be carried out. For example, the approximate line characteristics can be obtained by computing the approximate per unit-length inductance matrix, which is not affected by the inhomogeneity of the dielectric in the cable cross section. Relatively simple formulas which depend only on the cable geometry are available for these computations (ref. 24). The estimated inductance matrix and measured admittance matrix, based on the techniques of section III, can then be used to compute the capacitance matrix from equation (35). The L and C matrices completely specify the line characteristics (assumed lossless) since the eigenvalues and eigenvectors of the LC product are directly related to the modal amplitudes and modal velocities that the line will support.

The bulk or common mode impedance of segmented lines can be determined in some cases by an extension of the method illustrated in figure 44. In the analysis each reflected pulse observed back at the input measurement point is corrected for transmission through the discontinuities that lie between the measurement point and the reflection points. The individual reflected pulses from each segment can be unfolded in turn and used to compute the bulk characteristic impedance of each segment.

The pulse response of a line can be determined in a similar manner. For a line with a total of N discontinuities, the output pulse is just the product of the transmission coefficients and the input pulse

$$V_L = (\tau_1 \cdot \tau_2 \cdots \tau_N) V_i \quad (84)$$

where τ_N is the transmission coefficient of the N^{th} discontinuity, $\tau_N = (1 + \rho_N)$.

The common mode propagation velocity on cables of unknown length can be determined by introducing an external load at a known distance from the input and measuring the round trip travel time for reflection from the load. This can be accomplished by wrapping the cable with a grounded strip of conducting tape or foil, which acts as a capacitive load and produces a sharp reflection at the load point.

As an example, the sharp reflection shown on the TDR record of figure 48 was produced by placing a grounded two-inch wide strip of aluminum tape around a multiconductor at a point 5 meters from the free end.

The accuracy of time domain measurements on multiconductors is affected by small irregularities in the line cross section which causes partial reflections to occur over the entire line length. These effects appear

as noise superimposed on the main signal and reduce the accuracy of the measurements. Both the indirect and the direct methods for the determination of characteristic impedance or admittance are susceptible to noise. The first involves differences of small numbers and the latter involves the measurement of low signal levels.

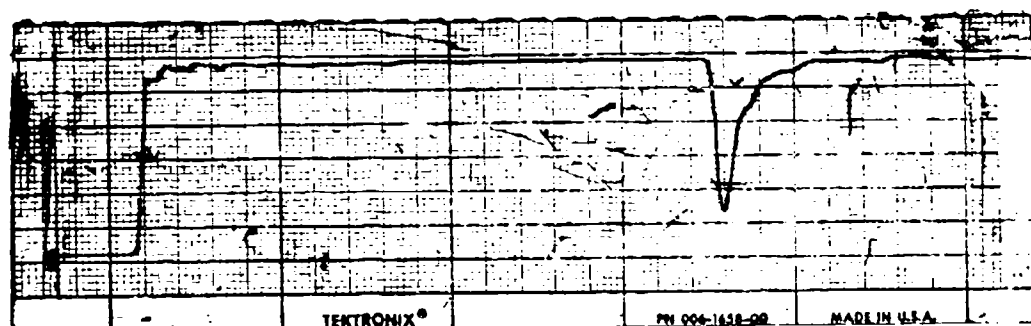


Figure 48. Example of the reflection produced by foil tape around a multiconductor. Vertical sens: 100 mp/div; horizontal sens: 0.305 m/div.

REFERENCES

1. Electromagnetic Pulse Handbook for Missiles and Aircraft in Flight. EMP Interaction Note 1-1, Sandia Laboratories, Albuquerque, NM, September 1972.
2. Frankel, S., Cable and Multiconductor Transmission Line Analysis. WOL-TR-091, Harry Diamond Labs, Washington, D.C., June 1974.
3. Pipes, L. A., "Matrix Theory of Multiconductor Transmission Lines," Phil. Mag., Vol. 24, pp. 97-113, July 1937.
4. Marx, R. D., "Propagation Modes, Equivalent Circuits, and Characteristic Terminations for Multiconductor Transmission Lines with Inhomogeneous Dielectrics," IEEE Trans. MTT, Vol. MTT-21, No. 7, July 1973.
5. Baum, C. E., T. K. Liu and F. M. Tesche, "On the General Analysis of Multiconductor Transmission Line Networks," AFML EMP Interaction Notes, Air Force Weapons Laboratory, Kirtland AFB, NM, to be published.
6. Baum, C. E., T. K. Liu, F. M. Tesche and S. K. Chang, "Numerical Results for Multiconductor Transmission Line Networks," AFML EMP Interaction Notes, Note 322, Air Force Weapons Laboratory, Kirtland AFB, NM, September 1977.
7. Paul, C. R., "On Uniform Multimode Transmission Lines," IEEE Trans. MTT, Vol. MTT-21, No. 8, pp. 556-558, August 1973.
8. Paul, C. R., "Useful Matrix Chain Parameter Identities for the Analysis of Multiconductor Transmission Lines," IEEE Trans. MTT, Vol. MTT-23, pp. 756-760, September 1975.
9. Paul, C. R., "Efficient Numerical Computation of the Frequency Response of Cables Illuminated by an Electromagnetic Field," IEEE Trans. MTT, Vol. MTT 22, No. 4, pp. 454-457, April 1974.
10. Amdinva, H., "Time Domain Analysis of Multiple Parallel Transmission Lines," RCA Review, pp. 241-276, June 1967.
11. Kunznetsov, P. I. and R. L. Stratonovich, The Propagation of Electromagnetic Waves in Multiconductor Transmission Lines. Oxford, England: Pergamon Press, 1964.
12. Chang, S. Y., "Transient Analysis of Lossless Coupled Transmission Lines in a Nonhomogeneous Dielectric Medium," IEEE Trans. MTT, Vol. MTT-18, No. 9, pp. 616-626, September 1970.

REFERENCES (Continued)

13. Krage, M. K. and G. I. Mammad, "Characteristics of Coupled Microstrip Transmission Lines With Inhomogeneous Dielectrics," IEEE Trans. MTT, Vol. MTT-21, No. 7, July 1973.
14. Scheikunoff, S. A., "Conversion of Maxwell's Equations Into Generalized Telegrapher's Equations," Bell System Technical Journal, Vol. 34, pp. 995-1043, September 1955.
15. Ramo, S., J. R. Whinnery and T. V. Duzer, Fields and Waves in Communication Electronics. New York: John Wiley & Sons, Inc., 1965.
16. Clements, J. C., C. R. Paul and A. T. Adams, "Computation of the Capacitance Matrix for Systems of Dielectric-Coated Cylindrical Conductors," IEEE Trans. EMC, Vol. EMC-17, No. 4, pp. 238-248, November 1975.
17. Paul, C. R. and A. E. Feather, "Computation of the Transmission Line Inductance and Capacitance Matrices from the Generalized Capacitance Matrix," IEEE Trans. EMC, Vol. EMC-18, No. 4, pp. 175-183, November 1976.
18. Agrawal, A. K., H. M. Fowles and L. D. Scott, "Experimental Characterization of Multiconductor Transmission Lines in Inhomogeneous Media Using Time Domain Techniques," AFML EMP Interaction Notes, Note 332, Air Force Weapons Laboratory, Kirtland AFB, NM.
19. Carey, V. L., T. R. Scott and M. T. Weeks, "Characterization of Multiple Parallel Transmission Lines Using Time Domain Reflectometry," IEEE Trans. IM, Vol. IM-18, No. 3, September 1969.
20. Collin, R. E., Foundations for Microwave Engineering. New York: McGraw-Hill, 1966.
21. Fowles, H. M., L. D. Scott, A. K. Agrawal and K. M. Lee, Aircraft Cable Parameter Study, AFML-TR-77-177, Air Force Weapons Laboratory, Kirtland AFB, NM, July 1977.
22. Bewley, L. V., Traveling Waves on Transmission Systems. New York: John Wiley & Sons, Inc., 1951.
23. Agrawal, A. K., K. M. Lee, L. D. Scott and H. M. Fowles, "Experimental Characterization of Multiconductor Transmission Lines in Frequency Domain," AFML EMP Interaction Notes, Note 311, Air Force Weapons Laboratory, Kirtland Air Force Base, NM, June 1977.
24. Grover, F. W., Inductance Calculations: Working Formulas and Tables. New York: Dover Publications, Inc., 1962.

APPENDIX

EXPERIMENTAL CHARACTERIZATION OF MULTICONDUCTOR TRANSMISSION LINES IN FREQUENCY DOMAIN

ABSTRACT

Although a number of papers have been published on the experimental characterization of multiconductor transmission lines, they are limited to the time domain for lossless multiconductor lines in homogeneous media. This appendix presents a method for the complete characterization of multiconductor transmission lines in inhomogeneous media. The experimental technique for the measurement of multiconductor line parameters is presented and the appropriate multiconductor line equations are solved to obtain these parameters. The experimental method is simple and involves only the short- and open-circuit impedance measurements for different configurations. The experimental results for multiconductors containing three, four, and five wires above a ground plane are found to be in good agreement with computed results and a low-frequency lumped model.

SECTION A-1

INTRODUCTION

The problem of multiconductor transmission line characterization has been a topic of interest for many years. Previous work (refs. 1, 2) provides methods of characterization for multiconductor lines in homogeneous media in the time domain, in which case, all the propagation modes have the same phase velocity. In general, for a multiconductor line (N conductors plus a ground reference) in an inhomogeneous medium, there will be N propagation modes each having a different phase velocity, and the inductance per unit-length and capacitance per unit-length matrices can not be obtained from the characteristic impedance matrix without the knowledge of the propagation matrix (refs. 3, 4).

Analysis of multiconductor transmission lines in frequency domain have been reported by several investigators (refs. 5, 6, 7, 8, 9, 10). Some useful matrix chain parameters were derived (ref. 5). Propagation modes and characteristics for multiconductor transmission lines with inhomogeneous dielectrics are discussed in reference 8. Measurement methods of the cable parameters at low frequencies have been presented (ref. 11); the correlation between the theoretical model and the measured data, to date, has not been entirely satisfactory (ref. 12).

This appendix describes a measurement technique for determining the parameters for a general parallel multiconductor transmission line system in the frequency domain. The measurement technique is an extension of the well known single-frequency technique for measuring the constants of a two-conductor line. It consists of measuring the impedances between all pairs of conductors under both short- and open-circuit load conditions with specific source conditions. A method of calculation utilizing a series of similarity transformations for obtaining the appropriate parameters from the measured data is used in solving the complex multiconductor equations.

SECTION A-1

INTRODUCTION

The problem of multiconductor transmission line characterization has been a topic of interest for many years. Previous work (refs. 1, 2) provides methods of characterization for multiconductor lines in homogeneous media in the time domain, in which case, all the propagation modes have the same phase velocity. In general, for a multiconductor line (N conductors plus a ground reference) in an inhomogeneous medium, there will be N propagation modes each having a different phase velocity, and the inductance per unit-length and capacitance per unit-length matrices can not be obtained from the characteristic impedance matrix without the knowledge of the propagation matrix (refs. 3, 4).

Analysis of multiconductor transmission lines in frequency domain have been reported by several investigators (refs. 5, 6, 7, 8, 9, 10). Some useful matrix chain parameters were derived (ref. 5). Propagation modes and characteristics for multiconductor transmission lines with inhomogeneous dielectrics are discussed in reference 8. Measurement methods of the cable parameters at low frequencies have been presented (ref. 11); the correlation between the theoretical model and the measured data, to date, has not been entirely satisfactory (ref. 12).

This appendix describes a measurement technique for determining the parameters for a general parallel multiconductor transmission line system in the frequency domain. The measurement technique is an extension of the well known single-frequency technique for measuring the constants of a two-conductor line. It consists of measuring the impedances between all pairs of conductors under both short- and open-circuit load conditions with specific source conditions. A method of calculation utilizing a series of similarity transformations for obtaining the appropriate parameters from the measured data is used in solving the complex multiconductor equations.

SECTION A-2

THEORETICAL BACKGROUND

Consider a line formed by N conductors, plus reference conductor ground. The line is assumed to be uniform along its length (z coordinate), but with arbitrary cross section. In general, the dielectric surrounding the line is inhomogeneous (e.g., cable made of insulated conductors with different dielectric constants).

In the presence of materials having different dielectric constants, the propagation mode can not in general be TEM. However, the low-frequency propagation mode is "quasi-TEM" (refs. 13, 14) and analysis can proceed from the generalized telegrapher's equations. These equations are (refs. 7, 13)

$$\frac{\partial [V_n(z,t)]}{\partial z} = -[R'_{nm}][i_m(z,t)] - [L'_{nm}] \frac{\partial [i_m(z,t)]}{\partial t} \quad (A-1a)$$

$$\frac{\partial [i_n(z,t)]}{\partial z} = -[G'_{nm}][V_m(z,t)] - [C'_{nm}] \frac{\partial [V_m(z,t)]}{\partial t} \quad (A-1b)$$

with $n = 1, 2, \dots, N$
 $m = 1, 2, \dots, N.$

where V_m and i_m represent the voltage with respect to the reference conductor and current on the m th conductor, respectively, as a function of distance z along the line and time, t . $[R'_{nm}]$, $[L'_{nm}]$, $[C'_{nm}]$ and $[G'_{nm}]$ are respectively per unit length resistance, and coefficients of inductance, capacitance and conductance matrices of $N \times N$ size. The resistance per unit-length matrix is in general diagonal and the others are symmetric. Also, in $[L'_{nm}]$, $[C'_{nm}]$ and $[G'_{nm}]$, the diagonal elements are self and the off diagonal elements are mutual quantities. The elements of the capacitance matrix $[C'_{nm}]$ and inductance matrix $[L'_{nm}]$ are further characterized by the following properties (ref. 15)

$$L'_{nm} \geq 0 \text{ for all } n \text{ and } m$$

$$C'_{nn} \geq 0 \text{ for all } n$$

$$C'_{nm} \leq 0 \text{ for all } n \neq m \quad (A-2)$$

$$\sum_{m=1}^N C'_{nm} \geq 0 \text{ for all } n$$

$$\sum_{n=1}^N C'_{nm} \geq 0 \text{ for all } m$$

We can rewrite equations (A-1a) and (A-1b) as

$$\frac{d}{dz} [\tilde{V}_n(z,s)] = -[Z'_{nm}(s)][\tilde{I}_m(z,s)] \quad (A-3a)$$

$$\frac{d}{dz} [\tilde{I}_n(z,s)] = -[Y'_{nm}(s)][\tilde{V}_m(z,s)] \quad (A-3b)$$

where $\tilde{V}_n(z,s)$ and $\tilde{I}_n(z,s)$ are the Laplace transforms of vectors $V_n(z,t)$ and $I_n(z,t)$, and $Z'_{nm}(z,s) = R'_{nm} + sL'_{nm}$ and $Y'_{nm}(z,s) = G'_{nm} + sC'_{nm}$ are the per unit-length series impedance and shunt admittance between n th and m th conductors. $s = \sigma + j\omega$. In general s is a complex frequency, but for sinusoidal excitation of the line we have $s = j\omega$.

The solution of the coupled set of equations (A-3a, A-3b) in general is given in the following form by Paul (refs. 5,6) as

$$\begin{bmatrix} \tilde{V}_n(z,s) \\ \tilde{I}_n(z,s) \end{bmatrix} = [s(z-z_0)^{-1}] \begin{bmatrix} \tilde{V}_n(z_0,s) \\ \tilde{I}_n(z_0,s) \end{bmatrix} \quad (A-4)$$

where z_0 is a suitably chosen reference location, and the characteristic impedance matrix $[Z_{c_{nm}}(s)]$ can be expressed in two forms (ref. 5) as

$$[Z_{c_{nm}}(s)] = [Y_{nm}^-(s)]^{-1} \left\{ [Y_{nm}^-(s)] [Z_{nm}^-(s)] \right\}^{\frac{1}{2}} = [Z_{nm}^-(s)] \left\{ [Y_{nm}^-(s)] [Z_{nm}^-(s)] \right\}^{-\frac{1}{2}} \quad (A-5)$$

and

$$[Z_{c_{nm}}(s)] = \left\{ [Z_{nm}^-(s)] [Y_{nm}^-(s)] \right\}^{\frac{1}{2}} [Y_{nm}^-(s)]^{-1} = \left\{ [Z_{nm}^-(s)] [Y_{nm}^-(s)] \right\}^{-\frac{1}{2}} [Z_{nm}^-(s)] \quad (A-6)$$

The order of multiplication of matrices is important and in general, $[Z_{nm}^-(s)] [Y_{nm}^-(s)] \neq [Y_{nm}^-(s)] [Z_{nm}^-(s)]$.

The chain parameter matrix, $[a(l)]$, may be expressed in partitioned form as

$$[a(l)] = \begin{bmatrix} [a_{11}(l)] & [a_{12}(l)] \\ [a_{21}(l)] & [a_{22}(l)] \end{bmatrix} \quad (A-7)$$

where submatrices $[a_{11}(l)]$, $[a_{12}(l)]$, $[a_{21}(l)]$ and $[a_{22}(l)]$ are of $N \times N$ order. The submatrices are expressed as follows (ref. 5):

$$\begin{aligned} [a_{11}(l)] &= [Y_{nm}^-(s)]^{-1} \left\{ \cosh \left\{ ([Y_{nm}^-(s)] [Z_{nm}^-(s)])^{\frac{1}{2}} l \right\} \right\} [Y_{nm}^-(s)] \\ &= \cosh \left\{ ([Z_{nm}^-(s)] [Y_{nm}^-(s)])^{\frac{1}{2}} l \right\} \end{aligned} \quad (A-8a)$$

$$\begin{aligned} [a_{12}(l)] &= -[Z_{c_{nm}}(s)] \left\{ \sinh \left\{ ([Y_{nm}^-(s)] [Z_{nm}^-(s)])^{\frac{1}{2}} l \right\} \right\} \\ &= -\left\{ \sinh \left\{ ([Z_{nm}^-(s)] [Y_{nm}^-(s)])^{\frac{1}{2}} l \right\} \right\} [Z_{c_{nm}}(s)] \end{aligned} \quad (A-8b)$$

$$\begin{aligned} [a_{21}(l)] &= -\left\{ \sinh \left\{ ([Y_{nm}^-(s)] [Z_{nm}^-(s)])^{\frac{1}{2}} l \right\} \right\} [Z_{c_{nm}}(s)]^{-1} \\ &= -[Z_{c_{nm}}(s)]^{-1} \left\{ \sinh \left\{ ([Z_{nm}^-(s)] [Y_{nm}^-(s)])^{\frac{1}{2}} l \right\} \right\} \end{aligned} \quad (A-8c)$$

$$\begin{aligned}
[\phi_{22}(L)] &= \cosh \left\{ ([Y_{nm}^*(s)][Z_{nm}^*(s)])^{\frac{1}{2}} L \right\} \\
&= [Y_{nm}^*(s)] \left\{ \cosh \left\{ ([Z_{nm}^*(s)][Y_{nm}^*(s)]^{\frac{1}{2}} L \right\} \right\} [Y_{nm}^*(s)]^{-1}
\end{aligned} \tag{A-8d}$$

The matrices $[\phi_{11}]$, $[\phi_{12}]$, $[\phi_{21}]$, and $[\phi_{22}]$ also satisfy the following identities (ref. 5):

$$[\phi_{12}][\phi_{22}][\phi_{12}]^{-1} = [\phi_{11}] \tag{A-9a}$$

$$[\phi_{21}][\phi_{11}][\phi_{21}]^{-1} = [\phi_{22}] \tag{A-9b}$$

and

$$[\phi_{11}(-L)] = [\phi_{11}(L)] \tag{A-10a}$$

$$[\phi_{22}(-L)] = [\phi_{22}(L)] \tag{A-10b}$$

$$[\phi_{12}(-L)] = -[\phi_{12}(L)] \tag{A-10c}$$

$$[\phi_{21}(-L)] = -[\phi_{21}(L)] \tag{A-10d}$$

With the above described theoretical background, we will now proceed in Section III to represent the line constants in terms of experimentally measured quantities, e.g., input impedance and admittance matrices.

SECTION A-3

DERIVATION OF PARAMETERS IN TERMS OF INPUT IMPEDANCE AND ADMITTANCE MATRICES

Consider that the load is located at $z_0 = 0$, then equation (A-4) becomes

$$\begin{bmatrix} \bar{V}_n(z,s) \\ \bar{I}_n(z,s) \end{bmatrix} = [a(z)] \begin{bmatrix} \bar{V}_n(0,s) \\ \bar{I}_n(0,s) \end{bmatrix} \quad (A-11)$$

Furthermore, it follows from the boundary condition at the load end, that

$$[\bar{V}_n(0,s)] = [Z_{Lnm}][\bar{I}_n(0,s)] \quad (A-12)$$

where $[Z_{Lnm}]$ is the load impedance matrix.

The voltage and current vectors at the input end of the line at $z = -L$ can be obtained from equations (A-6) and (A-11) as

$$\begin{aligned} [\bar{V}_n(-L,s)] &= \left\{ \cosh \left\{ ([Z_{nm}^0(s)][Y_{nm}^0(s)])^{\frac{1}{2}} L \right\} \right\} [\bar{V}_n(0,s)] \\ &\quad + \sinh \left\{ ([Z_{nm}^0(s)][Y_{nm}^0(s)])^{\frac{1}{2}} L \right\} [Z_{Cnm}(s)][\bar{I}_n(0,s)] \end{aligned} \quad (A-13a)$$

$$\begin{aligned} [\bar{I}_n(-L,s)] &= [Z_{Cnm}(s)]^{-1} \left\{ \sinh \left\{ ([Z_{nm}^0(s)][Y_{nm}^0(s)])^{\frac{1}{2}} L \right\} \right\} [\bar{V}_n(0,s)] \\ &\quad + [Y_{nm}^0(s)] \left\{ \cosh \left\{ ([Z_{nm}^0(s)][Y_{nm}^0(s)])^{\frac{1}{2}} L \right\} \right\} [Z_{Cnm}(s)]^{-1} [\bar{I}_n(0,s)] \end{aligned} \quad (A-13b)$$

For the short circuit load condition (i.e., all the conductors are shorted to the ground or reference conductor), $[Z_{Lnm}] = [0_{nm}]$ and $[\bar{V}_n(0,s)] = [0_{nm}]$. Then equation (A-13) becomes

$$[\bar{V}_n^{SC}(-L, s)] = \left\{ \sinh \left\{ ([Z_{nm}^{SC}(s)][Y_{nm}^{SC}(s)])^{\frac{1}{2}} L \right\} \right\} [Z_{Cnm}(s)] [\bar{I}_n(0, s)] \quad (A-14a)$$

$$[\bar{I}_n^{SC}(-L, s)] = [Y_{nm}^{SC}(s)] \left\{ \cosh \left\{ ([Z_{nm}^{SC}(s)][Y_{nm}^{SC}(s)])^{\frac{1}{2}} L \right\} \right\} [Y_{nm}^{SC}(s)]^{-1} [\bar{I}_n(0, s)] \quad (A-14b)$$

Let $[Z]_{nm}^{SC}(s)$ be the input impedance matrix when the load $[Z]_{nm} = [Z_{Cnm}]$, then the voltage and current vectors in equation (A-14) at the input end ($z = -L$) are related by

$$[\bar{V}_n^{SC}(-L, s)] = [Z]_{nm}^{SC}(s) [\bar{I}_n^{SC}(-L, s)] \quad (A-15)$$

Substituting equation (A-15) in equation (A-14), and rearranging we obtain

$$\begin{aligned} [Z]_{nm}^{SC}(s) [\bar{I}_n^{SC}(-L, s)] &= [Y_{nm}^{SC}(s)] \left\{ \cosh \left\{ ([Z_{nm}^{SC}(s)][Y_{nm}^{SC}(s)])^{\frac{1}{2}} L \right\} \right\} [Z_{Cnm}(s)]^{-1} \\ &\quad \times \left\{ \sinh \left\{ ([Z_{nm}^{SC}(s)][Y_{nm}^{SC}(s)])^{\frac{1}{2}} L \right\} \right\} [Z_{Cnm}(s)]^{-1} \end{aligned} \quad (A-16)$$

Pre-multiplying both sides by

$$\left\{ \sinh \left\{ ([Z_{nm}^{SC}(s)][Y_{nm}^{SC}(s)])^{\frac{1}{2}} L \right\} \right\} [Z_{Cnm}(s)]$$

in the above equation and using the identity (equation (A-9a)), we obtain

$$[Z]_{nm}^{SC}(s) = \left\{ \tanh \left\{ ([Z_{nm}^{SC}(s)][Y_{nm}^{SC}(s)])^{\frac{1}{2}} L \right\} \right\} [Z_{Cnm}(s)] \quad (A-17)$$

where, the definition

$$\begin{aligned} \tanh \left\{ ([Z_{nm}^{SC}(s)][Y_{nm}^{SC}(s)])^{\frac{1}{2}} L \right\} &= \left\{ \frac{\cosh \left\{ ([Z_{nm}^{SC}(s)][Y_{nm}^{SC}(s)])^{\frac{1}{2}} L \right\} - 1}{\cosh \left\{ ([Z_{nm}^{SC}(s)][Y_{nm}^{SC}(s)])^{\frac{1}{2}} L \right\} + 1} \right\} \\ &\quad \times \left\{ \sinh \left\{ ([Z_{nm}^{SC}(s)][Y_{nm}^{SC}(s)])^{\frac{1}{2}} L \right\} \right\} \end{aligned}$$

has been used. The order of multiplication of the two matrices on the right hand side does not matter, since it can be readily shown that the two functions of the same matrix commute.

For the open circuit load conditions, $[I_{nm}(0,s)] = [0_{nm}]$ and equation (A-13) becomes

$$[\tilde{V}_n^{OC}(-L,s)] = \left\{ \cosh \left\{ ([Z_{nm}'(s)][Y_{nm}'(s)])^{1/2} L \right\} \right\} [\tilde{V}_n(0,s)] \quad (A-16a)$$

$$[\tilde{I}_n^{OC}(-L,s)] = [Z_{c_{nm}}(s)]^{-1} \left\{ \sinh \left\{ ([Z_{nm}'(s)][Y_{nm}'(s)])^{1/2} L \right\} \right\} [\tilde{V}_n(0,s)] \quad (A-16b)$$

Let $[Z_{in_{nm}}^{OC}(s)]$ be the input impedance matrix when the load $[Z_{L_{nm}}] = [Z_{nm}]$, then the voltage and current vectors in equation (A-16) at the input and $(z = -L)$ are related by

$$[\tilde{V}_n^{OC}(-L,s)] = [Z_{in_{nm}}^{OC}(s)][\tilde{I}_n^{OC}(-L,s)] \quad (A-17)$$

Substituting equation (A-16) in equation (A-17) and rearranging we obtain

$$[Z_{in_{nm}}^{OC}(s)] = \left\{ \cosh \left\{ ([Z_{nm}'(s)][Y_{nm}'(s)])^{1/2} L \right\} \right\}^{-1} [Z_{c_{nm}}(s)] \quad (A-18)$$

Thus equations (A-17) and (A-18) give the input impedance matrices for the short- and open-circuit load conditions. Using the second form of $[Z_{nm}]$ in terms of $[Y_{nm}'(s)][Z_{nm}'(s)]$, it can easily be shown that

$$[Z_{in_{nm}}^{SC}(s)] = [Z_{c_{nm}}(s)] \left\{ \tanh \left\{ ([Y_{nm}'(s)][Z_{nm}'(s)])^{1/2} L \right\} \right\} \quad (A-19)$$

$$[Z_{in_{nm}}^{OC}(s)] = [Z_{c_{nm}}(s)] \left\{ \tanh \left\{ ([Y_{nm}'(s)][Z_{nm}'(s)])^{1/2} L \right\} \right\}^{-1} \quad (A-20)$$

This formulation clearly shows that matrices $\{Y_{nm}^I(s)\}$ and $\{Z_{nm}^I(s)\}$ do not commute, their order of multiplication should be properly maintained. However, it can be shown that $\{Y_{nm}^I(s)\}\{Z_{nm}^I(s)\}$ and $\{Z_{nm}^I(s)\}\{Y_{nm}^I(s)\}$ have the same eigenvalues (ref. 6).

Define

$$\{T_{nm}^I(s)\} = \{[Z_{nm}^I(s)][Y_{nm}^I(s)]\}^{\frac{1}{2}} \quad (A-23)$$

Then, equations (A-17) and (A-20) can be written as

$$\{Z_{nm}^{SC}(s)\} = \left[\tanh(\{T_{nm}^I(s)\}L) \right] \{Z_{nm}^I(s)\} \quad (A-24)$$

$$\{Z_{nm}^{SC}(s)\} = \left[\tanh(\{T_{nm}^I(s)\}L) \right]^T \{Z_{nm}^I(s)\} \quad (A-25)$$

Equations (A-24) and (A-25) can now be solved for $\{Z_{nm}^I(s)\}$ and $\{Y_{nm}^I(s)\}$ in terms of $\{Z_{nm}^{SC}(s)\}$ and $\{Z_{nm}^{SC}(s)\}$ and then from equation (A-6), the per unit length series impedance and shunt admittance matrices can be obtained.

From equation (A-25)

$$\{Z_{nm}^{SC}(s)\}^{-1} = \{Z_{nm}^I(s)\}^{-1} \left[\tanh(\{T_{nm}^I(s)\}L) \right] \quad (A-26)$$

Postmultiplying equation (A-24) by equation (A-26) and taking the positive square root of it, we obtain

$$\tanh(\{T_{nm}^I(s)\}L) = \left\{ \{Z_{nm}^{SC}(s)\} \{Z_{nm}^{SC}(s)\}^{-1} \right\}^{\frac{1}{2}} \quad (A-27)$$

or,

$$\{T_{nm}^I(s)\} = \frac{1}{L} \operatorname{arctanh} \left(\{Z_{nm}^{SC}(s)\} \{Z_{nm}^{SC}(s)\}^{-1} \right)^{\frac{1}{2}} \quad (A-28)$$

To solve for the characteristic impedance matrix $[Z_{c_{nm}}(s)]$, premultiply both sides of equation (A-24) by

$$\left[\tanh [T_{nm}^c(s)]L \right]^{-1}$$

to obtain

$$\left[\tanh ([T_{nm}^c(s)]L) \right]^{-1} [Z_{1_{nm}}^{sc}(s)] = [Z_{c_{nm}}(s)] \quad (A-29)$$

use equation (A-27) in equation (A-29) to obtain

$$[Z_{c_{nm}}(s)] = \left\{ [Z_{1_{nm}}^{sc}(s)] [Z_{1_{nm}}^{oc}(s)]^{-1} \right\}^{\frac{1}{2}} [Z_{1_{nm}}^{sc}(s)] \quad (A-30)$$

Thus once $[T_{nm}^c(s)]$ and $[T_{nm}^o(s)]$ are known, equations (A-26) and (A-30) give the matrices $[T_{nm}^c(s)]$ and $[Z_{c_{nm}}(s)]$. The eigenvalues of $[T_{nm}^c(s)]$ are the propagation constants for the different modes of propagation.

Using $[T_{nm}^c(s)]^2 = [Z_{c_{nm}}(s)]$ in equation (A-6) we can write the relations for $[Z_{c_{nm}}(s)]$ and $[V_{nm}^c(s)]$ matrices as,

$$[Z_{c_{nm}}(s)] = [T_{nm}^c(s)] [Z_{c_{nm}}(s)] \quad (A-31)$$

$$[V_{nm}^c(s)] = [Z_{c_{nm}}(s)]^{-1} [T_{nm}^c(s)] \quad (A-32)$$

Substituting for $[Z_{c_{nm}}(s)]$ and $[T_{nm}^c(s)]$ in equations (A-31) and (A-32) we arrive at

$$[Z_{c_{nm}}(s)] = \frac{1}{2} \left[\cosh ([Z_{1_{nm}}^{sc}(s)] [Z_{1_{nm}}^{oc}(s)]^{-1})^{\frac{1}{2}} \right] [Z_{c_{nm}}(s)] \quad (A-33)$$

$$[V_{nm}^c(s)] = \frac{1}{2} [Z_{c_{nm}}(s)]^{-1} \left[\cosh ([Z_{1_{nm}}^{sc}(s)] [Z_{1_{nm}}^{oc}(s)]^{-1})^{\frac{1}{2}} \right] \quad (A-34)$$

Since

$$[Z'_{nm}(s)] = [R'_{nm}] + s[L'_{nm}]$$

and

$$[Y'_{nm}(s)] = [G'_{nm}] + s[C'_{nm}]$$

and after setting $s = j\omega$, the per-unit-length parameters are given by

$$[R'_{nm}] = \operatorname{Re}[Z'_{nm}(s)] \quad (\text{A-35a})$$

$$[L'_{nm}] = \frac{1}{j\omega} \operatorname{Im}[Z'_{nm}(s)] \quad (\text{A-35b})$$

$$[G'_{nm}] = \operatorname{Re}[Y'_{nm}(s)] \quad (\text{A-35c})$$

$$[C'_{nm}] = \frac{1}{j\omega} \operatorname{Im}[Y'_{nm}(s)] \quad (\text{A-35d})$$

Thus from the knowledge of input impedance matrices for the short- and open circuit load conditions under prescribed source conditions, all the parameters of the multiconductor line can be obtained. Note that a similar solution can be obtained in terms of $[I'_{nm}][Z'_{nm}]$ giving the same final result.

In solving equations (A-28) and (A-30) for $[T'_{nm}(s)]$ and $[Z'_{nm}(s)]$, the calculation can be made easy when a series of similarity transformations are used. This simplification is based on the fact that, similar matrices have the same eigenvalues, and that, a polynomial matrix function $f([A'_{nm}])$ has eigenvalues $f(\lambda_n)$ when the matrix $[A'_{nm}]$ has eigenvalues λ_n . Also $f([A'_{nm}])$ has the same eigenvectors as those of $[A'_{nm}]$ (ref. 13). Thus, from the matrix

$$[A'_{nm}] = [Z'_{nm}(s)][Z'_{nm}(s)]^{-1}$$

one first determines its eigenvalues λ_n and corresponding eigenvectors $[U_n]$. From equation (A-29), it can be shown that $\tanh(\gamma_n l) = \sqrt{\lambda_n}$ where

γ_n is the n th eigenvalue of $[A_{nm}(s)]$. Since $[A_{nm}(s)]$ is a matrix function of $[A_{nm}]$, it can be determined from a similarity transformation, namely, $[A_{nm}(s)] = [X_{nm}][\Lambda_{nm}(s)][X_{nm}]^{-1}$, where $[X_{nm}]$ is the same as the eigenvector matrix of $[A_{nm}]$ and $[\Lambda_{nm}(s)]$ is a diagonal matrix formed by the eigenvalue γ_n 's. Calculation of $[Z_{nm}(s)]$ follows from equation (A-30) in a similar manner. This method of calculation offers a simple and straightforward procedure and is used in the following data reduction. Some other methods for the solution of such complex matrix equations are also available (ref. 16).

SECTION A-4

MEASUREMENT TECHNIQUE AND THE EXPERIMENTAL RESULTS

For the purposes of demonstrating the validity of the methods described, multiconductor lines of three-, four- and five-wires were constructed and tested. The experimental setup used is shown in figure A-1. The cross-sectional configurations of three-, four- and five-wire cables are shown in figures 2 and 6. These multiconductor cables were 20 meters in length, supported with Styrofoam blocks 4.16 cm above a 0.91 m by 21.33 m aluminum ground plane. Wires insulated with solid polyethylene, neoprene, rubber, foam polyethylene and semisolid polyethylene were used for the cable construction. The wires were wrapped with a dielectric tape to insure a constant cable cross section over the length of the cable. The wires were terminated in pin jacks so that each could be driven, shorted, or opened as necessary. Aluminum plates were placed at right angles to the ground plane at the driven and far ends of the cable in order to short the electric field at the cable end points and to provide a low impedance current path when a short circuit was required. A block diagram of the measurement setup is shown in figure A-2.

The voltage probe and current probe were selected to minimize probe loading effects. An active voltage probe with an input impedance of 1 M Ω , shunted by a capacitance of 1 pF was utilized for these measurements. The current probe was a clamp-on type with an insertion impedance of less than 0.1 Ω . The overall accuracy of the impedance measurements obtained was approximately $\pm 5\%$ over the frequency range studies.

The short circuit input impedance measurements were performed with the far end shorted (grounded) and the near end of all but the driver wire open (figure A-3a). The current in the driven wire and the voltage across each of the wires was measured with probes and the ratio of voltage to current was obtained as a function of frequency. This procedure was

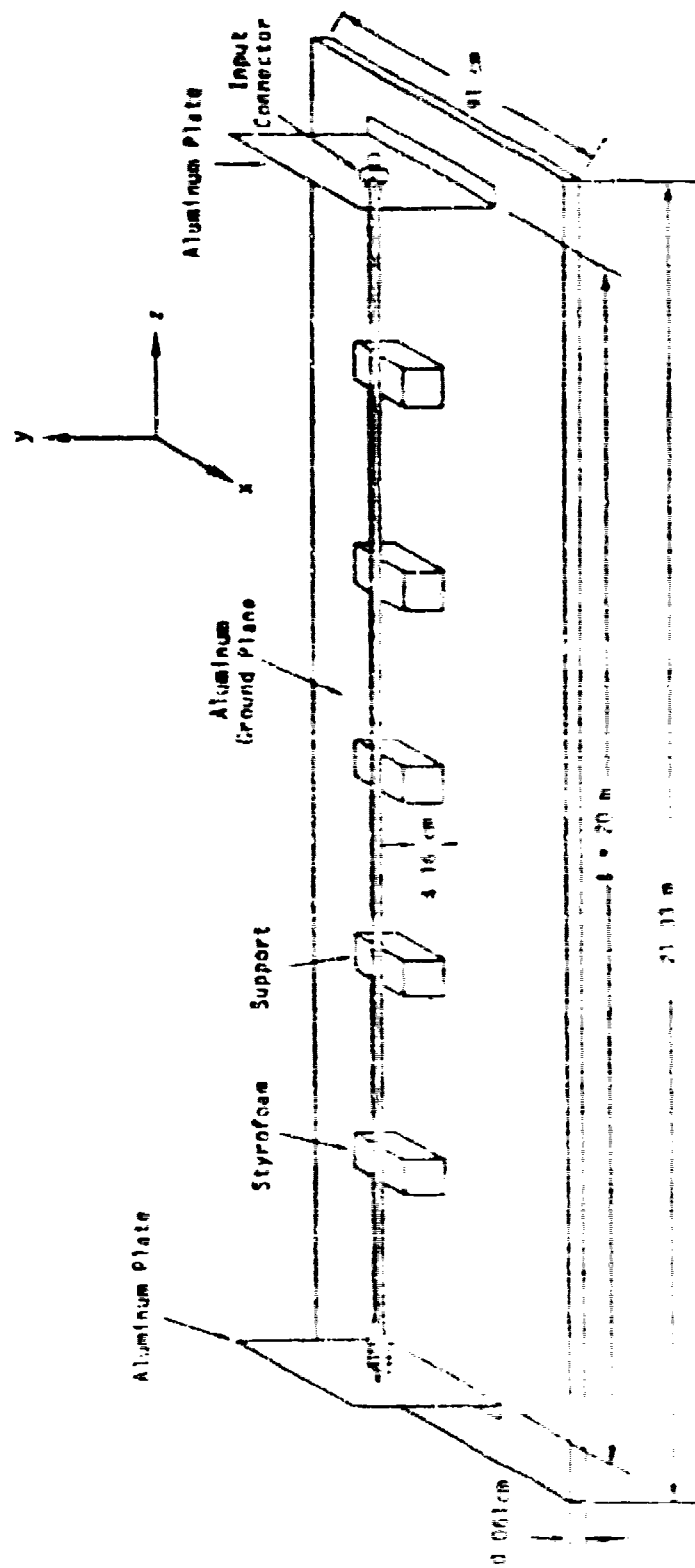


Figure A.1. Multiconductor Experimental Setup

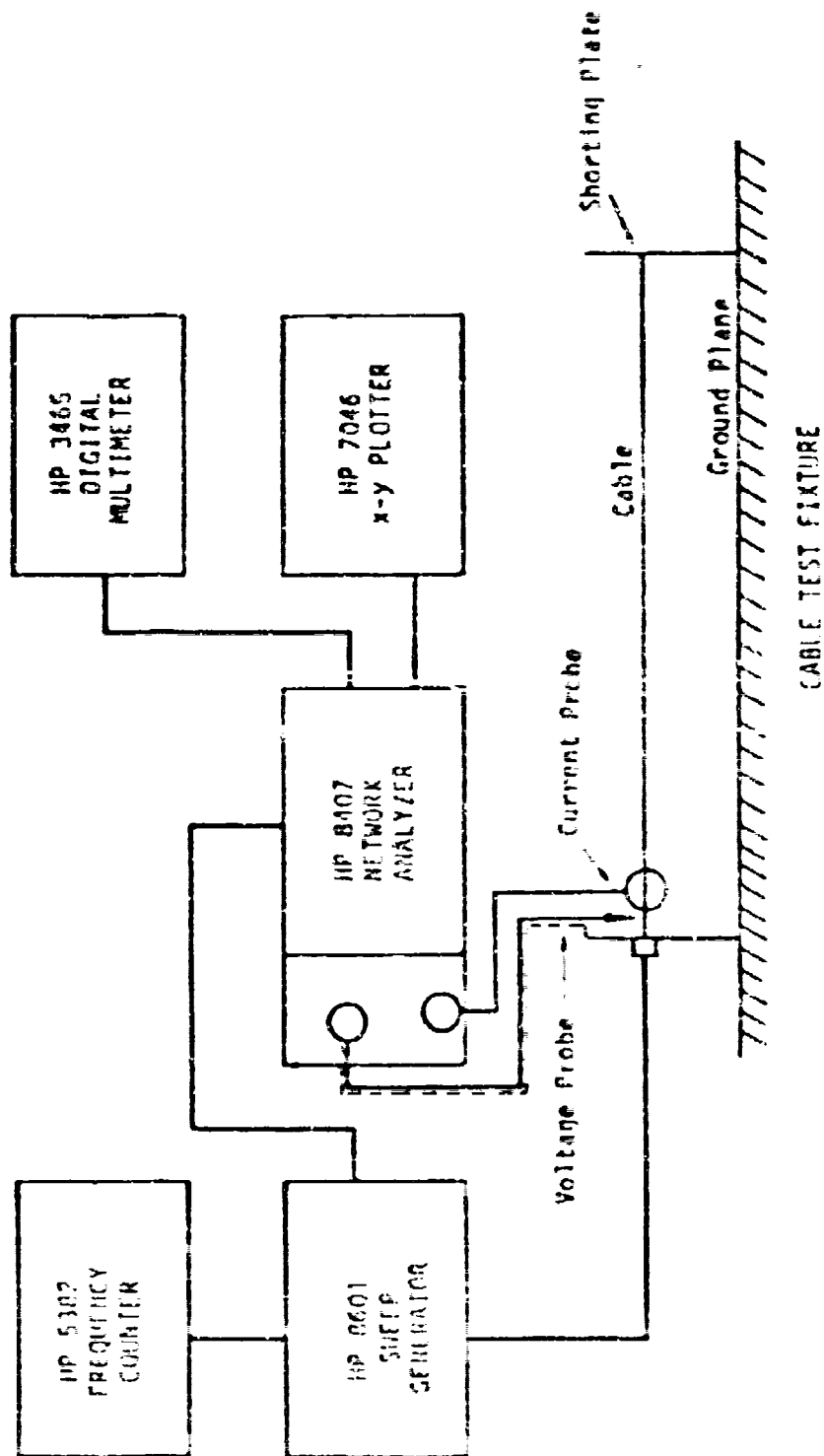


Figure A-2. Sweep Impedance Block Diagram

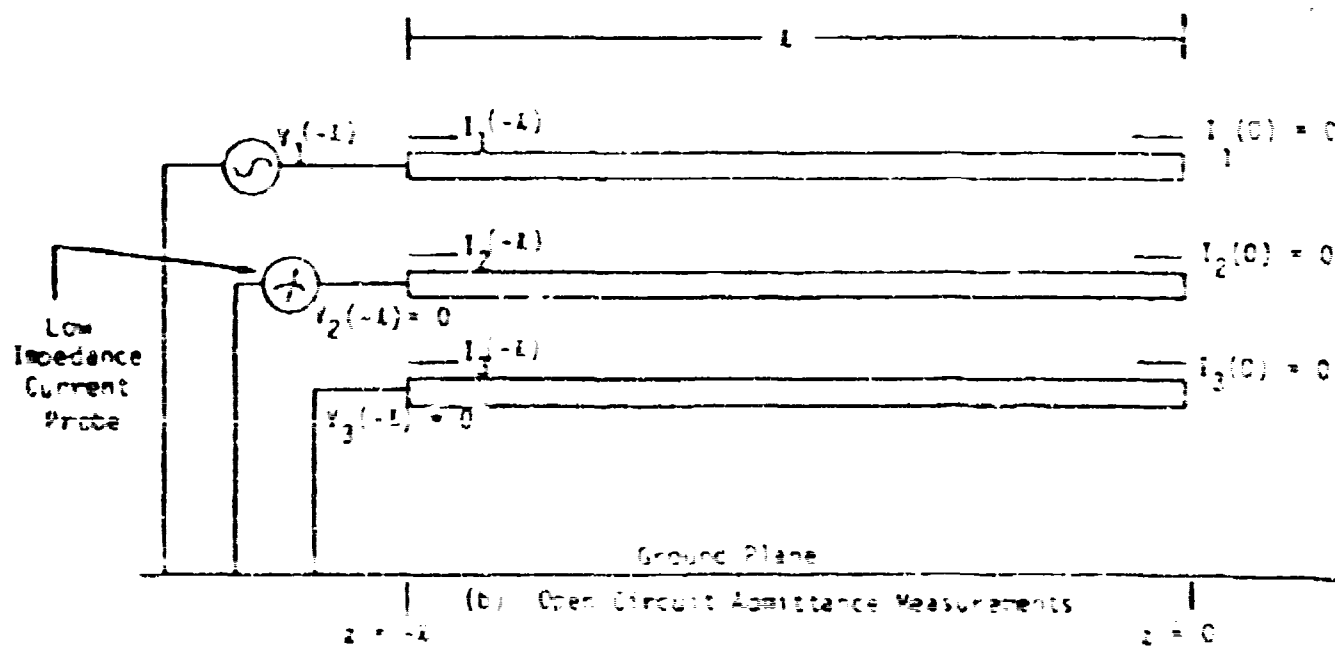
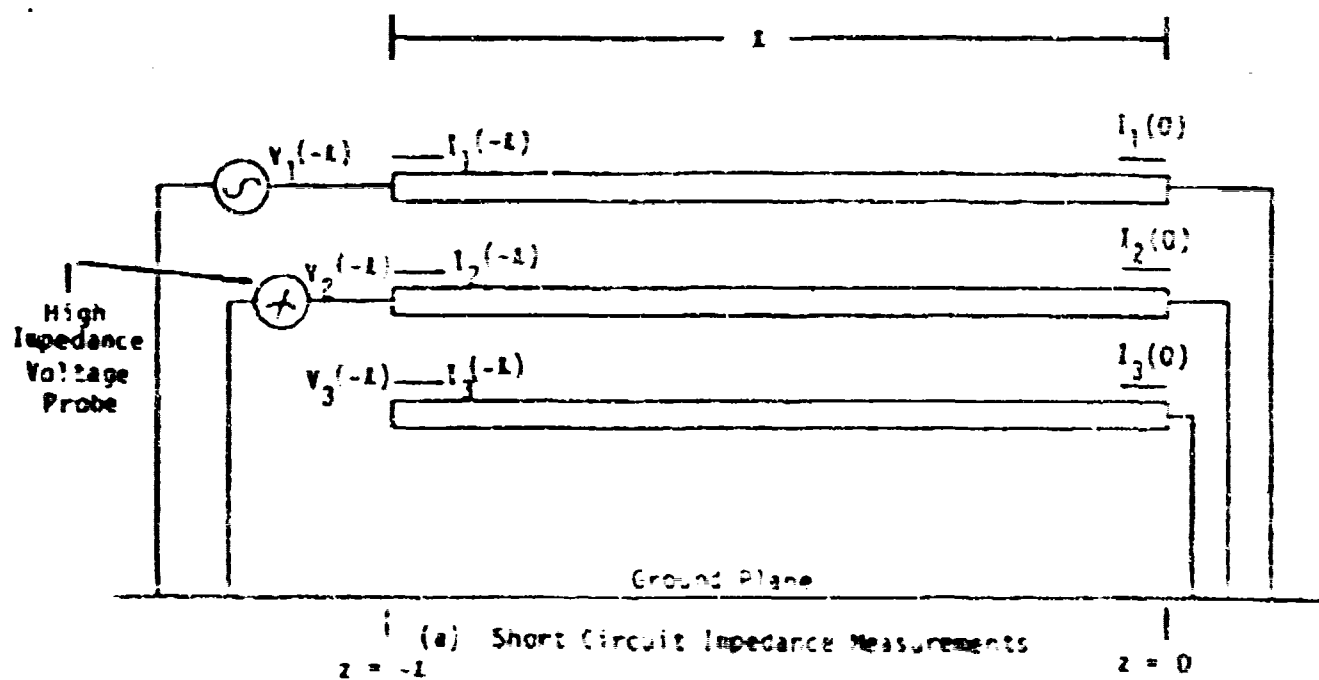


Figure 1-3. Schematic Diagram of Measurement Method (Three-wire Case Example)

repeated for each wire to isolate the self and mutual impedance terms in the circuit equations (e.g., in the three-wire case)

$$\begin{aligned}V_1 &= Z_{11}I_1 + Z_{12}I_2 + Z_{13}I_3 \\V_2 &= Z_{21}I_1 + Z_{22}I_2 + Z_{23}I_3 \\V_3 &= Z_{31}I_1 + Z_{32}I_2 + Z_{33}I_3\end{aligned}\tag{A-36}$$

The impedances are given by

$$Z_{nm}^{SC} = \frac{V_n}{I_m} \quad \begin{matrix} \text{for } n = 1,2,3 \\ m = 1,2,3 \end{matrix}\tag{A-37}$$

The open circuit input impedance matrix $[Z_{in}^{OC}(s)]$ or admittance matrix $[Y_{in}^{OC}(s)]$ measurements were performed with the far end open and the near end of all but the driven wire shorted (figure A-3b). The voltage across the driven wire and the current in each of the wires was measured with probes and the procedure repeated for all the wires to give the self and mutual admittance terms in the equations (e.g., in the three-wire case,

$$\begin{aligned}I_1 &= Y_{11}V_1 + Y_{12}V_2 + Y_{13}V_3 \\I_2 &= Y_{21}V_1 + Y_{22}V_2 + Y_{23}V_3 \\I_3 &= Y_{31}V_1 + Y_{32}V_2 + Y_{33}V_3\end{aligned}\tag{A-38}$$

with

$$Y_{nm}^{OC} = \frac{I_n}{V_m} \quad \begin{matrix} \text{for } n = 1,2,3 \\ m = 1,2,3 \end{matrix}\tag{A-39}$$

In the above measurements the losses in the line were found to be negligible and are neglected in further calculations. For a lossless case the per unit-length series impedance and shunt admittance matrices become

$$[Z_{nm}^0(s)] = s[L_{nm}^0] \quad (A-40a)$$

$$[Y_{nm}^0(s)] = s[C_{nm}^0] \quad \text{where } s = j\omega \quad (A-40b)$$

From the knowledge of $[Z_{nm}^{SC}(s)]$ and $[Y_{nm}^{OC}(s)]$, the parameters of the multiconductor line can be calculated using the equations described in section A-4. The parameters $[L_{nm}^0]$ and $[C_{nm}^0]$ and the velocities of propagation were calculated as a function of frequency (0.1 MHz - 2 MHz), using the experimental data. The measured average per unit-length inductance and capacitance matrices and velocities of propagation for the three-, four- and five-wire cables are as follows:

(a) Three-wire Cable

$$[L_{nm}^0]_{\text{meas}} = \begin{bmatrix} 0.864 & 0.484 & 0.535 \\ 0.484 & 0.939 & 0.379 \\ 0.535 & 0.379 & 0.992 \end{bmatrix} \mu\text{H/m}; \quad [C_{nm}^0]_{\text{meas}} = \begin{bmatrix} 46.48 & -20.909 & -20.553 \\ -20.909 & 33.834 & -4.152 \\ -20.553 & -4.152 & 31.099 \end{bmatrix} \text{pF/m}$$

$$v_1 = 2.829 \cdot 10^8 \text{ m/s}$$

$$v_2 = 2.178 \cdot 10^8 \text{ m/s}$$

$$v_3 = 2.009 \cdot 10^8 \text{ m/s}$$

(b) Four-wire Cable

$$[L_{nm}^0]_{\text{meas}} = \begin{bmatrix} 0.840 & 0.490 & 0.560 & 0.492 \\ 0.490 & 0.938 & 0.396 & 0.489 \\ 0.560 & 0.396 & 0.974 & 0.432 \\ 0.492 & 0.489 & 0.432 & 0.865 \end{bmatrix} \mu\text{H/m}$$

$$[C_{nm}^{(2)}]_{meas} = \begin{bmatrix} 57.256 & -16.745 & -22.754 & -11.595 \\ -16.745 & 43.769 & -2.329 & -15.815 \\ -22.754 & -2.329 & 34.994 & -4.774 \\ -11.595 & -15.815 & -4.774 & 37.672 \end{bmatrix} \text{ pF/m}$$

$$v_1 = 2.607 \cdot 10^8 \text{ m/s}; v_2 = 1.954 \cdot 10^8 \text{ m/s}$$

$$v_3 = 2.338 \cdot 10^8 \text{ m/s}; v_4 = 2.147 \cdot 10^8 \text{ m/s}$$

(c) Five-Wire Cable

$$[L_{nm}^{(2)}]_{meas} = \begin{bmatrix} 0.902 & 0.477 & 0.540 & 0.485 & 0.513 \\ 0.477 & 0.951 & 0.384 & 0.486 & 0.424 \\ 0.540 & 0.384 & 1.006 & 0.424 & 0.534 \\ 0.485 & 0.486 & 0.424 & 0.850 & 0.557 \\ 0.513 & 0.424 & 0.534 & 0.557 & 1.116 \end{bmatrix} \text{ uH/m}$$

$$[C_{nm}^{(2)}]_{meas} = \begin{bmatrix} 52.555 & -16.125 & -17.761 & -8.895 & -5.632 \\ -16.125 & 42.145 & -2.319 & -15.357 & -1.426 \\ -17.761 & -2.319 & 35.779 & -3.146 & -6.841 \\ -8.895 & -15.357 & -3.146 & 41.772 & -9.705 \\ -5.632 & -1.426 & -6.841 & -9.705 & 25.355 \end{bmatrix} \text{ pF/m}$$

$$v_1 = 1.917 \cdot 10^8 \text{ m/s}; v_2 = 2.762 \cdot 10^8 \text{ m/s}; v_3 = 2.071 \cdot 10^8 \text{ m/s}$$

$$v_4 = 2.465 \cdot 10^8 \text{ m/s}; v_5 = 2.260 \cdot 10^8 \text{ m/s}$$

A comparison of the measured coefficient for the inductance matrix with predicted values was carried out using the formulas (ref. 17)

$$L_{nn}^{(2)} = 0.2 \ln [4r_n / d_n], \quad (A-4'a)$$

$$L_{nm}^{(2)} = 0.2 \ln [5r_m / r_n], \quad (A-4'b)$$

where L'_{nn} is the self inductance term of the n th conductor, L'_{nm} is the mutual inductance term between n th and m th conductors. The other parameters are defined as:

- d = the diameter of the conductor
- h = the distance from a conductor to ground
- D = the distance between two conductors
- S = the distance from the conductor to the "image" of a second

The above formulas give quite accurate results if the ratio of conductor separation to radius is greater than 5. In this case the conductors can be assumed to be separated sufficiently such that the charge distribution around the periphery of each conductor is constant and the conductors can be replaced by filamentary lines of charge. For closer conductor spacings, proximity effect will alter the charge distributions from constant ones and numerical approximations must be employed.

The per unit-length inductance matrix $[L'_{nm}]$ calculated from the geometry using the formulas in (A-41a) and (A-41b) are

(a) Three-wire Cable

$$[L'_{nm}]_{\text{calc}} = \begin{bmatrix} 0.869 & 0.496 & 0.547 \\ 0.496 & 0.980 & 0.396 \\ 0.547 & 0.396 & 0.980 \end{bmatrix} \mu\text{H/m}$$

(b) Four-wire Cable

$$[L'_{nm}]_{\text{calc}} = \begin{bmatrix} 0.869 & 0.496 & 0.547 & 0.512 \\ 0.496 & 0.980 & 0.396 & 0.515 \\ 0.547 & 0.396 & 0.980 & 0.453 \\ 0.512 & 0.515 & 0.453 & 0.590 \end{bmatrix} \mu\text{H/m}$$

(c) Five-wire Cable

$$[L_{mm}]_{calc} = \begin{bmatrix} 0.869 & 0.496 & 0.547 & 0.512 & 0.539 \\ 0.496 & 0.980 & 0.396 & 0.515 & 0.433 \\ 0.547 & 0.396 & 0.980 & 0.453 & 0.579 \\ 0.512 & 0.515 & 0.453 & 0.690 & 0.555 \\ 0.539 & 0.433 & 0.579 & 0.555 & 1.325 \end{bmatrix} \text{ uH/m}$$

The comparison of the calculated values of the elements of the per unit-length inductance matrices with the measured values shows a maximum error of 6 percent. The error in most of the elements is less than 4 percent. The formulas in equations (A-4)a and (A-4)b are approximately valid for the present case of cables under investigation, since the ratio of conductor separation to radius is approximately greater than 6.

Finally, the error propagation in the process of calculation due to the experimental errors was studied. Two kinds of errors occur in the measurements, the error in the measurement of frequency and the error in the measurement of impedance or admittance. The propagation of the error in the process of calculation due to the error in the measurements was studied by perturbing the measured data and then noting the changes in the calculated values. It was observed that the percentage changes in the per unit-length inductance and capacitance matrices and the characteristic impedance matrix were of the same order as the percentage perturbation in the input data. This shows the stability of the method of calculation with respect to the errors in the measurements.

SECTION A-5

CONCLUDING REMARKS

A measurement technique for the characterization of parallel multi-conductor transmission lines in an inhomogeneous medium has been presented. The measurements are simple to perform and utilize commonly available laboratory equipment. It was found that data with a high confidence level could be obtained without difficulty; however, effects due to probe loading, probe cross coupling, stray impedances, etc. can produce erroneous results. Therefore, a careful measurement procedure was followed to minimize these effects. This method also gives the characteristics of different propagating modes so that explicit measurement of multiple phase velocities is not required. The measured data shows a good agreement with that calculated from theoretical formulas in literature. The matrices involved in the process of calculation are found to be well conditioned, so that the error propagation in calculations is minimized. Although the method was verified with a maximum of five wires, it is very general, and should work for any number of conductors.

REFERENCES

1. Armitage, H., "Time Domain Analysis of Multiple Parallel Transmission Lines," RCA Review, pp. 241-276, June 1967.
2. Carey, W. L., T. R. Scott and M. T. Weeks, "Characterization of Multiple Parallel Transmission Lines Using Time Domain Reflectometry," IEEE Trans. IM, Vol. IM-18, No. 3, September 1969.
3. Frenkel, S., Cable and Multiconductor Transmission Line Analysis, NOL-TR-091-1, Harry Diamond Labs, Washington, D. C., June 1974.
4. Fowles, H. W., L. D. Scott, A. K. Agrawal and C. M. Lee, Aircraft Cable Parameter Study, AFAL-TR-77-177, Air Force Weapons Laboratory, Kirtland Air Force Base, New Mexico, July 1977.
5. Paul, C. R., "Useful Matrix Chain Parameter Identities for the Analysis of Multiconductor Transmission Lines," IEEE Trans. MTT, Vol. MTT-23, pp. 756-760, September 1975.
6. Paul, C. R., "On Uniform Multinode Transmission Lines," IEEE Trans. MTT, Vol. MTT-21, pp. 556-558, August 1973.
7. Pipes, L. A., "Matrix Theory of Multiconductor Transmission Lines," Phil. Mag., Vol. 24, pp. 97-113, July 1937.
8. Mark, K. D., "Propagation Modes, Equivalent Circuits, and Characteristic Terminations for Multiconductor Transmission Lines with Inhomogeneous Dielectrics," IEEE Trans. MTT, Vol. MTT-21, No. 7, July 1973.
9. Tesche, F. M., "A General Multiconductor Transmission Line Model," Joint IEEE AP-S and URSI meeting, Ann Arbor, October 11-15, 1976.
10. Baum, C. E., "Coupling into Coaxial Cables from Currents and Charges on the Exterior," Joint IEEE AP-S and URSI meeting, Ann Arbor, October 11-15, 1976.
11. "Parameters for Aircraft Cables," The Boeing Company, D214-10015-1, June 1973.
12. Pretella, J. F. and R. A. Paost, "Analytical and Experimental Procedures for Determining Multiconductor Line Parameters," Joint EMF Technical Meeting, NIM 1913, Proceedings Vol. III, Interaction and Coupling, pp. 259-291, 5 June 1975.

REFERENCES (Continued)

13. Schelkunoff, S. A., "Conversion of Maxwell's Equations into Generalized Telegraphers Equations," Bell System Technical Journal, Vol. 34, pp. 995-1043, September 1955.
14. Krage, M. K. and G. I. Haddad, "Characteristics of Coupled Microstrip Transmission Lines - I: Coupled Mode Formulation of Inhomogeneous Lines," IEEE Trans. MTT, Vol. MTT-18, pp. 217-222, April 1970.
15. Ramo, S., I. R. Whinnery and T. V. Duzer, Fields and Waves in Communication Electronics, John Wiley & Sons, Inc., New York, 1965.
16. Chen, C. T., Introduction to Linear System Theory, Holt, Rinehart and Winston, Inc., New York, 1970.
17. Paul, C. R., "Applications of Multiconductor Transmission Line Theory to the Prediction of Cable Coupling," RADC-TR-76-101, Vol. I, Final Technical Report, Griffis Air Force Base, NY, April 1976.